U.PORTO
FEUP FACULDADE DE ENGENHARIA
UNIVERSIDADE DO PORTO

Master Thesis in Mechanical Engineering

Fracture envelope of automotive adhesives under impact

Author:
Catarina da Silva Pereira Borges

Supervisor:
Lucas F. M. da Silva
Co-Supervisors:
Alireza Akhavan
Eduardo A. S. Marques
Ricardo J.C. Carbas
Paulo D. P. Nunes

Integrated Master in Mechanical Engineering

June, 2019

Acknowledgements

First, I would like to express my gratitude to my supervisor, Lucas da Silva, for the opportunity to be a part of this project and for the knowledge and expertise shared throughout this project.

This work would not have been possible without the financial and technical support provided by ArcelorMittal Global R&D, in the context of a research internship on the dynamical behaviour of adhesive joints. Special appreciation goes to Hugo Leonardo Alfonso Medina for suggesting this work, and being constantly available for discussing and suggesting improvements to this work.

A special thank you to my co-supervisors Paulo Nunes, Eduardo Marques, Alireza Akhavan and Ricardo Carbas for the guidance, the knowledge shared, the long hours of work and constant availability and patience to help me along this project.

I would also like to express my gratitude to LOME, namely Pedro Moreira, Paulo Tavares and Nuno Viriato for the help given in the image acquisition with the high speed camera.

To all the members of the adhesives group, ADFEUP, for the constant availability, tips shared and friendship during this project. It was a pleasure to work with you all. A special thanks goes to Mário and Catarina for all the time spent working, dinning, and group whining.

To all my friends, both those who have been in my life for a long time and those with whom I have spent the last five years, thank you for your support, all the love and companionship you have given me over the years.

To my family, thank you for all your support throughout my life, and for always supporting my decisions. A special thanks to my mother who always brings me chocolate in times of stress, my father who gives me sushi when I need it the most and my grandmother, aunts and cousin who have always been there to make me laugh.

Abstract

Adhesives are increasingly being used in the automotive industry as an alternative to classical mechanical joining methods, as they improve strength to weight ratio and reduce the cost of the projected structure. Adhesives also suppress the need for holes, which not only results in a more uniform stress distribution along the surface, avoiding stress concentrations, but also enables the connection of composite materials, reducing the weight of the structure and, consequently, the fuel consumption. In the automotive industry, it is crucial to ensure passengers' safety if a collision occurs, for that, the behaviour of the entire structure should be analysed for impact conditions, including the adhesives.

The present work aims to understand how the mechanical properties of structural adhesives vary as a function of strain rate, through the definition of the strength and fracture toughness envelopes.

The envelope of the strength properties was defined through bulk tensile tests and thick adherend shear tests (TAST) at three different test speeds: quasi-static, 1 mm$\cdot$ min^{-1}, intermediate, $6 \cdot 10^3$ mm$\cdot$ min^{-1}, and impact, $180 \cdot 10^3$ mm$\cdot$ min^{-1}.

The fracture envelope was defined through mode I, mode II and mixed mode tests. The fracture toughness was determined, for mode I through double cantilever beam (DCB) tests, for mode II using end notched flexure (ENF) tests and for mixed mode using two in-house developed apparatus. The existing in-house developed apparatus for mixed mode testing was not designed to sustain high loading rates, thus, a new and more robust apparatus for mixed mode testing was developed and validated. All tests were performed for quasi-static conditions, 0.2 mm$\cdot$ min^{-1}, intermediate speed, $6 \cdot 10^3$ mm$\cdot$ min^{-1}, and impact conditions, $180 \cdot 10^3$ mm$\cdot$ min^{-1}.

As properties change with loading rate, when performing numerical simulations of bonded joints for different strain rates this variation should be accounted for. For that, the loading rate dependency was transformed in strain rate dependency and the trendlines for the properties variation were implemented in a cohesive zone model (CZM) using an Abaqus® subroutine - UMAT.

The tensile and shear strength, as well as the energy release rate for all mode mixities analysed showed an increase with increasing loading rate. The evolution of those properties was approximated using logarithmic relations.

The results of this numerical simulation were validated for DCB and ENF tests and revealed good agreement with the experimental results.

Resumo

Na indústria automóvel, os adesivos estruturais são cada vez mais utilizados como alternativa aos métodos clássicos de ligação mecânica, visto que contibuem para o aumento da razão entre a resistência e o peso da estrutura, e diminuem o custo. Os adesivos suprimem ainda a necessidade de furos, o que resulta não só numa distribuição de tensões mais uniforme, evitando zonas de concentração de tensões, mas também porque permitem a junção de materiais compósitos, muito sensíveis a entalhes, reduzindo o peso da estrutura e, consequentemente o consumo de combustível. Na indústria automóvel é crucial assegurar a segurança dos passageiros no caso de ocorrer uma colisão. Para tal, o comportamento de toda a estrutura, incluindo juntas adesivas, deve ser caracterizado para condições de impacto.

O presente trabalho pretende compreender como as propriedades do adesivo variam em função da taxa de deformação, através da definição dos envelopes de resistência e tenacidade.

O envelope de resistência mecânica foi definido através de ensaios de tração bulk e TAST para três velocidades de teste: quase-estático, 1 mm$\cdot$ min^{-1}, a velocidade intermédia, $6 \cdot 10^3$ mm$\cdot$ min^{-1}, e impacto, $180 \cdot 10^3$ mm$\cdot$ min^{-1}.

O envelope de fratura foi definido através de testes em modo I, double cantilever beam (DCB), testes em modo II, end notched flexure (ENF) e testes em modo misto. Um dispositivo para modo misto desenvolvido internamente foi utilizado para os testes quase estáticos. Porém, este dispositivo não foi projetado para testes a altas velocidades, pelo que um novo dispositivo, mais robusto, foi desenvolvido para estes ensaios e validado. Todos os testes foram realizados em regime quase-estático, 0.2 mm$\cdot$ min^{-1}, a velocidade intermédia, $6 \cdot 10^3$ mm$\cdot$ min^{-1}, e impacto, $180 \cdot 10^3$ mm$\cdot$ min^{-1}.

Visto que as propriedades do adesivo variam com a velocidade de teste, quando se simula numericamente uma junta adesiva para differentes taxas de deformação deve-se considerar esta variação. Para tal, a dependência da velocidade de teste foi transformada em variação da taxa de deformação, e estas relações foram implementadas num modelo de zonas coesivas (CZM) usando uma subrotina do interna do software Abaqus® - UMAT.

Foi determinado que a resistência do adesivo à tração e corte, bem como a energia de fratura para todos os modos analisados, aumenta com a velocidade de teste. A evolução destas propriedades foi aproximada utilizando uma relação logaritmica.

Os resultados desta simulação numérica foram comparados com os resultados experimentais para testes DCB e ENF tendo sido obtida uma boa aproximação.

Contents

List of Figures

List of Tables

List of acronyms

CBBM	Compliance based beam method
CBT	Corrected beam theory
CCM	Compliance based beam method
CZM	Compliance based beam method
DCB	Double cantilever beam
ENF	End notched flexure
FPZ	Fracture process zone
LVDT	Linear variable differential transformer
SHPB	Split Hopkinson pressure bar
TAST	Thick adherend shear test
TDCB	Tapered double cantilever beam

1 Introduction

1.1 Background and motivation

Adhesives are increasingly being used in a wide range of industries such as automotive, aerospace and aeronautical [1] due to their low weight, which allows a lower energy consumption, along with less emissions.

Adhesives are also used because of their unique advantages when compared to conventional mechanical joining methods. Among those advantages are a more uniform stress distribution, which leads to a good resistance to dynamic fatigue, higher stiffness and load transmission, the ability to bond dissimilar materials and thin sheets of material, the possibility of process automation, design flexibility and regular contours [1, 2].

In the automotive industry, it is crucial to ensure passengers' safety, both in daily use and in case of a collision. For that purpose, the impact behaviour of the adhesives used in the structures should also be assessed. For the simulation of the behaviour of an adhesive, the fracture energy, Young's modulus, shear modulus and shear and tensile strength should be determined for implementation on a cohesive zone model (CZM).

Although the static behaviour of adhesives has been extensively studied, the impact behaviour is noticeably less researched. Additionally, completely different trends for the strain rate dependent behaviour of different properties have been reported by different authors, which leads to a degree of uncertainty regarding the behaviour of adhesives under dynamic conditions.

1.2 Objectives

This thesis has two main objectives, the first is to fully understand how the adhesives' properties change with increasing strain rate, and establish a function that translates the variation of the properties of the adhesives under study as a function of strain rate.

The second objective is to implement the properties determined in a cohesive zone model (CZM) that takes into account the properties variation with strain rate, enabling the simulation of situations with different loading rates.

1.3 Research methodology

The objectives of this thesis were accomplished through the performance of several steps, which can be divided as follows:

- A careful literature review, focusing in detail on the state of the art regarding the variation of adhesives' properties with strain rate;
- Experimental tests, namely bulk tensile tests, thick adherend shear tests (TAST), double cantilever beam (DCB) tests, end notched flexure (ENF) tests and mixed mode fracture tests, performed at different levels of strain rate.

– Numerical simulation of the fracture specimens tested in mode I and mode II, considering material laws that reproduce the strain rate dependent behaviour of the adhesives under study.

1.4 Thesis outline

This thesis is divided in seven main parts. This introductory chapter contains a brief description of the problem addressed, as well as the background and motivation of this work and its objectives.

Chapter 2 comprehends a review about adhesive joints, their classification, failure modes, design, and their importance in the automotive industry. Since the main purpose of this work is to analyse the dependence of adhesives' properties on the strain rate, a brief literature review on the topic is also presented, focusing on the dependence of the strength and fracture behaviour, as well as numerical approaches proposed by some authors to reproduce adhesives' behaviour for different strain rates. Lastly, the approaches typically used to analyse the strength of an adhesive are discussed.

Chapter 3 clarifies the experimental procedures used throughout this work to assess the mechanical properties of the adhesives in study for different strain rates. This tests cover all the parameters typically used to simulate numerically an adhesive joint, from bulk to fracture properties. Chapter 4 explains the numerical model developed in this work and the double cantilever beam (DCB) and end notched flexure (ENF) models and its validation.

Chapter 5 presents the summary of the appended papers, with a brief description of its objectives and conclusions.

Chapter 6 presents the main conclusions about the topics of research and Chapter 7 presents suggestions for further work on these topics.

2 Literature review

2.1 Survey of adhesive joints

An adhesive can be defined as a material which, when applied to surfaces, can join them together and resist separation. Adhesive is, therefore, the general term which covers glue, cement, paste, and others [1].

An adhesive joint is the connection between two surfaces, made of similar or different materials, using non-metal fillers, adhesives. The materials that are bonded by the adhesive, before bonding, are called substrates. Generally, after bonding they are referred to as adherends. The region between the adherend and the adhesive is the interphase, which contains the interface, or boudary layer. The interface is the plane defined by the contact between the surface and the two materials [1].

Adhesives have been used for centuries but, until about 1900, the majority was obtained from natural products, such as skins, fish, milk and bones [1]. For example, early hunters included beeswax in feathers, used in arrows, to improve their aim, which can be consider a primitive adhesive [3]. In the last century, adhesives based on synthetic polymers, such as epoxy resins, have been introduced and adhesives were approached as an viable alternative to typical connection methods such as bolting, riveting, welding and brazing. This process eventually led to adhesives that are able to resist substantial loads, structural adhesives, which are also able to contribute to the stiffness and strength of the structure [4, 5].

On one hand, adhesive joints provide a wide variety of advantages when compared to conventional mechanical fasteners [1, 2]:

- More uniform stress distribution, which can be schematically observed in Figure 1. This leads to a good resistance to dynamic fatigue as well as higher stiffness and load transmission, reducing the weight and, thus, the cost;
- The ability to bond dissimilar materials;
- The ability to bond thin sheets of material;
- The possibility of process automation;
- Design flexibility, allowing new materials and design concepts;
- Regular contours, due to the absence of holes and welding marks.

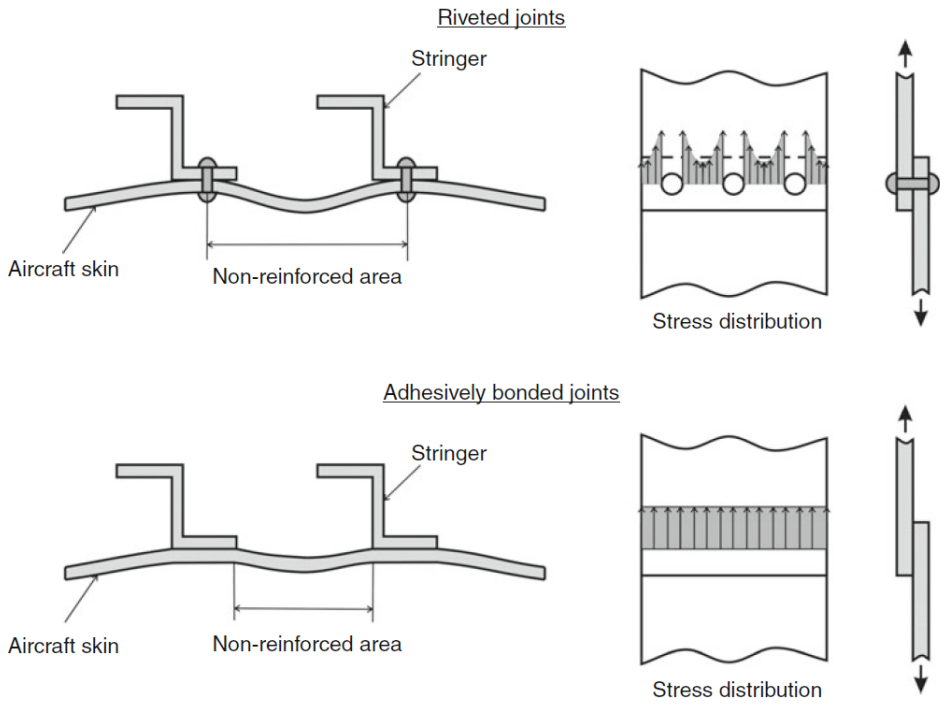

Figure 1: Comparison between riveted and adhesively bonded joints in terms of stiffness (left) and stress distribution (right) [1].

On the other hand, adhesive joints also present some disadvantages that should be considered [1, 2]:

- The need to avoid peel and cleavage stress because they create a load concentration in a small area, resulting in low strength;
- Limited resistance to extreme environmental conditions, such as high temperature and humidity, due to the polymeric nature of the adhesive;
- The necessity of fixtures to maintain the substrates in position, since the bonding is usually not instantaneous;
- The requirement of temperature for the hardening of a wide variety of adhesives;
- The necessity of extremely careful surface preparation to ensure good adhesion;
- Difficult quality control.

2.1.1 Classification of adhesives

Adhesives can be classified based on different parameters, the most common are: polymer base, functionality in the polymer "backbone", physical form, functional type, chemical family and method of application [1].

The polymer base can be either natural or synthetic. Adhesives that have a natural base include vegetable and animal based adhesives and natural gums. Those are, for

example, natural rubber, animal glue and casein-based and protein-based adhesives. Adhesives that have a synthetic base include all adhesives that are not natural. These are, for example, acrylics, epoxies, silicones and polyesters [1, 6].

The functionality of the polymer "backbone" can be thermosetting, thermoplastic, elastomeric (rubbers) and hybrid. Thermosetting adhesives are polymers that cure due to chemical reactions at room or high temperature and cannot be heated and melted after the initial cure. They can be supplied as one-part or multiple-part systems. The one-part system, typically requires high temperature to cure and its shelf life is reduced. Multiple-part systems often cure at room temperature and have a longer shelf life. Thermoplastic adhesives are cured from a melted state or by loss of solvent and can be melted without significant change in their properties. Elastomeric polymers typically have a higher elongation, toughness and peel strength. Hybrid adhesives result from a combination of the previous [1, 6].

The physical form can be liquid, paste, film or powder, and generally defines how the adhesive must be applied. Liquid adhesives can be applied using rolls, by spray or brushing and have good gap filling capabilities. Paste adhesives can be applied on vertical surfaces, because they have high viscosity and little tendency to sag or drip. Film adhesives ensure that the bondline thickness is constant and are very easy to handle. Powder adhesives usually have to be heated or dissolved into a solvent to be transformed into a liquid form, so that they can be applied [1, 6].

The functional type separates adhesives as structural and non-structural. Adhesives can also be referred to as hot-melt, pressure sensitive, water-base, ultraviolet/electron beam cured, conductive, among others [1].

The chemical family can be epoxy, acrylic, polyurethane, among others. Epoxy adhesives are very important in the structural adhesives family and are the most versatile. These thermosetting adhesives are strong and brittle, but can be formulated to be more flexible and tough without loss of tensile strength. Acrylics provide fast cure and high strength, but are more expensive than epoxies. Polyurethane is tough and flexible even at low temperature, but moisture and heat sensitive [1].

The method of application, depending on viscosity, can be coating, spraying or brushing [1, 6]

2.1.2 Failure modes and joint design

Adhesive joints, with metal substrates, can exhibit three different failure modes: cohesive failure in the adhesive, adhesive (interfacial) failure and cohesive failure in the adherend, as shown in Figure 2 [1].

Figure 2 clearly shows that, when cohesive failure in the adhesive occurs, the surfaces of both adherends remain covered in adhesive. This type of failure can be due to thermal stresses, gross void defects or inadequate overlap length. When adhesive failure occurs, the bond failure is between the adhesive and one of the adherends, which can result

from poor surface preparation. And, finally, when the adhesive bond is very strong, the adherend reaches its material strength limit and fails before the adhesive bond, which is referred to as cohesive failure in the adherend.

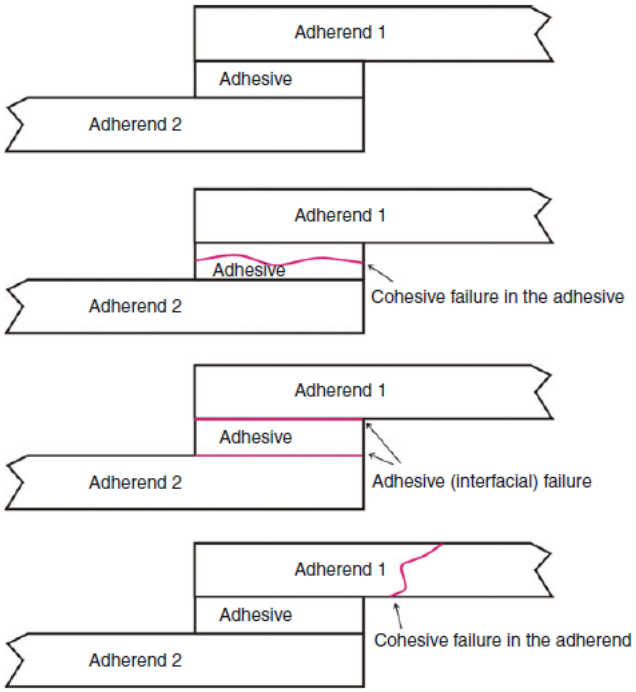

Figure 2: Schematic representation of cohesive and adhesive failures [1].

It is important to notice that adhesives can be exposed to different mechanical loading conditions. The most common types of stresses are: normal stresses - Figure 3a - , shear stresses - Figure 3b - , cleavage stresses - Figure 3c - and peel stresses - Figure 3d.

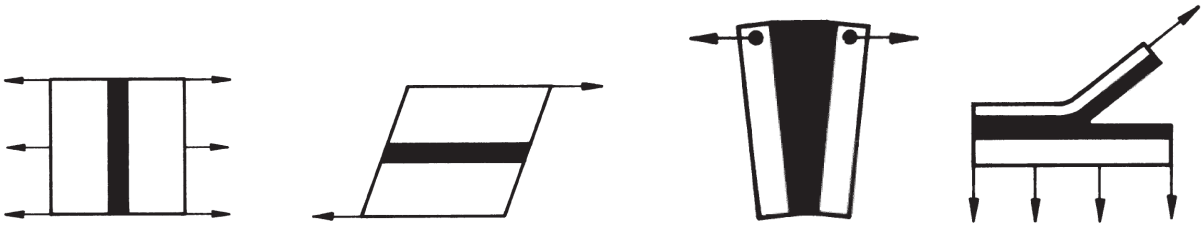

(a) Normal. (b) Shear. (c) Cleavage. (d) Peel.

Figure 3: Types of stress on adhesive joints. Adapted from [7].

The type of stress depends on the way the load is applied, the properties of the adhesive and substrates and on the geometry of the joint. Some of the most common joint configurations are: single-lap joints - the most studied configuration due to its simplicity -, double-lap joints, scarf joints and stepped-lap joints, which are represented in Figure 4 [8].

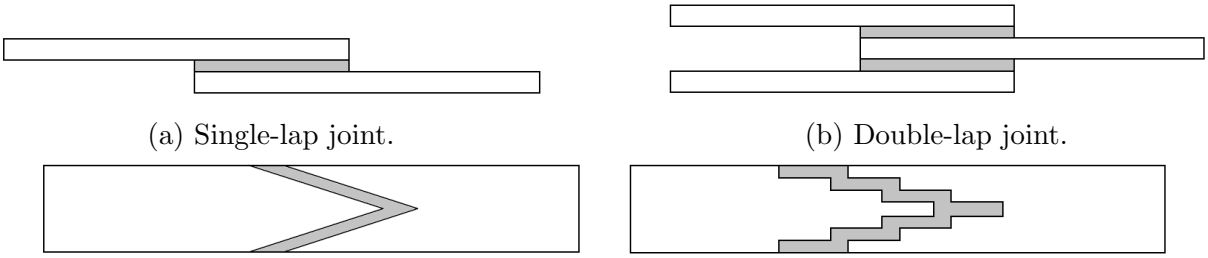

(a) Single-lap joint. (b) Double-lap joint.

(c) Scarf joint. (d) Stepped-lap joint.

Figure 4: Most common joint configurations.

2.2 Adhesives in the automotive industry

Adhesives are widely used in the automotive industry due to their light weight, which allows for improved energy economy and reduced emissions. They are used from applications where the loads involved are small, where non-structural adhesives are suitable, to numerous applications where loads are substantial and diverse structural adhesives must be used, which can be seen in Figure 5.

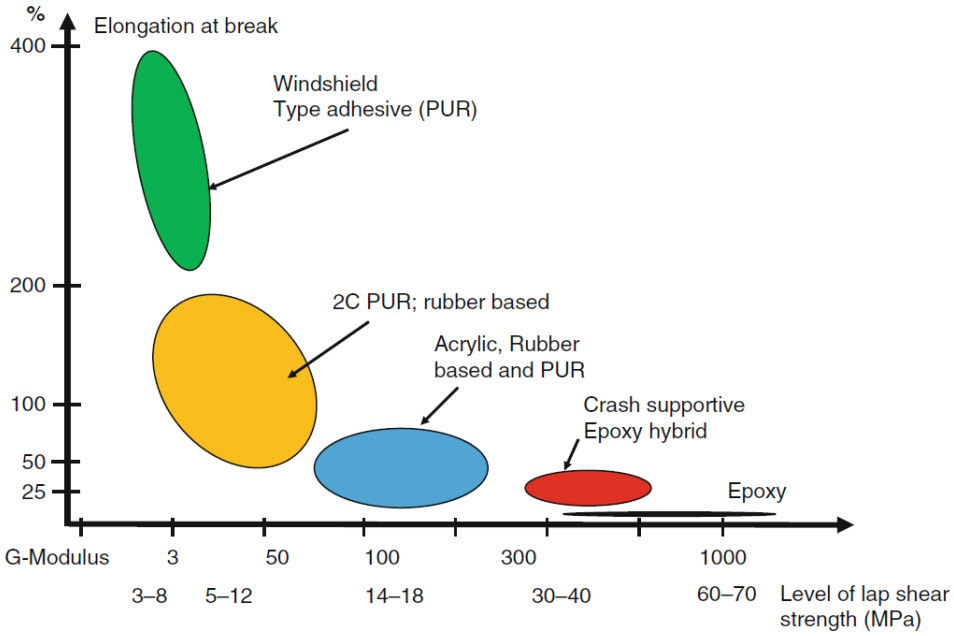

Figure 5: Overview of structural adhesives used in the automotive industry [1].

Figure 5 clarifies that, on one hand, polyurethane adhesives, with low modulus and high elongation are used, for example, in the windshield. And, on the other hand, very high strength crash-resistant epoxy-hybrid adhesives are used in vital areas of the car body.

Adhesives undergo a series of process conditions that can be distinguished, in the automotive industry, between three different areas of application: the body shop, the paint shop and the trim shop/assembly lane. In the body shop, adhesives are used for

anti-flutter bonding, hybrid joining and flange bonding. In the paint shop, the use of adhesives is limited to a few minor applications. However, most of the trim pieces are bonded to the vehicle so, in the trim shop, adhesives are extensively used [1].

Adhesives used in the car body should suit specific requirements [1]:

1. They need adhesion on oiled bare, eletrogalvanized or hot dip galvanized steel and on aluminum metal sheets;
2. They are designed to cure during the pretreatment process for the eletro coat;
3. They must be applied in a liquid stage to ensure proper wetting, so, a pre-curing or pre-gelation is often required to withstand the conditions of the pretreatment baths;
4. They should resist about 200°C over half an hour, the time and temperature can change according to the production process used;
5. They must be prepared to be stored or shipped uncured because, under those conditions, adhesives may absorb moisture from the atmosphere, which will cause bubbles when curing, reducing the strength of the adhesive.
6. They should be resistant to corrosion because all body shop adhesives are applied directly on the metal surface.

In the automotive industry, it is crucial to ensure passengers' safety in case of a collision. Due to the viscoelastic nature of polymeric materials, it is known that adhesives' properties change with loading rate and, consequently, strain rate. Therefore, it is very important do study the behaviour of adhesives under impact to know how they would behave in case of a crash.

2.3 Strength prediction approaches

Adhesive joints should be carefully designed to sustain the loads imposed in service. There are three main approaches to predict the failure of the adhesive: continuum mechanics, fracture mechanics and damage mechanics.

2.3.1 Continuum mechanics

Continuum mechanics assumes that both the adhesive and the adherends are continuous and that the connection between them is perfect, not taking into account the properties of the interface [9]. This approach relies on the study of stresses and deformations and on the determination of the maximum load that can be applied to the bonded parts, specially in the most common types of loading conditions, discussed in subsection 2.1.2, and shown in Figure 3.

Continuum mechanics presents various fracture criteria, such as the maximum stress and maximum strain but, the available criteria fails to describe faithfully the failure of an adhesive joint due to singularities of the joint tip geometry, shown in Figure 6. Here, using finite element analysis, the value of stress increases with mesh refinement, not converging. Different authors presented approaches to solve this problem. However, they are only applicable for continuous structures, making it impossible to describe defects or different materials [9].

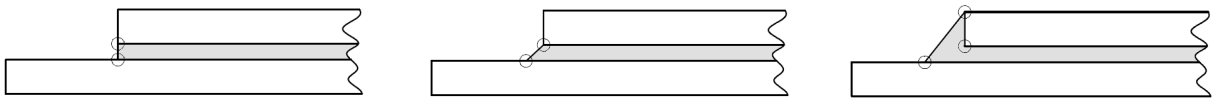

Figure 6: Singularities of the joint tip geometry. Adapted from [9].

2.3.2 Fracture mechanics

Fracture mechanics, in contrast to continuum mechanics, assumes that the structure has discontinuities, allowing the consideration of manufacture defects or other damage caused during its life [9]. Fracture mechanics intends to analyse quantitatively the behaviour of solid bodies containing cracks, evaluating if the size of one defect overcomes the critical fracture size. There are two main criteria in which fracture mechanics is based: the stress intensity factor criterion and the energy criterion.

Cracks with different shapes can create the same type of stress concentration, leading to infinite stress at the crack tip. Therefore, the stress concentration factor would not be suited to distinguish between those different cases, where it would be always equal to infinity although the stress distribution in the region of the crack tip is not the same in all cases. The stress intensity factor, K, represents a scale parameter that reflects the stress distribution in the neighbourhood of the crack tip. Generically,

$$K = Y\sigma_r\sqrt{\pi a} \tag{1}$$

where Y is a non dimensional factor, dependent on the geometry and load distribution, σ_r is the remote tension applied and a is related to the crack length. The crack will occur when the stress intensity factor, K, is equal to the material fracture toughness K_c.

There are three different loading modes: mode I (opening mode), mode II and mode III (shear modes), Figure 7. In most real situations, the applied load creates a combination of these fracture modes at the crack tip.

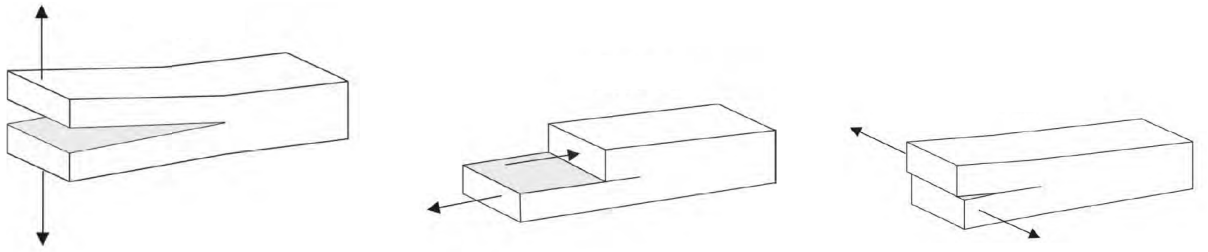

(a) Mode I. (b) Mode II. (c) Mode III.

Figure 7: Fracture modes for an adhesive joint [9].

For each fracture mode, a stress intensity factor is defined, K_I, K_{II} and K_{III} for mode I, II and III respectively.

The energetic criterion considers that the crack will propagate when the available energy at the crack tip, G - energy release rate - is equal to the energy needed for the propagation of the crack, G_c - critical energy release rate [9].

The two criteria can be related, for plane stress, by [10]:

$$G = \frac{K^2}{E} \tag{2}$$

where E is the Young's modulus. And, for plane strain by [10]:

$$G = \frac{K^2}{E}(1 - \nu^2) \tag{3}$$

where ν is the Poisson's ratio.

This criterion is more used than the stress intensity factor because it is difficult to obtain reliable values of K, specially when the crack grows near the interface [9].

In adhesives, for bulk materials the crack tends to grow in mode I but, in an adhesive joint, the adherends constrict the crack growth and the crack is compelled to propagate in mixed mode I+II. The combination of mode I and II, the ratio mode, can be given by [9]:

$$\varphi = tan^{-1}\sqrt{\frac{G_{II}}{G_I}} \tag{4}$$

When mixed mode crack propagation occurs, it is necessary to take into account both mode I and II, using suitable criteria, such as [9]:

$$\left(\frac{G_I}{G_{Ic}}\right)^{\alpha} + \left(\frac{G_I}{G_{IIc}}\right)^{\beta} = 1 \tag{5}$$

where G_{Ic} is the critical energy release rate in mode I, G_{IIc} is the critical energy release rate in mode II, and α and β are constants.

To represent the energy release rate in mode I, II and for mixed modes that result from a combination of the previous, a fracture envelope is often used. Knowing the mode

I and II critical energy release rate, the fracture envelope is often approximated using the linear or quadratic criterion, which can be seen in Figure 8.

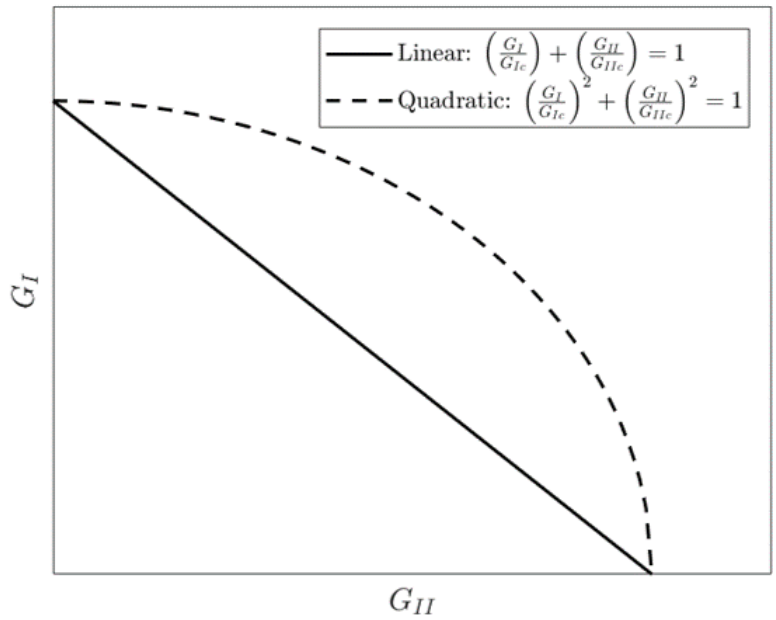

Figure 8: Schematic representation of fracture envelope approximations, using linear and quadratic criterion.

The inconvenient of fracture mechanics is that it is not suited to describe damage initiation, only damage propagation [9].

2.3.3 Damage mechanics

Damage mechanics takes into account continuum mechanics and fracture mechanics to study damage initiation and propagation, respectively. A cohesive zone model (CZM) is usually used for this type of study. CZMs are typically based on elements with no thickness, which establish the connection between two solid surfaces. For each of those elements, when a stress criterion is satisfied, a relaxation process based on fracture energy criterion, used to simulate material degradation, starts. It is important to notice that no pre-crack is needed and the propagation does not need use interference to occur [9].

The behaviour of the adhesive is, then, simulated using suitable traction-separation laws. The most common, due to its simplicity, are the triangular laws. The trapezoidal laws are also used, specially for very ductile adhesives. Triangular and trapezoidal traction separation laws are schematically represented in Figure 9.

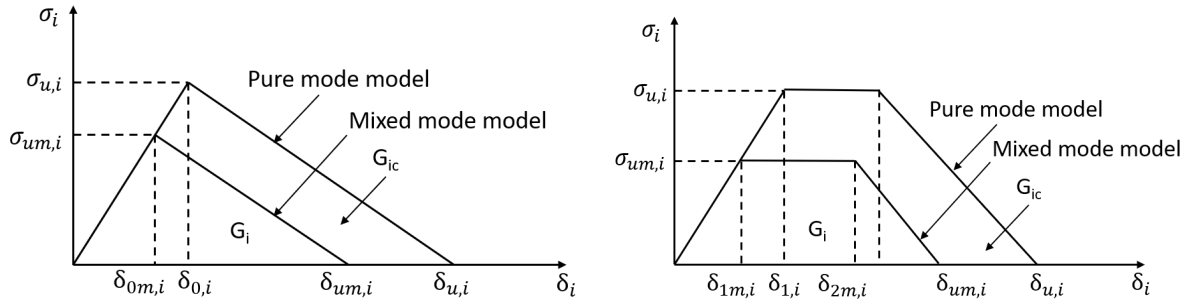

(a) Triangular traction-separation law. (b) Trapezoidal traction-separation law.

Figure 9: Schematic representation of traction separation laws, i=I,II.

2.4 Effect of strain rate on adhesives

2.4.1 Tensile and shear properties

Among the first to study the dynamic behaviour of polymers were Tardif and Marquis [11] and Lindholm [12]. Analysing an epoxy resin under compression, using strain rates up to 1000 s^{-1}, it was concluded the resin was highly strain rate sensitive. The resin showed an increase in modulus and ultimate stress along with a decrease in ultimate strain over the static value, indication of a strongly viscoelastic behaviour.

Chalkley and Chiu [13], in 1993, and Zgoul [14], in 2002, concluded that while yield stress and maximum strain exhibited a strain rate dependent behaviour, modulus remained practically unaffected - which was supported by other authors [15–20]. Most of them recorded an increase in maximum stress and a reduction in elongation.

In 2011, Sugaya et al. [15] analysed two different one-part epoxy adhesives, one showed a brittle behaviour while the other was more ductile. The brittle adhesive was tested for $4 \cdot 10^{-4}$ s^{-1} and $1 \cdot 10^{-4}$ s^{-1} while the ductile was tested for $2.8 \cdot 10^{-3}$ s^{-1} and $7 \cdot 10^{-4}$ s^{-1}. The brittle epoxy increased both stress and strain in impact conditions, which was explained by the Kalthoff-and-Shockey's theory that states that there is a particular minimum loading duration needed for the fracture of a material, that may not be satisfied the dynamic loading imposed. The ductile adhesive showed a brittle behaviour under impact, combined with an increase in maximum stress, which was explained by brittle transition due to the time-temperature superposition, which states that the effect caused by increasing strain rate is similar to that of decreasing temperature. Considering this, the author expects that with increasing strain rate adhesives become stronger and more brittle.

Avendaño et al. [21] stated that the strength of adhesives with large strain to failure values usually increases substantially with strain rate.

Machado et al. [22], in 2019, also studied the behaviour of an crash resistant tough epoxy and observed that the tension behaviour is highly dependent on the strain rate and the Young's modulus increases with the increase of strain rate.

2.4.2 Fracture behaviour

Regarding the fracture behaviour of adhesives, while static conditions have been extensively studied, impact conditions present noticeably more limited research [23]. In 1981, Bascom et al. [24] performed a compact tension study, using elastomer-modified epoxy polymers, with strain rates from 10^{-2} s^{-1} to 10^{3} s^{-1} and concluded that, in general, a decrease in fracture energy in mode I was verified with increasing strain rate.

A decrease in toughness with increasing strain rate was also detected by Britner et al. [25], Hunston et al. [26], Lataillade et al. [27], Blackman et al. [28, 29], Raghavan et al. [30], Karac et al. [16] and Jia et al. [31].

Britner et al. [25] also affirmed that fracture behaviour of adhesives may be controlled by a viscoelastic behaviour and that loading rate and temperature increases have reverse effects. Once again, for brittle materials, loading rate dependence proved to be very small over most of its useful range. This conclusion was again mentioned by Avendaño et al. [21], in 2016.

Lataillade et al. [27], in 1994, developed a new device, based on the split Hopkinson pressure bar (SHPB) apparatus and studied the variation of fracture energy in mode I (or peel mode), mode II (a shear mode) and mixed mode I+II, for adhesives with different bondline thicknesses, over a range of temperatures. A slight decrease in fracture energy with increasing strain rate was determined for all bondline thicknesses and modes tested.

In 2002, Raghavan et al. [30] stated that, at most rates, the behaviour of an acrylic rubber was approximately linear elastic with little to no R-curve behaviour. However, bellow a critical rate, a transition to ductile failure with a large R-curve and high fracture energies was observed. The transition was said to be very sudden, which could explain why it was only detected by a few authors. As a possible explanation for the decrease in fracture energy with increasing loading rate it was discussed that, slower loading rates allow a more significant crack-tip deformation, which can result in increased toughness. Lowering loading rates has also shown to generate a transition from unstable to stable crack growth.

Blackman et al. [29], in 2009, studied the dynamic behaviour of an epoxy adhesive in mode I, using double cantilever beam (DCB) and tapered double cantilever beam (TDCB) tests. The displacement rate ranged from quasi-static to up to 15 $m{\cdot}s^{-1}$. A decrease in the fracture energy of approximately 40% of its quasi-static value was noticed when increasing the loading rate over six decades.

May et al. [32] tried to justify the reduction in fracture toughness with increasing loading rate using thermodynamics, stating that when a critical crack propagation speed is reached, the conditions at the crack tip change from isothermal to adiabatic. The reduction of fracture toughness is then caused by the poor properties of polymers at high temperature.

The trend lines obtained by Blackman et al. [29] from DCB and TDCB tests and by Karac et al. [16] from TDCB tests can be observed in Figure 10.

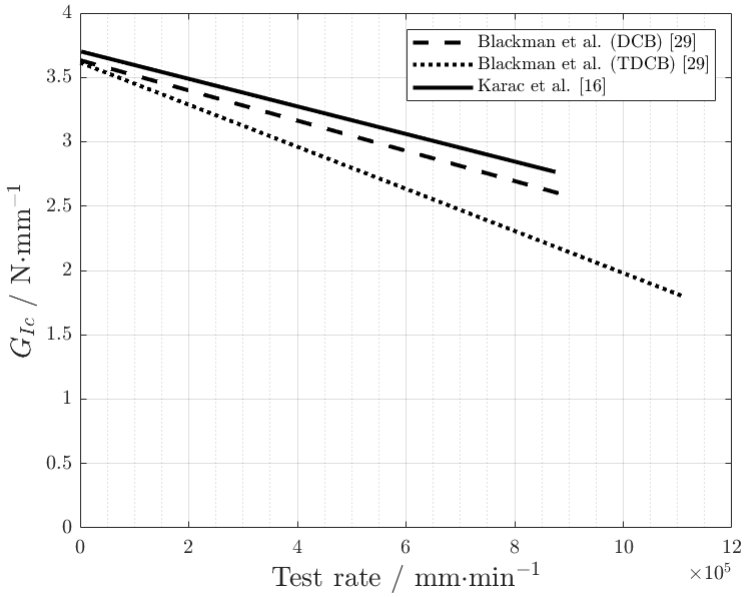

Figure 10: Energy release rate in mode I decreasing as a function of test rate. Adapted from [16, 29].

However, the notion that fracture energy decreases with increasing strain rate is not unanimous in literature. Kinloch et al. [33], in 1987, analysed both an unmodified and a rubber-modified epoxy and concluded that while the improvement noticed in the unmodified adhesive was not very pronounced, the multiphase microstructure of the rubber-modified epoxy led to a significant increase of the fracture energy with increasing strain rate. An increase in fracture energy with increasing strain rate was also reported by Biel et al. [34], Carlberger et al. [35], Marzi et al. [36, 37] and May et al. [32].

Carlberger et al. [35], in 2009, concluded that, regarding the fracture of adhesive materials, in mode I the fracture energy increases slightly with increasing strain rate, while in mode II a decrease in the fracture energy is observed. Peak stress was shown to increase for both mode I and II. Minor effects of plasticity were expected in mode I while in mode II the dissipation through plasticity was not negligible, which can explain the different influence of strain rate in these modes. Aditionally, Carlberger et al. [35] and Avendaño et al. [21] both discussed that the dependence of fracture energy in mode I and maximum tension with stain rate can be considered linear in a semi-logarithmic scale.

May et al. [32], in 2014, concluded that the fracture energy in mode I is constant bellow a limit strain rate, increasing following linear relation in a semi-logarithmic scale until a second boundary strain rate is reached. After that limit, the fracture energy is once again constant. Fracture energy in mode II did not show a dependency of strain rate.

Viana et al. [38], in 2018, studied the mechanical behaviour of a crash resistant toughened epoxy with 1 mm thick mild steel plates adherends, and concluded that, for different temperatures, impact tested specimens were able to withstand higher loads and absorb

higher amounts of energy than the quasi-static tested specimens. An outcome corroborated by Machado et al. [22] in 2019.

Figure 11 shows the tendencies for energy release rate as a function of strain rate reported by Carlberger et al. [35] from DCB tests, Marzi et al. [36] from T-joint tests and May et al. [32] from TDCB tests.

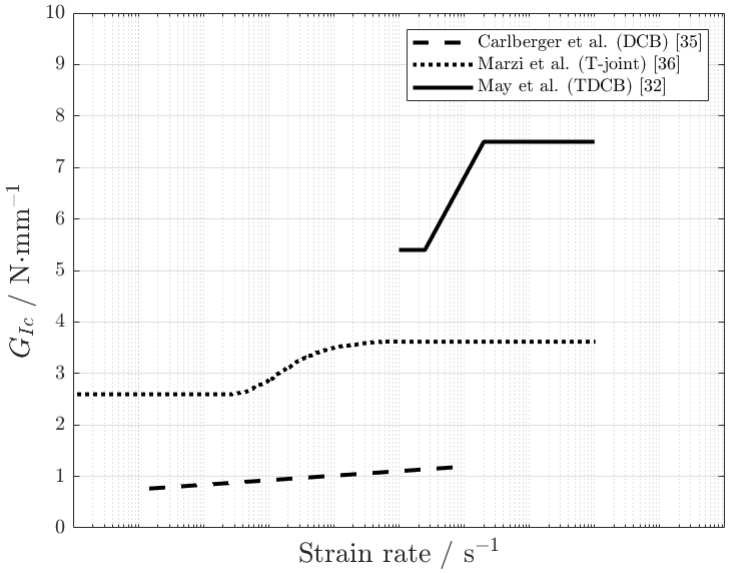

Figure 11: Energy release rate in mode I increasing as a function of strain rate. Adapted from [32, 35, 36].

2.4.3 Numerical simulation approaches

Although an universal trend has not been found, authors agree that the behaviour of adhesives is highly dependent on strain rate. Therefore, when analysing or creating a numerical simulation to model adhesive joints, this property variation should be accounted for. Different cohesive zone models (CZM) have been developed to consider this effect.

Rahulkumar et al. [39], in 2000, developed a computational model technique, using cohesive elements, to simulate fracture propagation in viscoelastic materials in mode I. For this purpose, a viscoelastic adhesive model was combined with a rate-independent CZM. The numerical results did not show a proper fit to experimental analysis.

Xu et al. [40, 41] in 2003, developed a model of a rate-independent CZM in parallel with a Maxwell element. A fracture behaviour consisting of three different regimes, the equivalent modulus becomes constant if the loading rate is higher or lower than a reference rate, and, at intermediate rates, the equivalent modulus varies with strain rate. The application of this model was then compared with experimental results revealing a proper adjustment.

Zhang et al. [42] in 2003, used a multi-scale approach to describe the non-linear zone, which is the combination of the plastic and damage region. It is considered that each

region has its own power law, the damage region is described in terms of ultimate strength, softening index and rate-sensitivity factor, and the plastic region as a function of strain hardening and rate. The rate-dependency in each regions is accounted for using a viscous coefficient. No experimental validation of the model was shown.

Giambanco et al. [43], in 2006, developed an interface model in the framework of viscoplasticity for generalized standard materials. This model intends to describe the mixed mode decohesion phenomena at the contact layer, considering its time-dependent effects. No experimental validation of the model was shown.

Marzi et al. [36] in 2009, developed a model, via an user defined subroutine, considering the rate-dependency of the CZM parameters traction and fracture energy, considering stiffness rate-independent. Rate-dependent simulations of mode I exhibited good agreement with the experimental analysis.

3 Experimental procedures

3.1 Materials

Two different adhesives manufactured by DOW Automotive (Michigan, USA) were used in this work, Betamate^{TM}120EU and Betamate^{TM}1480R. These are crash-resistant, one component adhesives used in the automotive industry - especially developed for the body shop - to increase durability in service, crash performance and body stiffness. The general properties of the adhesive can be seen in Table 1.

Table 1: General properties of the adhesives used.

Adhesive	Type of adhesive	Supplied as	Cure cicle
Betamate^{TM} 120EU	Epoxy resin	One-part	180 °C / 30 min
Betamate^{TM} 1480R	Epoxy resin	One-part	180 °C / 30 min

The mechanical properties given by the supplier for Betamate^{TM} 120EU and Betamate^{TM} 1480R can be seen in Table 2.

Table 2: Mechanical properties of the adhesives used, given by the supplier.

Property	Betamate^{TM} 120EU	Betamate^{TM} 1480R
Density/ g·mL^{-1}	1.26	1.22
Viscosity/ Pa·s	160	25
Tensile strength/ MPa	32	36
Elongation at break/ %	≈ 6	≈ 10
Young's modulus/ MPa	2100	1600

The substrates were machined from DIN 40CrMnMo7 steel, a high strength steel. The objective of using a high strength steel is avoiding plastic deformation. The general properties of the substrates can be seen in Table 3.

Table 3: Mechanical properties of the substrates used.

Young's modulus/ MPa	210000
Poisson's ratio	0.3

3.2 Testing methods

The main objective of the experimental part of this work is the definition of the strength and fracture properties of the adhesives for different loading rates, which allows the definition of expressions for the property variation with loading rate and, consequently, strain rate.

For that, strength and fracture envelopes were defined for three different test speeds: quasi-static, intermediate and impact.

For the strength characterization, bulk tensile tests and thick adherend shear tests (TAST) were preformed to determine tensile and shear properties, respectively. Those tests were preformed at 1 mm·min^{-1}, $6 \cdot 10^3$ nmm·min^{-1} or 100 mm·s^{-1} and $180 \cdot 10^3$ mm·min^{-1} or 3 m·s^{-1}.

For the fracture characterization double cantilever beam (DCB), end notched flexure (ENF) and mixed mode tests were preformed to determine fracture toughness in mode I, mode II and mixed mode, respectively.

For each condition at least three specimens were tested.

3.2.1 Strength tests

Bulk specimen tensile test

Bulk specimens are obtained from a cured sheet of adhesive to have a specific shape, based on the standard BS 2782 [44], shown in Figure 12.

These specimens are tested under tensile loads until failure. Load and displacement of the specimen are recorded and a stress-strain curve is created. This curve allows the determination of the Young's modulus, tensile strength and the assessment of the ductility.

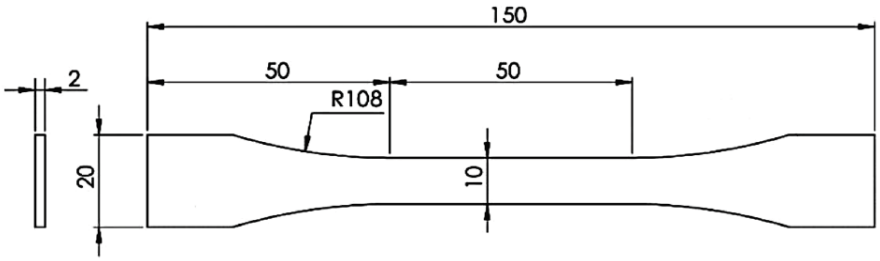

Figure 12: Representation of bulk specimen's geometry, in mm.

Thick adherend shear test (TAST)

TAST specimens are manufactured creating an adhesive joint, as shown in Figure 13, with hard steel adherends. A tension load is applied in the loading holes. Load and displacement are recorded. This procedure allows the determination of the shear strength and the assessment of ductility.

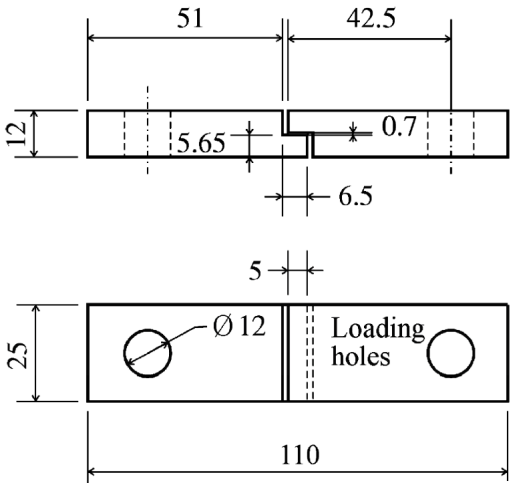

Figure 13: Representation of TAST specimen's geometry, in mm.

3.2.2 Mode I and mode II facture tests

Double cantilever beam (DCB)

DCB tests were performed to determine the fracture energy in mode I. The DCB specimen consists on two bonded beams with the same length and thickness, as represented in Figure 14.

It is important to notice that a_0, the length of an initial region without adhesive, is considered to be the pre-crack length, h is the thickness of each adherend and t the adhesive thickness.

A tension load is applied to the specimen as shown in Figure 14.

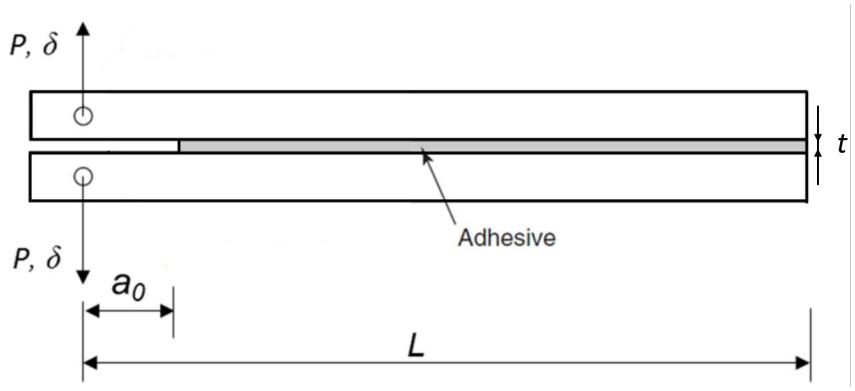

Figure 14: Schematic representation of DCB test.

The load and displacement are recorded during the test and, with an appropriate data reduction scheme, discussed in the Subsection 3.3, the critical energy release rate in mode I, G_{Ic}, can be determined.

End notched flexure (ENF)

ENF tests were performed to determine the fracture energy in mode II. The specimens used were the same as described for the DCB test.

A schematic representation of the ENF test can be observed in Figure 15.

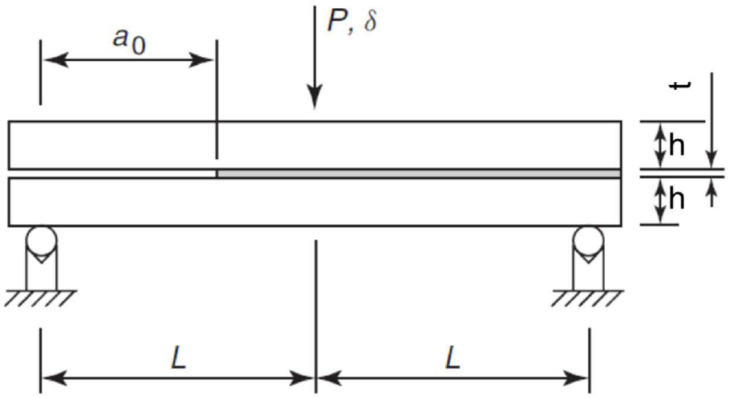

Figure 15: Schematic representation of ENF test.

where a_0 is the initial crack length, P the load applied, δ the displacement of the center of the ENF, h the height of each specimen, t the adhesive thickness and L the distance from each support to the vertical line where the load is applied. As in the DCB test, load and displacement are recorded and, with an appropriate data reduction scheme, shown in the Subsection 3.3, the critical energy release rate in mode II, G_{IIc}, may be determined.

3.2.3 Mixed mode fracture tests

There are several tests developed to characterize the behaviour of an adhesive in mixed mode. The method used in this work was developed by ADFEUP group [45], and the main objective of this test is to determine the mixed mode fracture toughness of the adhesive. A new apparatus, based on the previous one, was also developed to sustain impact loading. Both of them will be detailed bellow.

Existing apparatus for mixed mode testing

This apparatus can be configured for different phase angles between mode I and II, which allows more flexibility when comparing with other mixed mode testing methods, that only allow a strict range of mode mixities. The configuration of the phase angles can be done adjusting the beam lengths (s_1, s_2, s_3 and s_4), represented in Figure 16. This apparatus allows a wide variety of phase angles between 0° and 90°. The angle, as a function of the upper beam load, F_1 and the lower beam load, F_2 is given by [46]:

$$\varphi = tan^{-1} \frac{\sqrt{3}\left(\frac{F_1}{F_2}+1\right)}{2\left(\frac{F_1}{F_2}-1\right)} \tag{6}$$

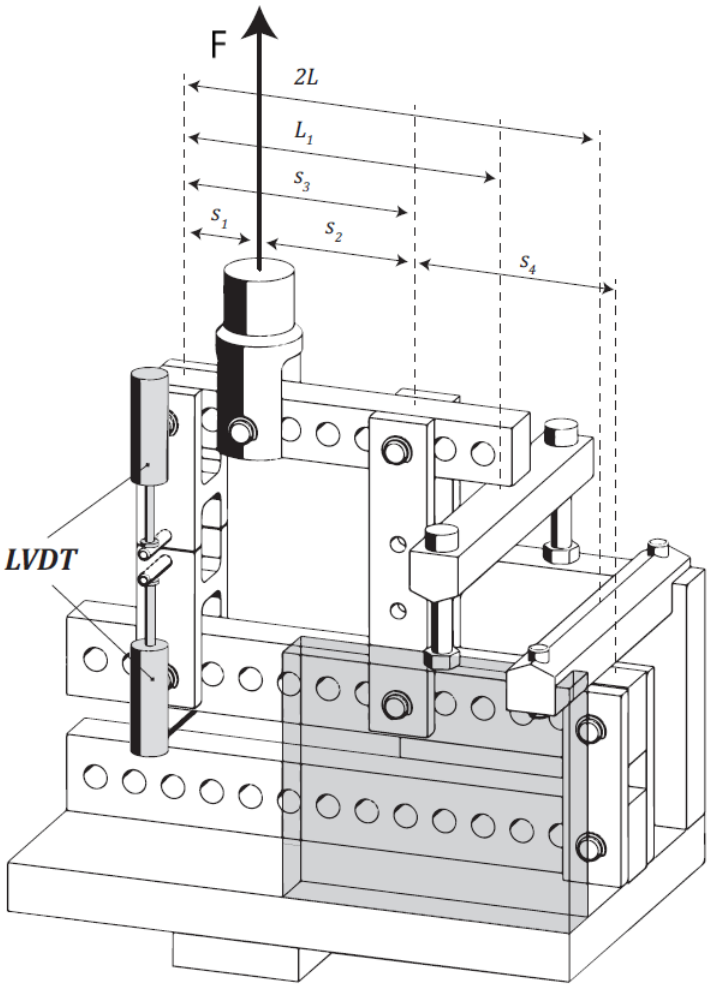

Figure 16: Schematic representation of the existing apparatus for mixed mode testing [46].

The load applied is a combination of mode I and II, as shown in Figure 17, and can be decomposed in F_1 and F_2 by:

$$F_1 = F\frac{s_2}{s_3}; \qquad F_2 = F\frac{s_1 s_4}{s_3(s_3+s_4)} \tag{7}$$

Mode I and II load components, P_I and P_{II} are then determined by:

$$P_I = \frac{F_1 - F_2}{2}; \qquad P_{II} = F_1 + F_2 \tag{8}$$

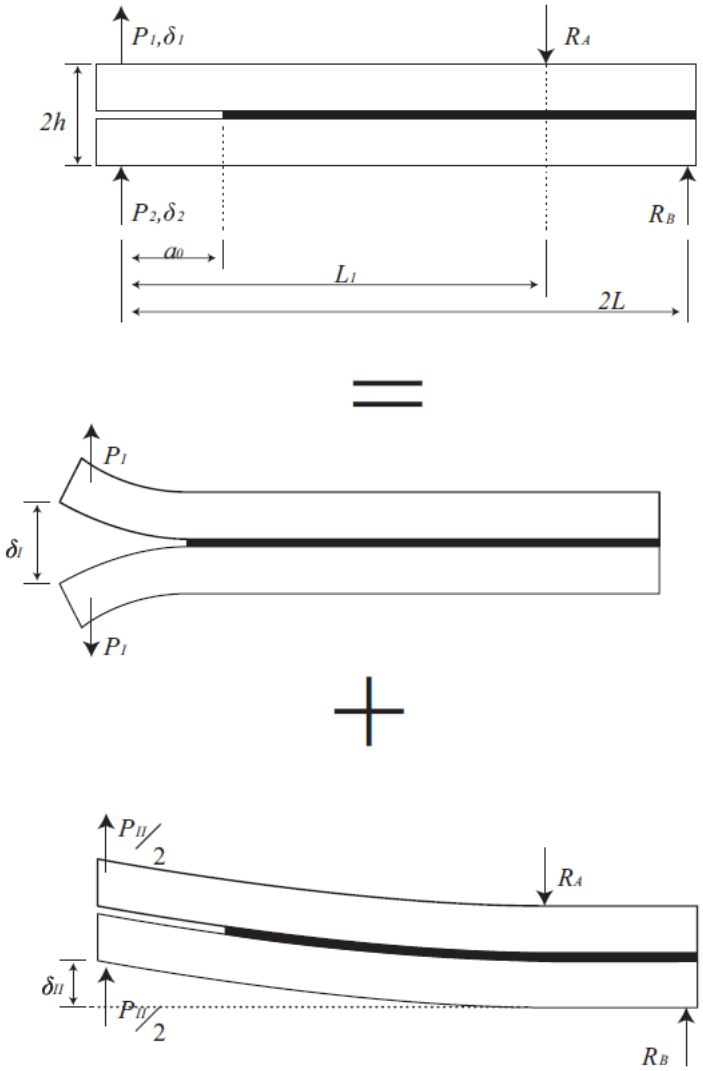

Figure 17: Schematic representation of the mixed mode test [46].

The specimens used to perform tests are the ones described for the DCB and ENF tests, also simplifying the manufacture process when compared with other testing methods for mixed mode.

The existing apparatus for mixed mode testing was not designed with impact loads in consideration, therefore, a new apparatus was developed.

New apparatus for mixed mode testing

The design of the new apparatus was adjusted to ensure that tests can be performed at enough mode mixities to represent the complete fracture envelope of the adhesive, reducing as much as possible the number of holes and load concentration zones for a more robust configuration. With that in mind, the angles of $\varphi = 0°$, $22.5°$, $45°$, $72.5°$ and $90°$ were chosen.

Mode details about the apparatus and its validation are presented in Section 3.4.

3.3 Data reduction scheme

A data reduction scheme must be used to obtain the energy release rate in mode I and mode II, thus determining mode-mixity and the total fracture energy [47]. The classical methods - Compliance Calibration Method (CCM) [48, 49] and Corrected Beam Theory (CBT) [49–53] - rely on the determination of the exact crack length, which can be a difficult task, specially when analyzing mode II and mixed mode and when a sudden fracture occurs [45, 48, 49]. Additionally, a fracture process zone (FPZ), seen in Figure 18, develops ahead of the major crack tip caused by plasticization and the nucleation of multiple micro-cracks. With increasing ductility, the energy dissipated in the FPZ also increases and must be considered in the data reduction scheme [47].

The method used was the compliance-based beam method (CBBM) that exclusively depends on the specimen's compliance during the test and is based on the concept of equivalent crack length, taking into account the phenomena previously described [47, 54].

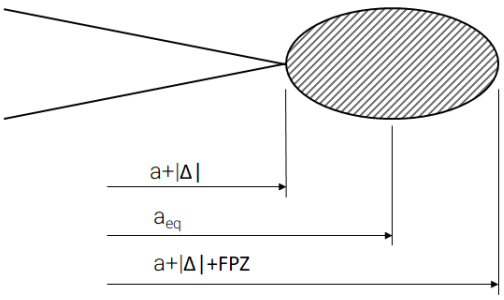

Figure 18: Schematic representation of equivalent crack length and the FPZ concept. Adapted from [47].

Considering this method, in mode I, the fracture energy is given by [47]:

$$G_I = \frac{6P^2}{B^2 h}\left(\frac{2a_{eq}^2}{h^2 E_f} + \frac{1}{5G_{13}}\right) \tag{9}$$

where P is the load, B is the specimen width, h is the height of each specimen, G_{13} is the substrates' shear modulus, a_{eq} is the length of the crack equivalent, given by the solution of the following equation, derived from Timoshenko's beam theory [47]:

$$C = \frac{\delta}{P} = \frac{8a_{eq}^3}{Bh^3 E_f} + \frac{12a_{eq}}{5G_{13}Bh} \tag{10}$$

and E_f is the corrected flexural modulus, used because this method does not take into consideration stress concentration and substrates' rotation near the crack tip [47]:

$$E_f = \left(C_0 - \frac{12(a_0 + |\Delta|)}{5BhG_{13}}\right)^{-1} \frac{8(a_0 + |\Delta|)^3}{Bh^3} \tag{11}$$

where the index 0 refers to initial values - being a_0 que initial crack length and C_0 the initial compliance - and Δ is a correction factor for the crack length given by [55]:

$$\Delta = h\sqrt{\frac{E}{11G_{13}}\left(3-2\left(\frac{\Gamma}{1+\Gamma}\right)^2\right)} \tag{12}$$

where

$$\Gamma = \frac{1.18E}{G_{13}} \tag{13}$$

where E is the substrates Young's modulus.

The crack length correction can be determined using a linear regression, obtained experimentally, after loading the specimen at three different load levels, which can be schematically observed in Figure 19.

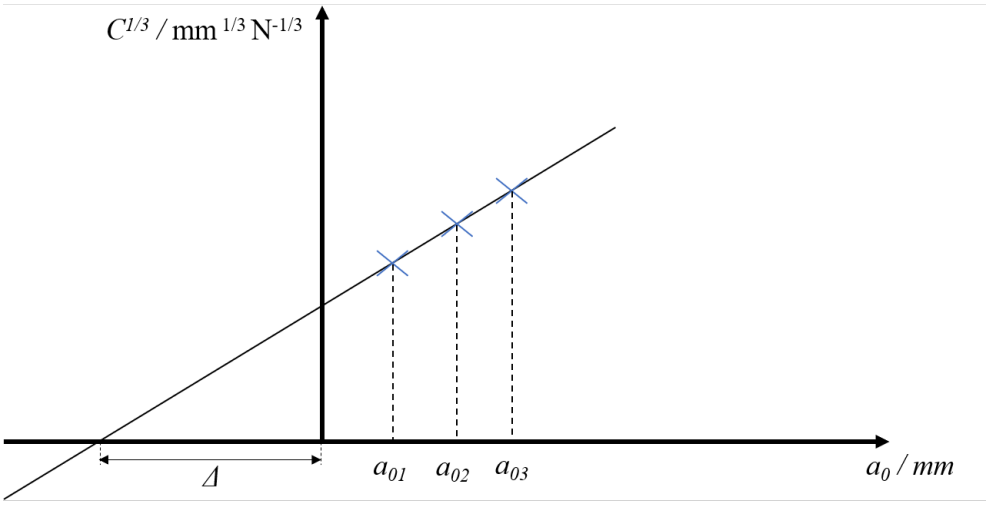

Figure 19: Method for crack length correction,Δ. Adapted from [9].

Mode II fracture energy can be determined by [56]:

$$G_{IIc} = \frac{9P^2a_{eq}^2}{16B^2Eh^3} \tag{14}$$

where

$$a_{eq} = \left(\frac{a_0^3C_c}{C_{0c}} + \left[\frac{C_c}{C_{0c}} - 1\right]\frac{2L^3}{3}\right)^{1/3} \tag{15}$$

where

$$C_c = C - \frac{3L}{10BhG_{13}} \tag{16}$$

and

$$E = \frac{3a_0^3 + 2L^3}{8Bh^3C_{0c}} \tag{17}$$

where L is half of the specimen total length, considering the ENF test. The index c refers to the correct value of the variable.

Analysing mixed mode, knowing δ_1 and δ_2 - which are represented in Figure 17-, separated G_I and G_{II} curves can be obtained. Mixed mode phase angle is then estimated by:

$$\varphi = \tan^{-1}\sqrt{\frac{G_{II}}{G_I}} \tag{18}$$

3.4 New apparatus for mixed mode testing

The main working principle, in terms of load decomposition and phase angle calculation, is the same used for the previous apparatus and the specimens used are also the ones described for DCB tests, to simplify the manufacture process.

The Solidworks ® model and photograph of the new apparatus can be seen in Figures 20 and 21, respectively. The Solidworks ® model represents how the apparatus is used on the drop-weight machine, where the arrow represents the impactor.

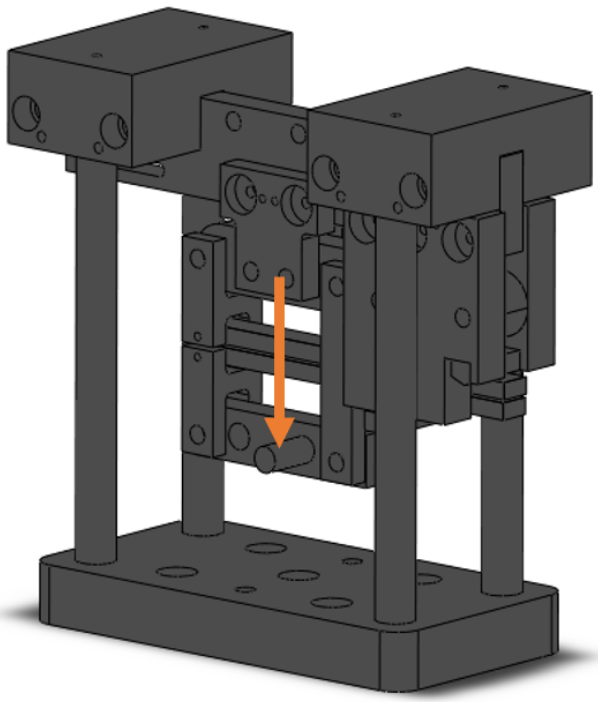

Figure 20: Schematic representation of the new apparatus for mixed mode testing, configured for impact tests.

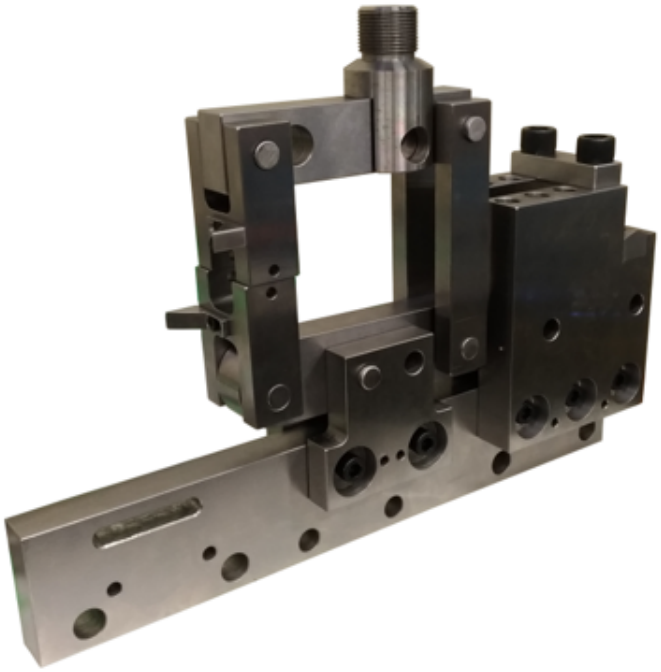

Figure 21: New apparatus for mixed mode testing.

This new apparatus, as said, is capable of performing tests at different mode mixities: $\varphi = 0°$, 22.5°, 45°, 72.5° and 90°. For that, the lengths s_1, s_2, s_3 and s_4, Figure 22, should be adjusted adequately, placing a pin in the upper and lower beam in the corresponding position, Figure 23.

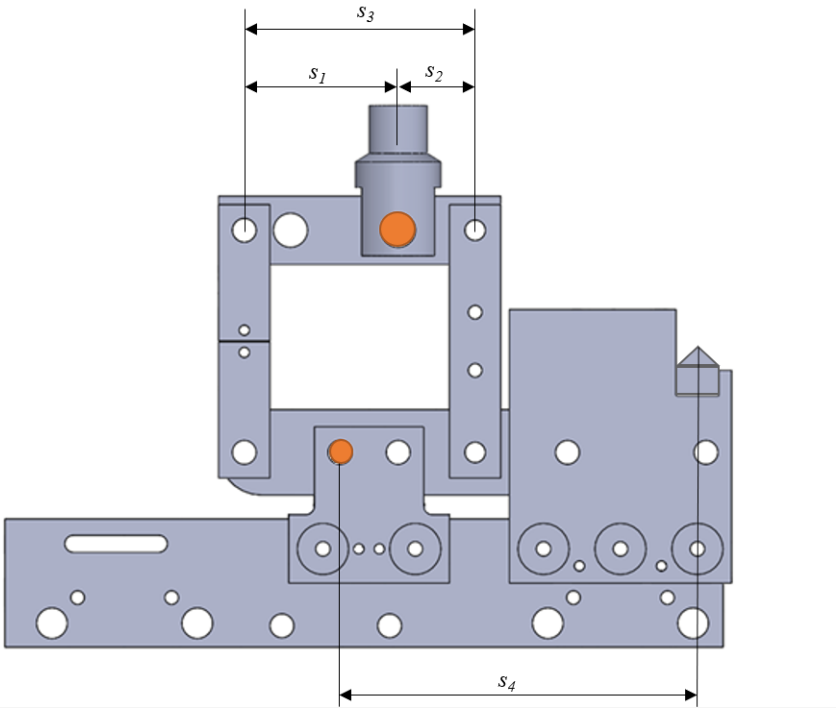

Figure 22: Schematic representation of the lengths that should be changed to adjust mode mixity.

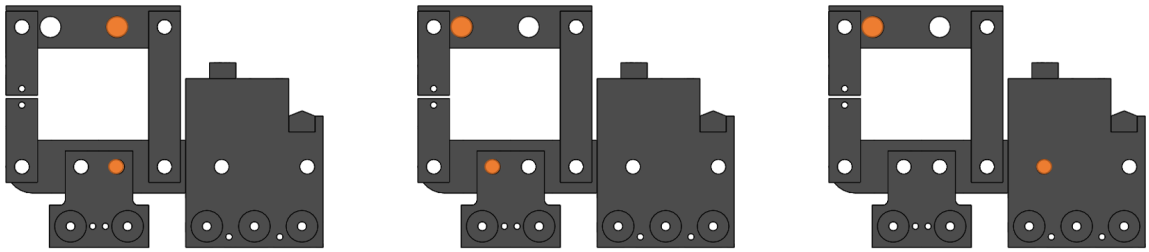

(a) 0° (b) 22.5° (c) 45°

(d) 72.5° (e) 90°

Figure 23: Positions where the pins should be placed to perform tests in each mode mixity.

Apparatus validation

The apparatus developed was used to perform tests at high speeds, however, a validation procedure was carried out before the testing began.

The validation of the apparatus was done for pure mode I and mixed mode I+II, at 45°. For comparison, the quasi-static fracture envelopes of both adhesives tested, represented in **Paper B**, were used. Those fracture envelopes were determined at 0.2 mm·min^{-1}, using standard DCB and ENF tests for mode I and II, respectively, and the existing apparatus for mixed mode testing for 45°.

The load was recorded by the universal testing machine used, an INSTRON® 3367 with a load cell of 30 kN. The displacement of the extremity of each substrate was measured using LVDTs. The data was then treated using the compliance based beam method, explained in detail in Section 3.3.

The fracture envelopes determined for quasi-static conditions, with the previous apparatus, and the points obtained using this new apparatus can be seen in Figures 24 and 25 for Betamate™ 120EU and Betamate™ 1480R, respectively.

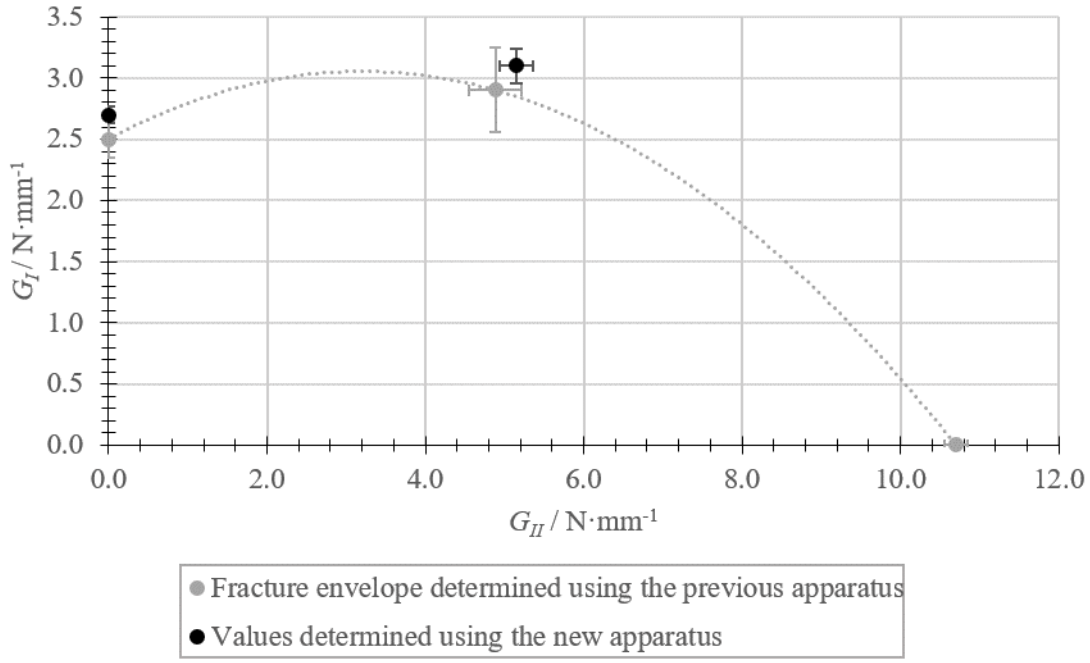

Figure 24: Comparison between the fracture envelope previously determined and the results obtained with the new apparatus, Betamate^{TM} 120EU.

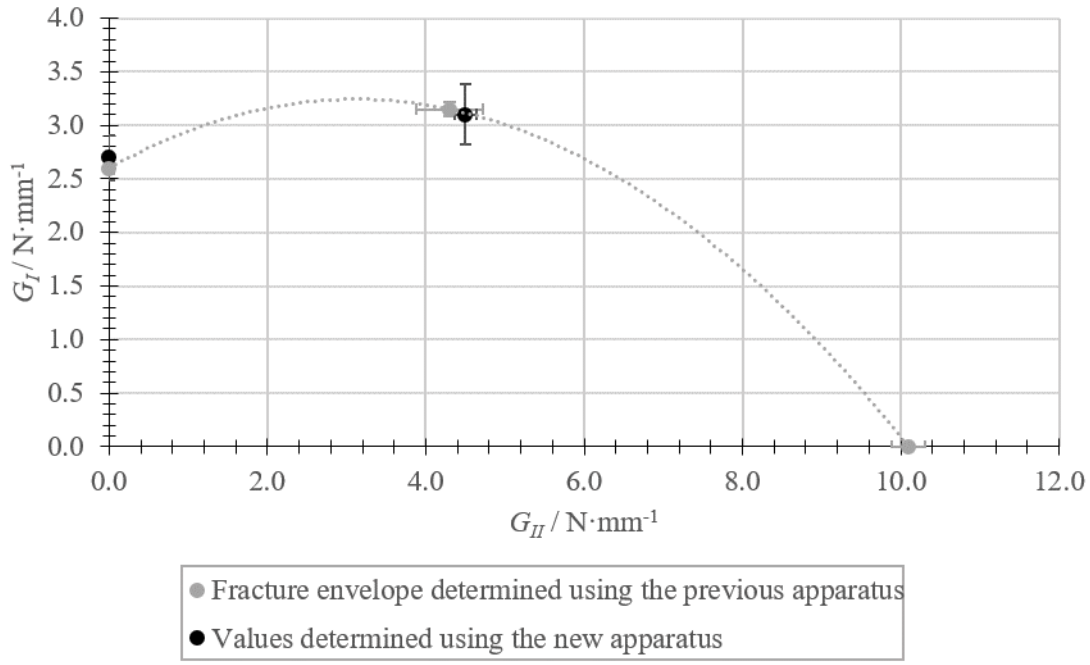

Figure 25: Comparison between the fracture envelope previously determined and the results obtained with the new apparatus, Betamate^{TM} 1480R.

The results obtained are also represented, for both adhesives, in Table 4.

Table 4: Comparison between the fracture envelope determined using conventional tests and the new apparatus for mixed mode testing.

Adhesive			Betamate™ 120EU	Betamate™ 1480R
Mode I	G_I / N·mm^{-1}	Fracture envelope	2.5 ± 0.15	2.6 ± 0.05
		New apparatus	2.7 ± 0.07	2.7 ± 0.21
		Error/%	8.0	3.8
Mode I+II	G_I / N ·mm^{-1}	Fracture envelope	2.9 ± 0.35	3.2 ± 0.07
		New apparatus	3.1 ± 0.14	3.1 ± 0.28
		Error/%	6.9	3.1
	G_{II} / N·mm^{-1}	Fracture envelope	4.9 ± 0.33	4.3 ± 0.42
		New apparatus	5.2 ± 0.21	4.5 ± 0.14
		Error/%	6.1	4.7

4 Numerical details

Adhesives exhibit a highly strain rate dependent behaviour, thus, when modelling adhesive joints for different loading rates, the variation of the adhesive's properties with strain rate for each element should be considered. Therefore, an Abaqus® user defined subroutine was created to define the behaviour of the adhesive.

The subroutine adopted was UMAT, which defines the Jacobian matrix, for the mechanical constitutive model, updating stress. A scheme of the integration of UMAT for each increment can be seen in Figure 26. UMAT is a subroutine compatible with standard and dynamic implicit models in Abaqus®.

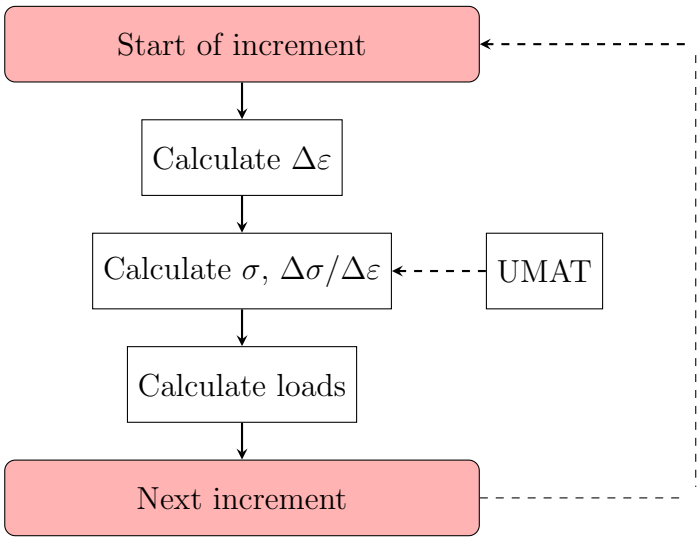

Figure 26: Scheme representing the integration of UMAT in Abaqus®.

It should be noted that the code developed can be implemented in both two and three-dimensional models.

Figure 27 encloses a flowchart that clarifies the code implemented in the user defined material - UMAT. The input mechanical properties of the adhesive in the program are:

- Young's modulus, E;
- Shear modulus, G_s;
- Expression that characterizes tensile strength, σ_{max}, as a function of strain rate;
- Expression that characterizes shear strength, τ_{max}, as a function of strain rate;
- Expressions that characterize energy release rate in peel mode - mode I - and shear modes - mode II and III - as a function of strain rate.

Abaqus® also provides, for each time increment, the strain increment and duration of the time increment, which are used to calculate the strain rate for each element and each

time increment. With the strain rate, the energy release rate rate in mode I, II and III are determined, based on the inputted expressions.

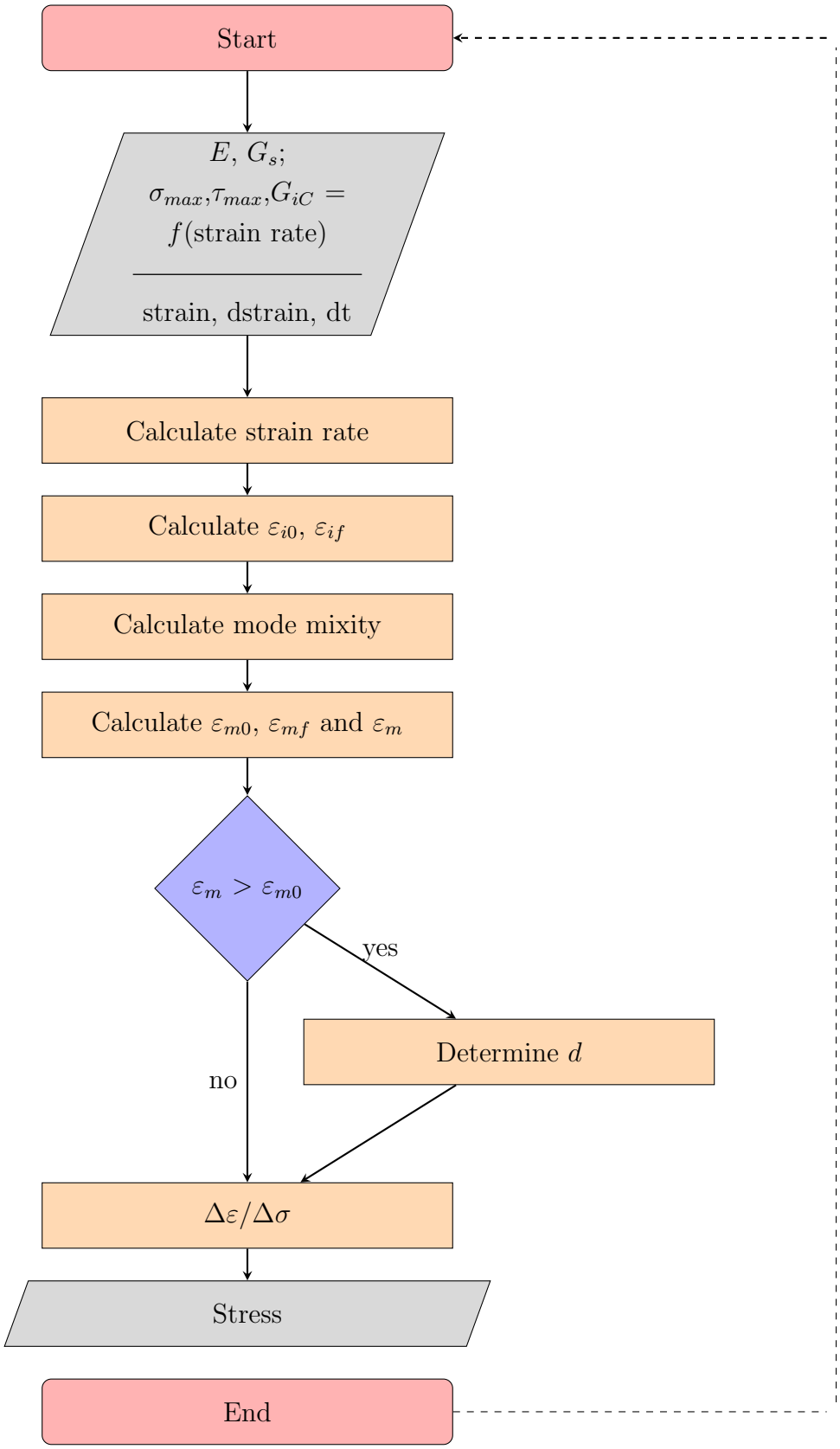

Figure 27: Scheme representing the code developed in UMAT.

The maximum stress in mode I, $\sigma_{I,max}$, is the tensile strength σ_{max} and maximum stress in mode II, $\sigma_{II,max}$, and III, $\sigma_{III,max}$, is the tensile strength τ_{max}.

With the properties of the adhesive for peel and shear modes, the strain when maximum stress is reached, ε_{i0}, and maximum strain, ε_{if}, are calculated. The schematic representation of the triangular law used can be observed in Figure 28, where I refers to loadings in mode I, II in mode II and III in mode III. For this calculation, the stiffnes, k, is considered to be the adhesive's Young's modulus and shear modulus, respectively for peel and shear modes, and the area below the curve is G_{iC}.

The current strain ε_i, in the direction of modes I, II and III, respectively, is also given by Abaqus®. Afterwards, with the current strains, mode mixity is determined. For that mode mixity, a triangular law is established, based on the laws for the pure modes combined, as it can be seen in Figure 29, with this, strain when maximum tension is reached, ε_{m0}, maximum strain, ε_{mf}, and current strain, ε_m, are determined for the mode under analysis.

It is considered that, when the strain in one element reaches ε_{m0}, damage initiates, and as strain progresses from ε_{m0} to ε_{mf} a damage coefficient, d, progresses linearly from 0 to 1 reaching 1 when the strain reaches ε_{mf}.

When ε_m is less than ε_{m0}, the Jacobian matrix is calculated, and stress is determined. When ε_m is higher than ε_{m0}, damage is calculated and then stress is determined. The degradation of the properties when damage occurs can be seen in Figure 30.

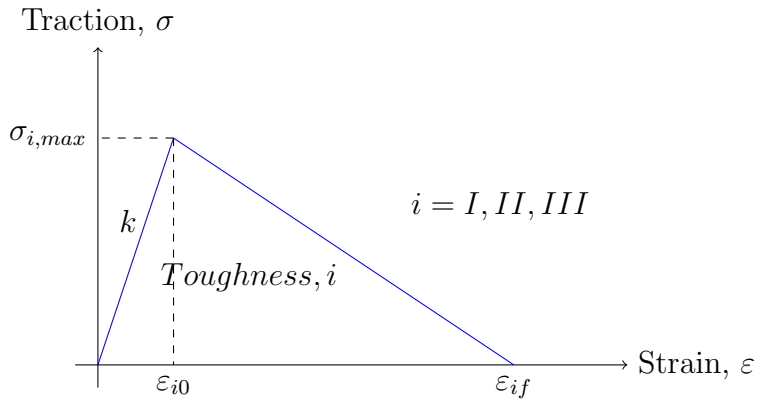

Figure 28: Triangular law used in UMAT, for each pure mode.

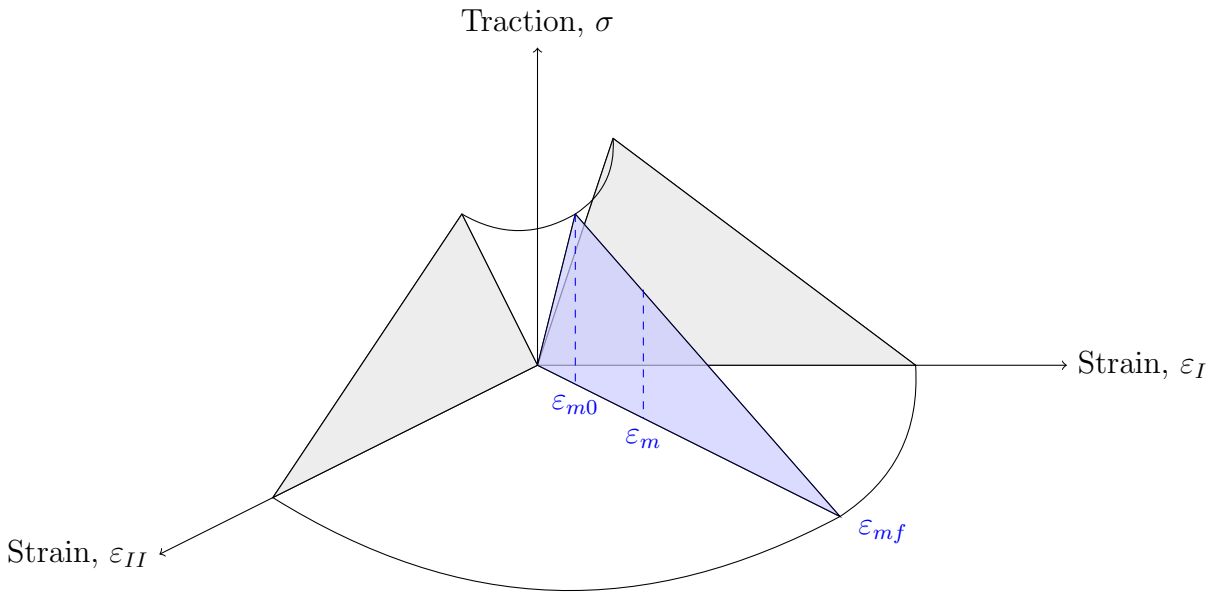

Figure 29: Combination of the pure modes in mixed mode.

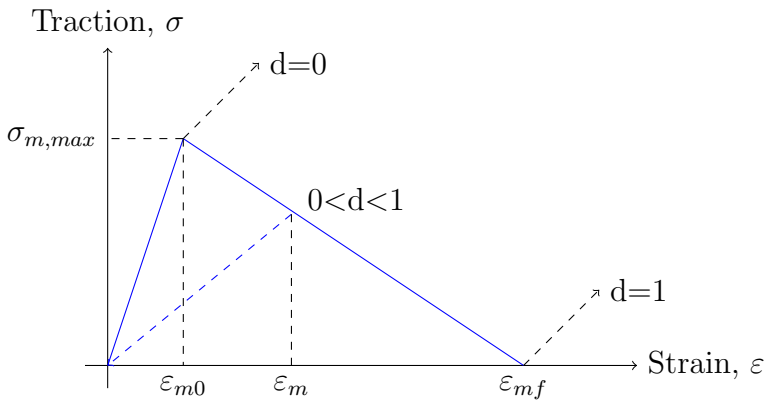

Figure 30: Triangular law used in UMAT, mixed mode, with degradation due to damage.

4.1 Mode I - DCB model

Double cantilever beam specimens were tested experimentally at 0.2 mm·min^{-1}, $6 \cdot 10^3$ mm·min^{-1} and $180 \cdot 10^3$ mm·min^{-1}.

Two models were created to simulate the conditions described, one for tests performed in universal testing machines, at 0.2 mm·min^{-1} and $6 \cdot 10^3$ mm·min^{-1}, and other for impact tests at $180 \cdot 10^3$ mm·min^{-1}. Based on those numerical models, strain rate in mode I determined by Abaqus® along each specimen and critical energy release rate in mode I were determined. Thus defining critical energy release rate in mode I as a function of strain rate. The results were then compared with the experimental results obtained. This process is described in further detail in **Paper A**.

4.2 Mode II - ENF model

End notched flexure specimens were tested experimentally for 0.2 mm·min^{-1} and $6 \cdot 10^3$ mm·min^{-1}, because for higher strain rates plastic deformation of the substrates was observed. The experimental results and the procedures and machines used in the tests are presented in **Paper B**. The shear modulus G_s was adjusted to fit the experimental results.

The numerical model created was two dimensional, used solid elements for the substrates and cohesive elements for the adhesive. The substrates properties are presented in Section 3 and the adhesive was connected to the UMAT developed.

In the substrates the mesh was squared, with a side length of 1 mm . In the adhesive the mesh was formed using rectangles with 1 mm by 0.2 mm, which is the thickness of the adhesive.

Quasi-static and intermediate speed

Contact between the rolls, represented by half a circumference, and the specimen was imposed, and the boundary conditions applied were encastres in the bottom supports and a downward displacement in the upper roll, Figure 31.

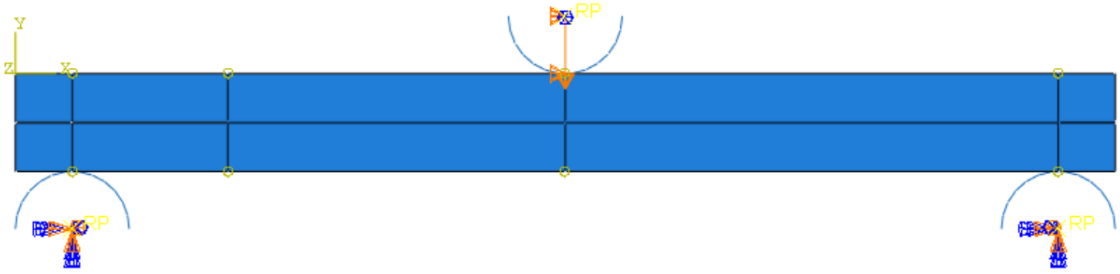

Figure 31: Boundary conditions for the ENF test simulation for quasi-static and intermediate speed.

The loading rate was controlled by the displacement imposed and the total time of the test. For each condition, the maximum displacement and testing time can be seen in Table 5.

Table 5: Displacement and duration inputted for the each end notched tests simulated.

Loading rate / mm·min^{-1}	Displacement / mm	Duration of the test / s
0.2	20	$6 \cdot 10^3$
$6 \cdot 10^3$	20	0.2

Impact speed

This model is similar to the one described previously, but the upper roll is a circle, and its density was adjusted to match the mass of the impactor of the drop-weight machine. A velocity field of $180 \cdot 10^3$ mm·min^{-1} was applied to the circle.

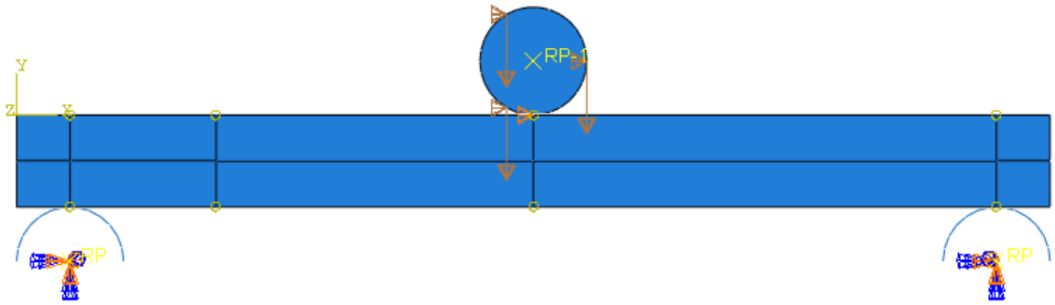

Figure 32: Boundary conditions for the ENF test simulation for impact conditions.

Numerical results

The load displacement curves obtained with the previous models were then analysed using CBBM. The r-curves obtained were similar to the one shown in Figure 33, comparing with a representative experimental curve, which is for Betamate^{TM}120EU at 0.2 mm·min^{-1}.

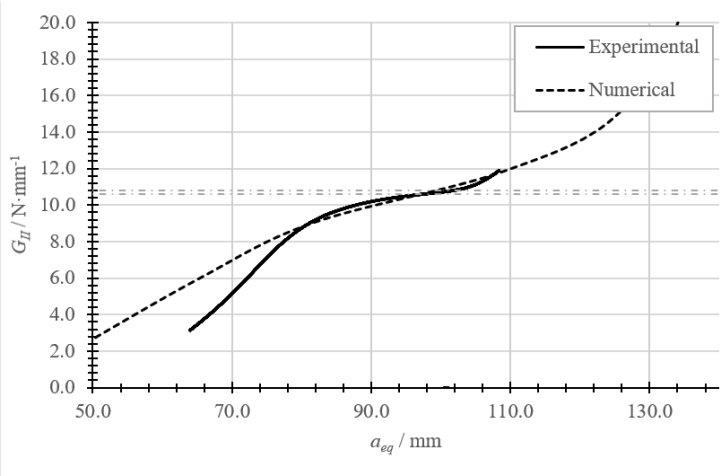

Figure 33: Representative curve for the experimental results for ENF tests, compared with a numerical curve.

The numerical R-curve does not exhibit a clear plateau, therefore, the energy release rate in mode II was considered in the inflection, where a evidence of the plateau is found. The results for energy release rate in mode II, compared with the experimental results obtained can be seen in Figure 34 and Table 6.

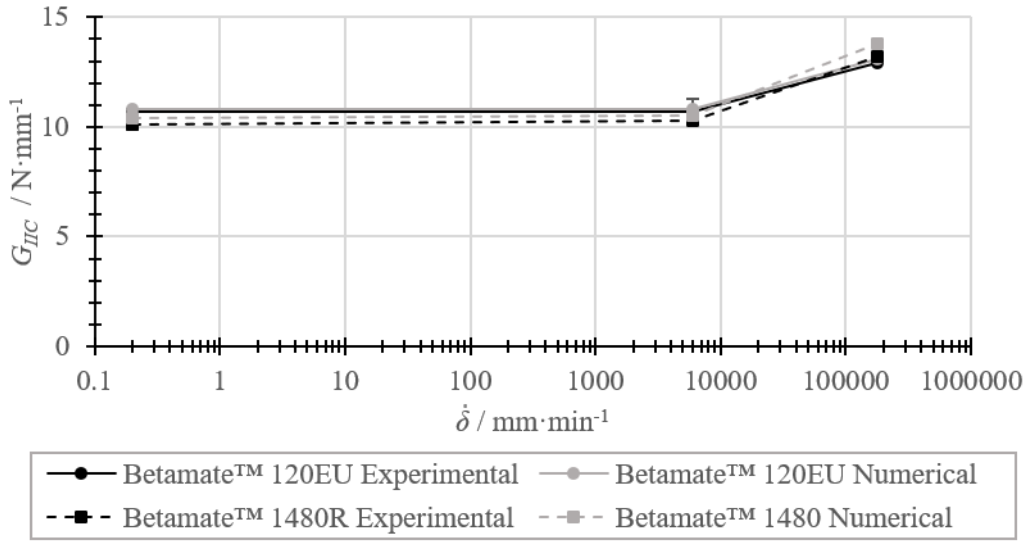

Figure 34: Comparison between experimental and numerical energy release rate, G_{IIC}, for the three different loading rates, $\dot{\delta}$, tested.

Table 6: Experimental and numerical energy release rate, G_{IIC}, for the three different loading rates, $\dot{\delta}$, tested.

Adhesive	$\dot{\delta}$ / mm·min^{-1}	Experimental G_{IIC} / N·mm^{-1}	Numerical G_{IIC} / N·mm^{-1}	Error /%
Betamate^{TM}120EU	0.2	10.7 ± 0.1	10.8	0.9
	$6 \cdot 10^3$	10.7 ± 0.6	10.8	0.9
	$180 \cdot 10^3$	12.9	13.1	1.5
Betamate^{TM}1480R	0.2	10.1 ± 0.2	10.4	3.0
	$6 \cdot 10^3$	10.3 ± 0.1	10.5	1.9
	$180 \cdot 10^3$	13.2	13.8	4.5

Strain rate determination

To implement the functions describing energy release rate in mode II as a function of the strain rate in mode II defined by Abaqus ® this strain rate should be known for each time increment and along the specimen, which is possible as it is one of the output variables of the UMAT subroutine developed. Damage for each time increment and each element is also an output variable, d, which changes from $d = 0$, when no damage can be found on the element, to $d = 1$, when the element fails. With those two variables, the strain rate when each element along the bondline fails can be determined.

The strain rate at the time of element failure was plotted as a function of the distance from the crack tip, and trends for that evolution were defined. The trends obtained for the strain rate for each test speed are represented in Figure 35 and all loading rates are compared in Figure 36, considering a pre-crack of 45 mm and the Betamate120EU adhesive.

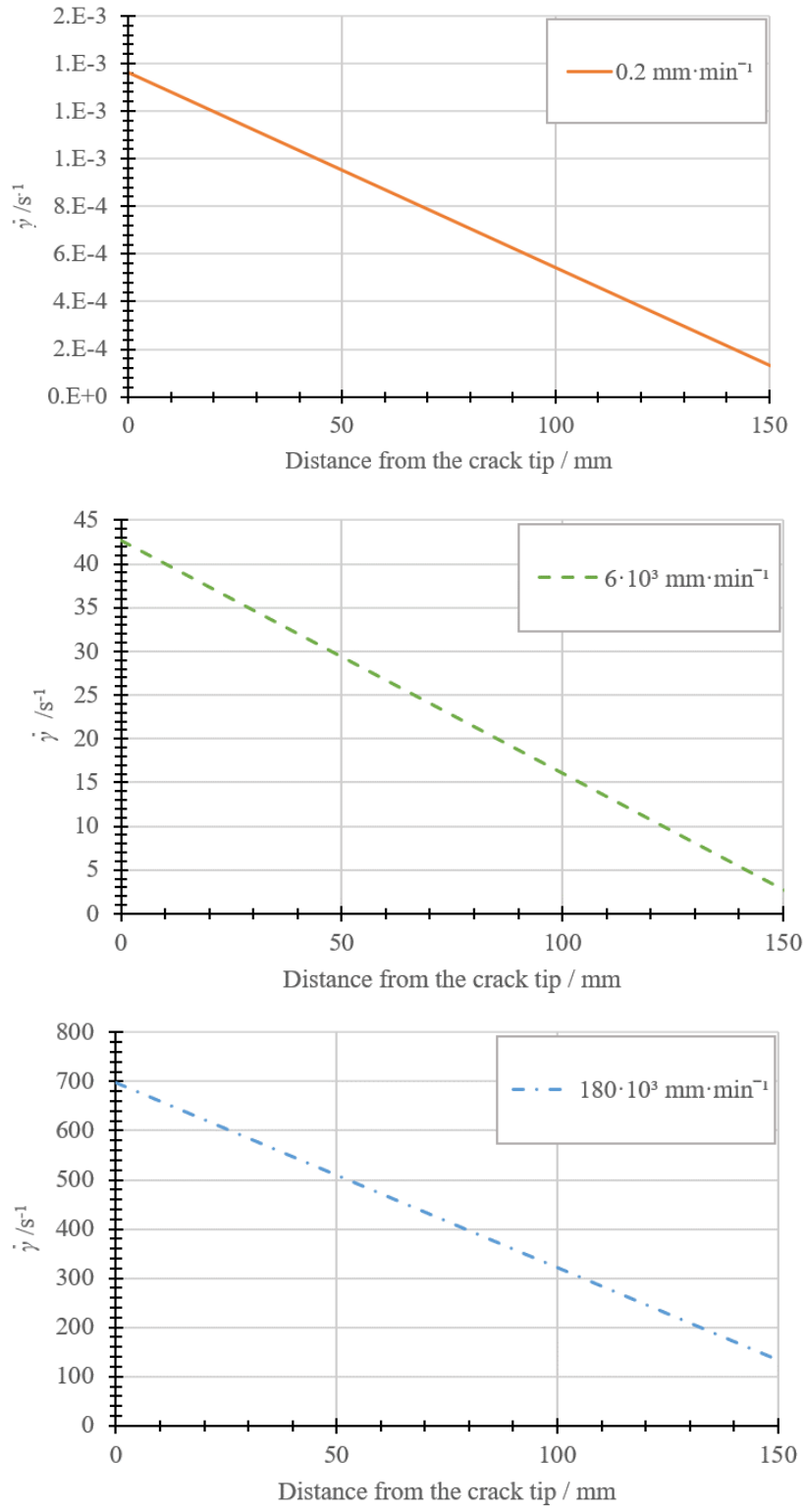

Figure 35: Strain rate for each loading rates tested, with a pre-crack length of 45 mm.

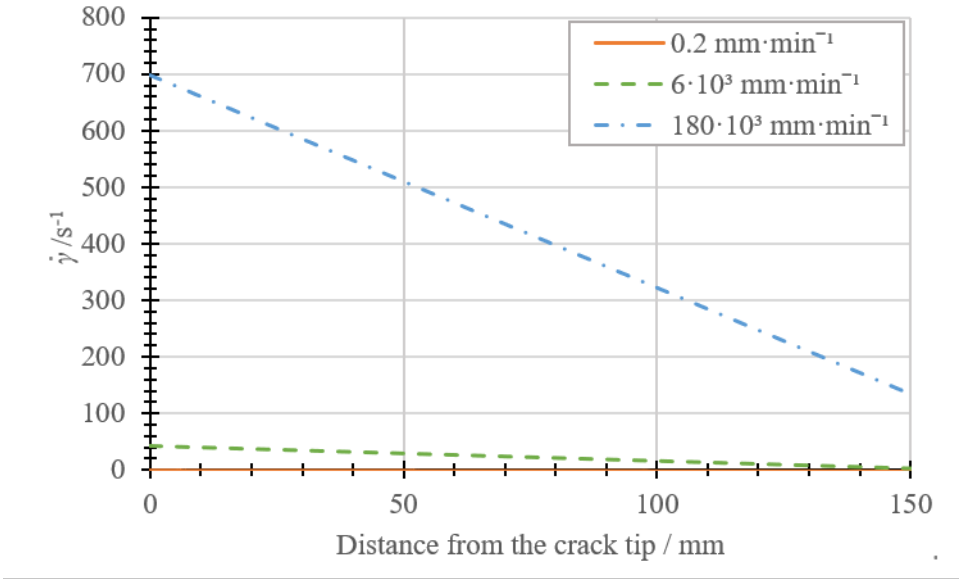

Figure 36: Strain rate for all loading rates tested, with a pre-crack length of 45 mm.

5 Summary of appended papers

Paper A	This paper explores the development of a finite element which takes into account the strain rate dependent behaviour of two structural adhesives, in mode I. Tensile strength and energy release rate in mode I are defined as a logarithmic function of the strain rate, determined experimentally. For this, two adhesives were tested under three different conditions: quasi-static, intermediate speed and impact. The strength was determined using bulk tensile tests and toughness using double cantilever beam (DCB) specimens. Both adhesives studied have shown an increase in ultimate stress and critical energy release rate with increasing strain rate. The functions were then implemented on a finite element, which was found to be good agreement with the experimental results.
Paper B	The main aim of this paper is the definition of the strength and fracture envelopes of two epoxy based crash-resistant adhesives at quasi-static conditions, an intermediate speed and impact conditions. Mode I and tensile properties had already been determined in **Paper A**. Therefore, for the characterization of the strength envelope, thick adherend shear tests (TAST) were performed. For the characterization of the fracture envelopes, mode II fracture toughness was studied using energy release rate (ENF) tests, and mixed mode was studied with two in-house developed apparatus, one for quasi-static conditions and a more robust one for intermediate speed and impact. Strength was found to increase for tensile and shear loading with increasing strain rate. An increase was also recorded for the energy release rate at all mode-mixities studied, function of the loading rate and following a logarithmic trend.

6 Conclusions

The strength and fracture envelopes of two epoxy adhesives were established for three different loading rates.

The strength envelopes were defined using bulk tensile tests and thick adherend shear tests. All tests were performed for both adhesives under quasi-static conditions, 1 mm·min^{-1}, at an intermediate speed, $6 \cdot 10^3$ mm·min^{-1}, and impact $180 \cdot 10^3$ mm·min^{-1}.

The fracture envelopes were defined using the energy release rate in mode I, mode II and mixed mode (I+II). All fracture tests were performed at quasi-static rate 0.2 mm·min^{-1}, intermediate speed, $6 \cdot 10^3$ mm·min^{-1}, and impact $180 \cdot 10^3$ mm·min^{-1}. Critical energy release rate in mode I was defined using double cantilever beam (DCB) tests, in mode II using end notched flexure (ENF) tests and in mixed mode using two in-house developed apparatus. For quasi-static conditions, an existing apparatus was used. However, this apparatus was not designed to sustain high loading rates and, for that purpose, a new apparatus was developed. This apparatus was validated for mode I and mixed mode using the quasi-static fracture envelopes obtained with DCB, ENF and with the first apparatus for both adhesives.

A numerical model that takes into account the variation of properties with strain rate was also developed and used for mode I, DCB tests, and mode II, ENF tests. Based on this model, strain rate along the specimen during the test was determined and, consequently, the strain rate at which each element fails along the test established. Experimental tests were also reproduced using this model.

The main conclusions drawn from this work are:

- Strength and fracture behaviour of adhesives show a strain rate dependency, corresponding to what is expected from viscoelastic materials.

- Tensile and shear strength increase with increasing loading rate and can be approximated by linear behaviour in a logarithmic scale.

- Fracture envelopes are defined by a quadratic curve, and its shape is similar for all loading rates.

- Energy release rate, for all mode mixities studies revealed an increase with increasing loading rate. The evolution of energy release rate can also be defined using logarithmic relations.

- The user defined material, UMAT, was updated with the relationship established for the variation of properties with strain rate and showed good agreement with the experimental results.

7 Future work

In the future, it would be interesting to determine energy release rate for more test speeds and more mode mixities to solidify the developed relations, both regarding energy release rate as a function of strain rate and the fracture envelopes.

Regarding the numerical simulation, it would be interesting to adapt the code from UMAT, used with standard and dynamic implicit models, to VUMAT, used with dynamic explicit models. This would allow the use of the adhesives properties as a function of strain rate for a wider variety of models.

Since the model was developed considering mode I, II and III and is compatible with both two dimensional and three dimensional models, it would be worthy to create an experiment with more complex loadings combining different modes and different strain rates, and compare the results with numerical simulations.

Additionally, and because these adhesives exhibit a viscoelastic behaviour, it would be interesting to repeat this study for different temperatures and establish a general law for the behaviour of the adhesives. The numerical model could also be updated with this condition.

References

[1] Lucas FM Da Silva, Andreas Öchsner, and Robert D Adams. *Handbook of adhesion technology*. Springer Science & Business Media, 2011.

[2] WA Lees. Adhesive selection. In *Adhesives in Engineering Design*, pages 92–123. Springer, 1984.

[3] E.Petrie. *Handbook of adhesives and sealants.* McGraw-Hill Education, 2007, 2007.

[4] Robert D Adams, Robert D Adams, John Comyn, William Charles Wake, and WC Wake. *Structural adhesive joints in engineering*. Springer Science & Business Media, 1997.

[5] Robert D Adams. *Adhesive bonding: science, technology and applications*. Elsevier, 2005.

[6] Sina Ebnesajjad and Arthur H Landrock. *Adhesives technology handbook*. William Andrew, 2014.

[7] Anthony J Kinloch. *Adhesion and adhesives: science and technology*. Springer Science & Business Media, 2012.

[8] MD Banea and Lucas FM da Silva. Adhesively bonded joints in composite materials: an overview. *Proceedings of the Institution of Mechanical Engineers, Part L: Journal of Materials: Design and Applications*, 223(1):1–18, 2009.

[9] Filipe JP Chaves, LFM Da Silva, MFSF De Moura, DA Dillard, and VHC Esteves. Fracture mechanics tests in adhesively bonded joints: a literature review. *The Journal of Adhesion*, 90(12):955–992, 2014.

[10] David Broek. *Elementary engineering fracture mechanics*. Springer Science & Business Media, 2012.

[11] HP Tardif and H Marquis. Some dynamic properties of plastics. *Canadian Aeronautics and Space Journal*, 9:205–213, 1963.

[12] US Lindholm. Some experiments with the split hopkinson pressure bar. *Journal of the Mechanics and Physics of Solids*, 12(5):317–335, 1964.

[13] PD Chalkley and WK Chiu. An improved method for testing the shear stress/strain behaviour of adhesives. *International Journal of Adhesion and Adhesives*, 13(4):237–242, 1993.

[14] Moudar Zgoul. *Characterising the rate dependent response of adhesively bonded structures*. PhD thesis, University of Surrey, 2002.

[15] Toru Sugaya, Tatsuya Obuchi, and Chiaki Sato. Influences of loading rates on stress-strain relations of cured bulks of brittle and ductile adhesives. *Journal of Solid Mechanics and Materials Engineering*, 5(12):921–928, 2011.

[16] Aleksandar Karac, BRK Blackman, V Cooper, AJ Kinloch, S Rodriguez Sanchez, WS Teo, and A Ivankovic. Modelling the fracture behaviour of adhesively-bonded joints as a function of test rate. *Engineering Fracture Mechanics*, 78(6):973–989, 2011.

[17] GD Dean, Bryan Eric Read, and BC Duncan. *An evaluation of yield criteria for adhesives for finite element analysis*. National Physical Laboratory, 1999.

[18] W Chen, F Lu, and M Cheng. Tension and compression tests of two polymers under quasi-static and dynamic loading. *Polymer testing*, 21(2):113–121, 2002.

[19] Amos Gilat, Robert K Goldberg, and Gary D Roberts. Strain rate sensitivity of epoxy resin in tensile and shear loading. *Journal of Aerospace Engineering*, 20(2):75–89, 2007.

[20] Luca Goglio, L Peroni, M Peroni, and M Rossetto. High strain-rate compression and tension behaviour of an epoxy bi-component adhesive. *International journal of adhesion and adhesives*, 28(7):329–339, 2008.

[21] R Avendaño, RJC Carbas, EAS Marques, LFM da Silva, and AA Fernandes. Effect of temperature and strain rate on single lap joints with dissimilar lightweight adherends bonded with an acrylic adhesive. *Composite Structures*, 152:34–44, 2016.

[22] JJM Machado, A Hayashi, PDP Nunes, EAS Marques, RJC Carbas, C Sato, and LFM da Silva. Strain rate dependence of a crash resistant adhesive as a function of temperature for the automotive industry. *Proceedings of the Institution of Mechanical Engineers, Part L: Journal of Materials: Design and Applications*, page 1464420719836914, 2019.

[23] JJM Machado, EAS Marques, and Lucas FM da Silva. Adhesives and adhesive joints under impact loadings: an overview. *The Journal of Adhesion*, 94(6):421–452, 2018.

[24] WD Bascom, RY Ting, RJ Moulton, CK Riew, and AR Siebert. The fracture of an epoxy polymer containing elastomeric modifiers. *Journal of Materials Science*, 16(10):2657–2664, 1981.

[25] JL Bitner, JL Rushford, WS Rose, DL Hunston, and CK Riew. Viscoelastic fracture of structural adhesives. *The Journal of Adhesion*, 13(1):3–28, 1981.

[26] DL Hunston and GW Bullman. Viscoelastic fracture behaviour for different rubber-modified epoxy adhesive formulations. *International journal of adhesion and adhesives*, 5(2):69–74, 1985.

[27] JL Lataillade, D Grapotte, and F Cayssials. The impact resistance of ctbn-modified epoxy adhesive joints. *Le Journal de Physique IV*, 4(C8):C8–771, 1994.

[28] BRK Blackman, AJ Kinloch, AC Taylor, and Y Wang. The impact wedge-peel performance of structural adhesives. *Journal of materials science*, 35(8):1867–1884, 2000.

[29] BRK Blackman, AJ Kinloch, FS Rodriguez Sanchez, WS Teo, and JG Williams. The fracture behaviour of structural adhesives under high rates of testing. *Engineering Fracture Mechanics*, 76(18):2868–2889, 2009.

[30] D Raghavan, J He, D Hunston, and D Hoffman. Strain rate dependence of fracture in a rubber-toughened epoxy system. *The Journal of Adhesion*, 78(8):723–739, 2002.

[31] Zhemin Jia, Guoqing Yuan, David Hui, Xiaoping Feng, and Yun Zou. Effect of high loading rate and low temperature on mode i fracture toughness of ductile polyurethane adhesive. *Journal of Adhesion Science and Technology*, 33(1):79–92, 2019.

[32] Michael May, Holger Voß, and Stefan Hiermaier. Predictive modeling of damage and failure in adhesively bonded metallic joints using cohesive interface elements. *International Journal of Adhesion and Adhesives*, 49:7–17, 2014.

[33] AJ Kinloch, GA Kodokian, and MB Jamarani. Impact properties of epoxy polymers. *Journal of materials science*, 22(11):4111–4120, 1987.

[34] Anders Biel. *Constitutive behaviour and fracture toughness of an adhesive layer*. PhD thesis, Chalmers tekniska högskola, 2005.

[35] Thomas Carlberger, Anders Biel, and Ulf Stigh. Influence of temperature and strain rate on cohesive properties of a structural epoxy adhesive. *International Journal of Fracture*, 155(2):155–166, 2009.

[36] S Marzi, O Hesebeck, M Brede, and F Kleiner. A rate-dependent cohesive zone model for adhesively bonded joints loaded in mode i. *Journal of Adhesion Science and Technology*, 23(6):881–898, 2009.

[37] S Marzi. Measuring the critical energy release rate in mode ii of tough, structural adhesive joints using the tapered end-notched flexure (tenf) test. *The European Physical Journal Special Topics*, 206(1):35–40, 2012.

[38] G Viana, J Machado, R Carbas, M Costa, LFM da Silva, M Vaz, and MD Banea. Strain rate dependence of adhesive joints for the automotive industry at low and high temperatures. *Journal of Adhesion Science and Technology*, 32(19):2162–2179, 2018.

[39] P Rahulkumar, A Jagota, SJ Bennison, and S Saigal. Cohesive element modeling of viscoelastic fracture: application to peel testing of polymers. *International Journal of Solids and Structures*, 37(13):1873–1897, 2000.

[40] Chongchen Xu, Thomas Siegmund, and Karthik Ramani. Rate-dependent crack growth in adhesives: I. modeling approach. *International journal of adhesion and adhesives*, 23(1):9–13, 2003.

[41] Chongchen Xu, Thomas Siegmund, and Karthik Ramani. Rate-dependent crack growth in adhesives ii. experiments and analysis. *International journal of adhesion and adhesives*, 23(1):15–22, 2003.

[42] Xi Zhang, Yiu-Wing Mai, and Rob G Jeffrey. A cohesive plastic and damage zone model for dynamic crack growth in rate-dependent materials. *International journal of solids and structures*, 40(21):5819–5837, 2003.

[43] G Giambanco and G Fileccia Scimemi. Mixed mode failure analysis of bonded joints with rate-dependent interface models. *International journal for numerical methods in engineering*, 67(8):1160–1192, 2006.

[44] Lucas FM Da Silva and RD Adams. Measurement of the mechanical properties of structural adhesives in tension and shear over a wide range of temperatures. *Journal of Adhesion Science and Technology*, 19(2):109–141, 2005.

[45] Filipe José Palhares Chaves. Fracture mechanics applied to the design of adhesively bonded joints. 2013.

[46] M Costa, R Carbas, E Marques, G Viana, and LFM Da Silva. An apparatus for mixed-mode fracture characterization of adhesive joints. *Theoretical and Applied Fracture Mechanics*, 91:94–102, 2017.

[47] MFSF De Moura, RDSG Campilho, and JPM Gonçalves. Crack equivalent concept applied to the fracture characterization of bonded joints under pure mode i loading. *Composites Science and Technology*, 68(10-11):2224–2230, 2008.

[48] Lucas Filipe Martins Da Silva and Andreas Öchsner. *Modeling of adhesively bonded joints*. Springer, 2008.

[49] DFS Saldanha, C Canto, LFM Da Silva, RJC Carbas, FJP Chaves, K Nomura, and T Ueda. Mechanical characterization of a high elongation and high toughness epoxy adhesive. *International journal of adhesion and adhesives*, 47:91–98, 2013.

[50] Y Wang and JG Williams. Corrections for mode ii fracture toughness specimens of composites materials. *Composites Science and Technology*, 43(3):251–256, 1992.

[51] Raul Duarte Salgueiral Gomes Campilho et al. Repair of composite and wood structures. 2009.

[52] Hiroshi Yoshihara and Takuji Kawamura. Mode i fracture toughness estimation of wood by dcb test. *Composites Part A: applied science and manufacturing*, 37(11):2105–2113, 2006.

[53] MFSF De Moura, JPM Gonçalves, JAG Chousal, and RDSG Campilho. Cohesive and continuum mixed-mode damage models applied to the simulation of the mechanical behaviour of bonded joints. *International Journal of adhesion and Adhesives*, 28(8):419–426, 2008.

[54] MFSF De Moura, JPM Gonçalves, and AG Magalhães. A straightforward method to obtain the cohesive laws of bonded joints under mode i loading. *International Journal of Adhesion and Adhesives*, 39:54–59, 2012.

[55] MFSF De Moura and AB De Morais. Equivalent crack based analyses of enf and els tests. *Engineering Fracture Mechanics*, 75(9):2584–2596, 2008.

[56] M Costa, R Carbas, M Benedita, E Marques, G Viana, LFM da Silva, E Yokoi, S Nakada, and T Furusawa. Static assessment of the mixed-mode behaviour of three epoxy adhesives. *Engineering Fracture Mechanics*, 182:552–565, 2017.

Appendices

A Paper A

A strain rate dependent cohesive zone element for mode I modelling of the fracture behaviour of adhesives.

C.S.P. Borges[1], P.D.P. Nunes[1], A. Akhavan[1], E.A.S. Marques[1], R.J.C. Carbas[1] L.F.M. Silva[2]

1 Instituto de Ciência e Inovação em Engenharia Mecânica e Engenharia Industrial (INEGI), Portugal

2 Departamento de Engenharia Mecânica, Faculdade de Engenharia (FEUP), Universidade do Porto, Portugal

Abstract

Adhesives are widely used in the automotive industry as they can be used to manufacture lightweight multimaterial structures with improved strength to weight ratio, contributing to lower energy consumption and emissions. In this industry it is also crucial to ensure passengers' safety thus, mechanical behaviour of the complete automotive structure should be tested for impact conditions, including the adhesive joints within it. This work presents the development of a finite element which models the mechanical behaviour of adhesives and takes into account strain rate dependent property variation, in mode I. The trends for the property variation were set based on an experimental study of two adhesives under three different impact conditions: quasi-static, intermediate speed and impact. The strength was determined using bulk tensile tests and toughness using double cantilever beam (DCB). Both adhesives studied have shown an increase in ultimate stress and critical energy release rate with increasing strain rate. The property variation was then implemented on a finite element, which revealed good agreement with the experimental results.

A.1 Introduction

Adhesive joints are increasingly being used in detriment of mechanical joints due to their ability to create a more uniform stress distribution along the bonded area, which translates into higher stiffness, load transmission and fatigue resistance at reduced weight and cost [1–4]. Adhesives are used in several sectors, such as the automotive and, in this industry it is mandatory to ensure passengers' safety if a collision occurs and, consequently, the behaviour of the bonded areas found in the automobile structure must be studied and optimized for impact conditions.

Among the first to study the dynamic behaviour of polymers were Tardif and Marquis [5] and Lindholm [6], they concluded that an epoxy resin under compression is highly strain rate sensitive. The resin showed an increase in modulus and ultimate stress paired with a decrease in ultimate strain over the static value.

Chalkley and Chiu [7], in 1993, and Zgoul [8], in 2002, concluded that while yield stress and maximum strain exhibited a strain rate dependent behaviour, modulus remained practically unaffected. This conclusion was supported by other authors [9–14]. Most of them recorded an increase in maximum stress and a reduction in elongation. In 2011, Sugaya et al. [9] discussed that it is expected that adhesives become stronger and more brittle with increasing strain rate.

Regarding the fracture toughness of adhesives, the behaviour under static conditions has been widely researched, but impact conditions have been significantly less studied.

Bascom et al. [15], in 1981, concluded that, in general, a decrease in fracture energy in mode I was verified with increasing strain rate. A decrease in toughness with increasing strain rate was also reported by Britner et al. [16], Hunston et al. [17], Lataillade et al. [18], Blackman et al. [19, 20], Raghavan et al. [21], Karac et al. [10] and Jia et al. [22].

Raghavan et al. [21], in 2002, presented a possible explanation for the decrease in fracture energy with increasing loading rate, stating that slower loading rates allow a more significant crack-tip deformation, which can result in increased toughness. Other justification was presented by May et al. [23], in 2014, saying that when a critical crack propagation speed is reached, the conditions at the crack tip change from isothermal to adiabatic, which causes a reduction in fracture toughness due to the poor properties of polymers at high temperature.

The trends obtained by Blackman et al. [20] from DCB and tappered double cantilever beams (TDCB) tests and Karac et al. [10] from DCB tests can be observed in Figure 1.

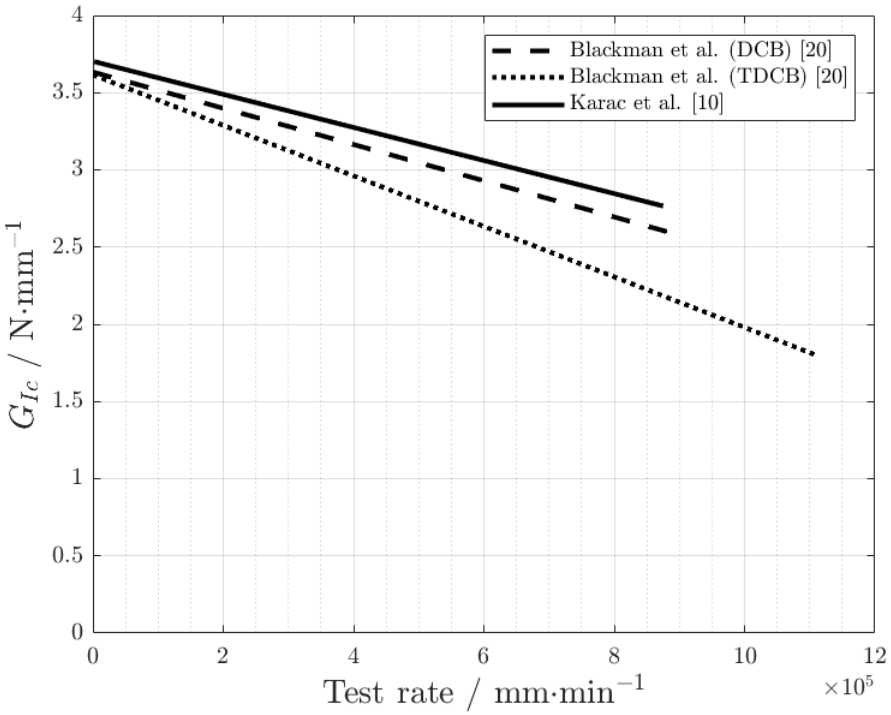

Figure 1: Energy release rate in mode I decreasing as a function of test rate. Adapted from [10, 20].

However, the concept that fracture energy decreases with increasing strain rate is not unanimous in literature. Kinloch et al. [24], in 1987, declared that a rubber-modified epoxy showed a significant increase of the fracture energy with increasing strain rate. An increase in fracture energy with increasing strain rate was also reported by Biel et al. [25], Carlberger et al. [26], Marzi et al. [27, 28] and May et al. [23].

Additionally, Carlberger et al. [26] and Avendaño et al. [29] both stated that the dependence of fracture energy in mode I and maximum tension with stain rate can be considered linear in a semi-logarithmic scale.

May et al. [23], in 2014, showed a different tendency for the variation of the fracture energy, saying that it is constant below a limit strain rate, increasing following linear relation in a semi-logarithmic scale until a second boundary strain rate is reached. After that limit, the fracture energy is once again constant.

Viana et al. [30], in 2018, studied the static and impact behaviour of adhesives, and concluded that, for different temperatures, impact tested specimens were able to withstand higher loads, and absorb higher amounts of energy than the quasi-static tested specimens. An outcome corroborated by Machado et al. [31] in 2019.

Figure 2 shows the evolution of energy release rate as a function of strain rate, reported by Carlberger et al. [26] from DCB tests, Marzi et al. [27] from T-joint tests and May et al. [23] from TDCB tests.

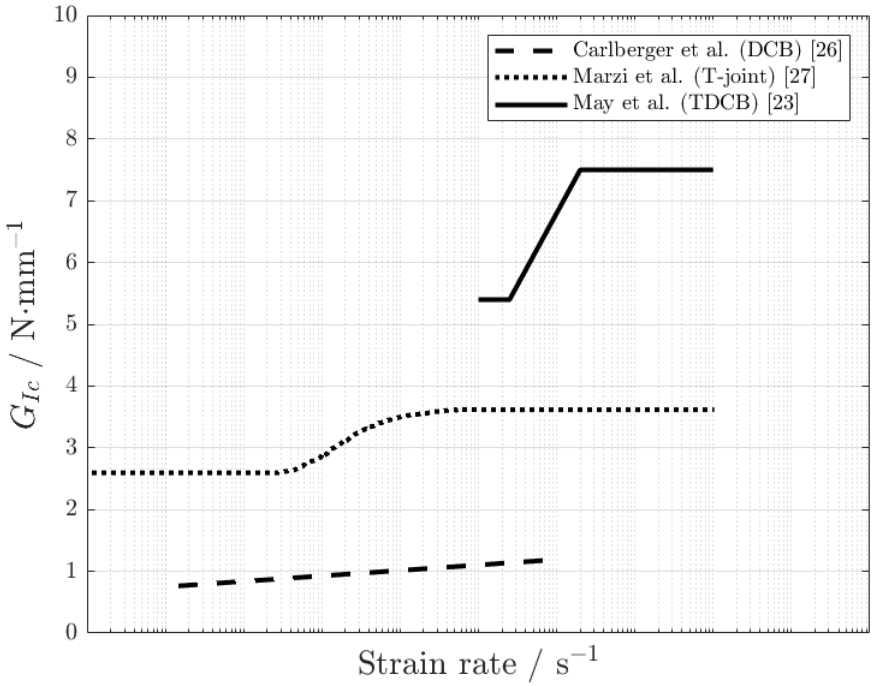

Figure 2: Energy release rate in mode I increasing as a function of strain rate. Adapted from [23, 26, 27].

Although a universal trend has not yet been found, authors agree that the behaviour of adhesives is dependent on strain rate. Therefore, when analysing or running a numerical simulation to model adhesive joints, the properties' variation should be accounted for.

In this work, the variation with strain rate of fracture energy in mode I and tensile strength properties were determined, using DCB and bulk tensile tests, respectively, performed at three different loading rates: quasi-static, intermediate speed, and impact. Afterwards, ultimate tensile stress and energy release rate in mode I were defined as a function of strain rate. Those functions were then implemented on a cohesive zone model using Abaqus® UMAT, an user-defined subroutine, for the correct simulation of the adhesive for different loading rates. The user defined material, UMAT, was then validated using DCB models.

A.2 Experimental details

This section presents the adhesives used in this study and the detailed manufacturing and testing processes. Tensile specimens and DCB specimens were tested, to determine tensile properties and energy release rate in mode I, respectively.

A.2.1 Crash resistant adhesive

The adhesives analysed in this work were the Betamate^{TM} 120EU and the Betamate^{TM} 1480R. Both adhesives are one component crash-resistant adhesives from DOW Automotive (Michigan, USA), and were developed to increase durability, crash performance and body stiffness. The cure for both adhesives consists of a stage at 180 °C for 30 minutes, Figure 3.

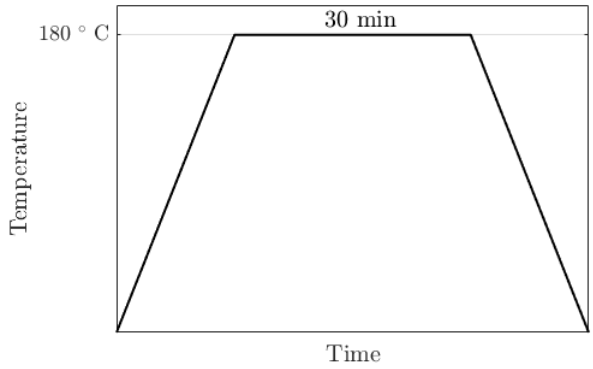

Figure 3: Cure cicle of the adhesives used.

A.2.2 Specimen fabrication

Tensile specimens. Tensile specimens were machined from adhesive plates, manufactured following the French standard NF T 76-142 [32], with the thickness of 2 mm. Uncured adhesive is pressed between steel plates, with a silicone rubber frame being used to restrict the adhesive and create hydrostatic pressure, which promotes a good surface finish and prevents the creation of voids. Appropriate temperature and pressure were then applied to ensure the correct cure of the adhesive. The specimens were then machined following the British standard BS 2782 [33], obtaining specimens with the configuration observed in Figure 4.

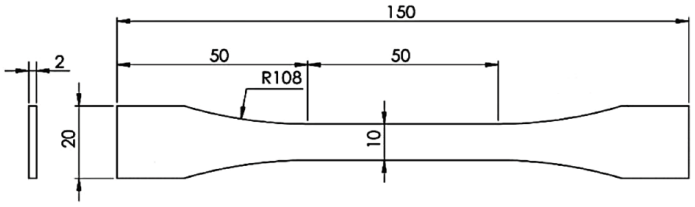

Figure 4: Representation of tensile specimens' geometry, according to BS 2782 [33], in mm.

DCB specimens. DCB specimens, Figure 5, were manufactured using hard steel substrates to avoid plastic deformation. Those substrates were grit blasted and degreased with acetone before the application of the adhesive to ensure good adhesion. The initial

crack length was 45 mm and the crack was introduced positioning a sharp razor blade, with the thickness of 0.1 mm, in the mid-thickness of the bondline. The bondline thickness of 0.2 mm was established with calibrated tape. The specimens were then subjected to pressure and temperature to ensure the proper cure of the adhesive.

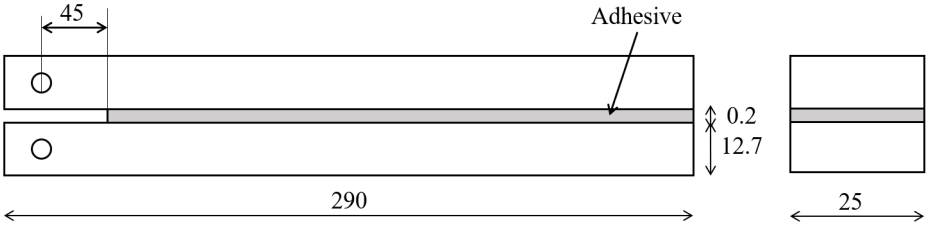

Figure 5: Representation of DCB specimens' geometry, in mm.

A.2.3 Testing procedures

Mode I tests were performed at three different test speeds referred in this document as quasi-static, intermediate and impact. The quasi-static speed adopted was 1 mm·min $^{-1}$ for tensile tests and 0.2 mm·min $^{-1}$ for DCB tests. The intermediate speed used was $6 \cdot 10^3$ mm·min $^{-1}$ and the impact speed was $180 \cdot 10^3$ mm·min $^{-1}$.

For the tests, three different machines were used, two of them were universal testing machines, INSTRON® 3367 with a load cell of 30 kN, used for quasi-static tests, and INSTRON® 8801 with a load cell of 100 kN, used for intermediate speed. For impact tests, an in-house developed drop weight machine [34] was used. This machine allows to test using a drop mass of up to 56 kg, released from a maximum height up to 1.27 m, achieving an impact speed of 5 m·s^{-1}, and has a load cell of 30 kN.

For each condition, at least three specimens were tested.

Tensile tests. Load displacement ($P - \delta$) curves were recorded for each test, until failure. For the test at loading rates of 1 mm·min $^{-1}$ and $6 \cdot 10^3$ mm·min $^{-1}$, the displacement was recorded using an extensometer, but for higher loading rates, this proved to be ineffective, due to slippage of the specimen during the test, therefore, a high speed camera at 5000 fps and digital image correlation was used. Tensile strength and Young's modulus were determined using this test.

DCB tests. Critical energy release rate in mode I was determined using DCB tests, Figure 6. DCB specimens were previously loaded in mode I at low load levels to ensure a stable crack propagation and a sharp pre-crack, for which a new initial crack length, a_0, was recorded. Afterwards, load displacement curves were recorded. At quasi-static and intermediate speed both load and displacement were registered by the machines used, for impact loading, load was determined by the machine and displacement was determined using a high speed camera at 5000 fps and digital image correlation.

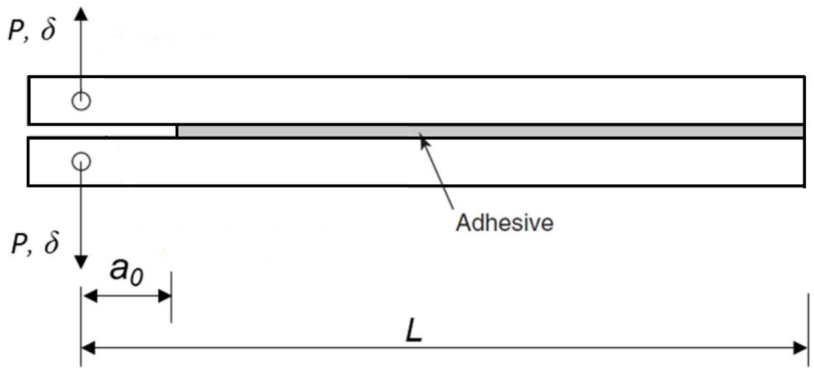

Figure 6: Representation of DCB test, in mm.

Energy release rate in mode I was determined using the compliance based beam method (CBBM), which is a data reduction scheme that has the advantage of not needing the exact crack length determination and taking into account the fracture process zone [35]. Considering this method, fracture energy is given by [35]:

$$G_I = \frac{6P^2}{B^2 h}\left(\frac{2a_{eq}^2}{h^2 E_f} + \frac{1}{5G_{13}}\right) \tag{1}$$

where P is the load, B is the specimen width, h is the thickness of the substrates, G_{13} is its shear modulus, a_{eq} is the length of the crack equivalent and E_f is the corrected flexural modulus, needed because this method does not take into account stress concentration and substrates' rotation near the crack tip [35].

A.3 Numerical model

Adhesives, as said, exhibit a strain rate dependent behaviour thus, when analysing them at different loading rates, the variation of their properties with strain rate should be accounted for. Consequently, numerical modelling of the DCB tests for different displacement rates was done using an user defined material in Abaqus® - UMAT. This subroutine allows the determination of the strain rate for each element and the definition of G_{Ic} for each strain rate, through a function previously characterized using experimental data.

UMAT defines the Jacobian matrix, $\partial\Delta\sigma/\partial\Delta\varepsilon$, for the mechanical constitutive model, updating stress. A scheme of the integration of UMAT for each increment can be seen in Figure 7.

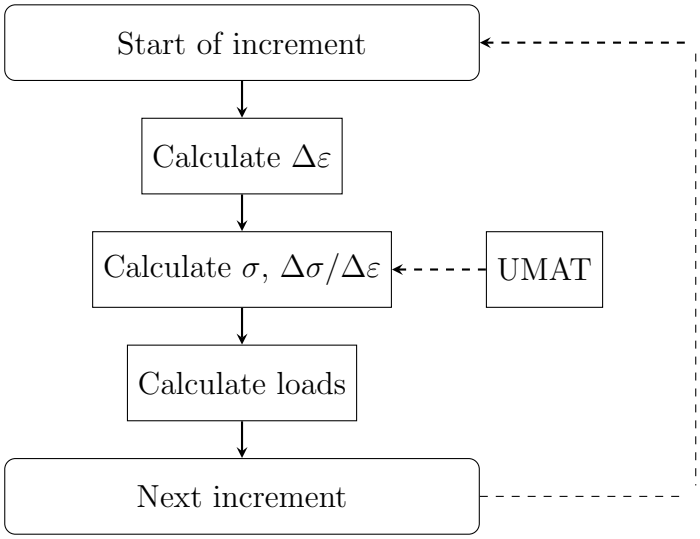

Figure 7: Scheme representing the integration of UMAT in Abaqus®.

The properties of the adhesive that should be inputted are: Young's modulus, E, shear modulus, G_s, the expression that characterizes tensile strength, σ_{max}, as a function of strain rate, shear strength, τ_{max}, the expression that characterizes critical energy release rate in mode I, G_{IC}, as a function of strain rate and critical energy release rate in mode II, G_{IIC}.

The ultimate stress in mode I, $\sigma_{I,max}$, is the maximum tensile strength σ_{max} and ultimate stress in mode II $\sigma_{II,max}$ is the maximum tensile strength τ_{max}.

It is important to note that, although the code was developed to analyse cases in which the loading is mainly in mode I, it should be able to accommodate minor loadings in mode II that may appear during the test. Therefore, the UMAT was developed considering a mixed mode I+II. In this way, if the loading is in pure mode I, only mode I properties will be considered but, if small mode II loads emerge, their contribution can be accounted for.

Abaqus® provides, for each time increment, the strain increment and its duration, which allows the determination of strain rate. As mentioned above, if the strain rate is known, the critical energy release rate in mode I can be determined, based on the inputted expression. Afterwards, and considering a triangular traction-separation law, the strain when maximum stress is reached, ε_{i0} $(i = I, II)$, and the maximum strain, ε_{if} $(i = I, II)$, are determined through the area of the triangle represented in Figure 8. The stiffness k, is considered the Young's modulus and the shear modulus for mode I and II, respectively.

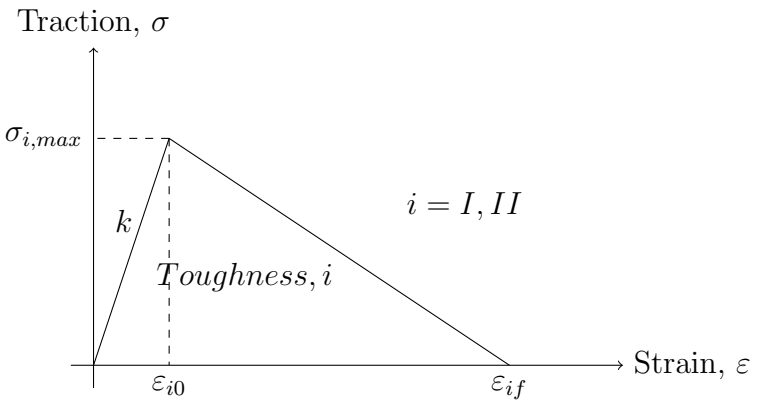

Figure 8: Triangular law used in UMAT, for each pure mode.

The current strain in the direction of mode I and II, ε_i $(i = I, II)$, is also provided by Abaqus®, enabling the calculation of the mode mixity of the loading. Afterwards, a new triangular law is established for that mode mixity, combining the properties for pure mode I and pure mode II, as clarified in Figure 9. Strain when maximum stress is reached, ε_{m0}, maximum strain, ε_{mf}, and current strain, ε_m, are determined for the mode under analysis.

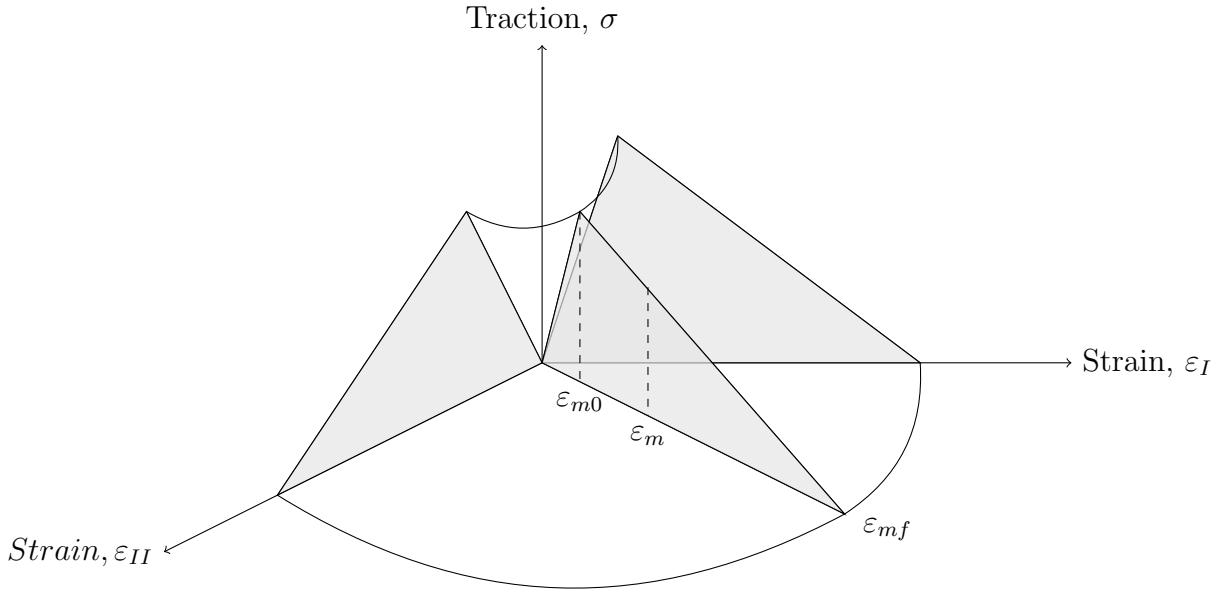

Figure 9: Combination of the pure modes in mixed mode.

It is considered that, when the strain in one element reaches ε_{m0}, damage initiates, and as strain progresses from ε_{m0} to ε_{mf} a damage coefficient, d, progresses linearly from 0 to 1 reaching 1 when the strain reaches ε_{mf}.

When ε_m is less than ε_{m0}, the Jacobian matrix is calculated, and stress is determined. When ε_m is higher than ε_{m0}, damage is calculated and then stress is determined. The degradation of the properties when damage occurs can be seen in Figure 10.

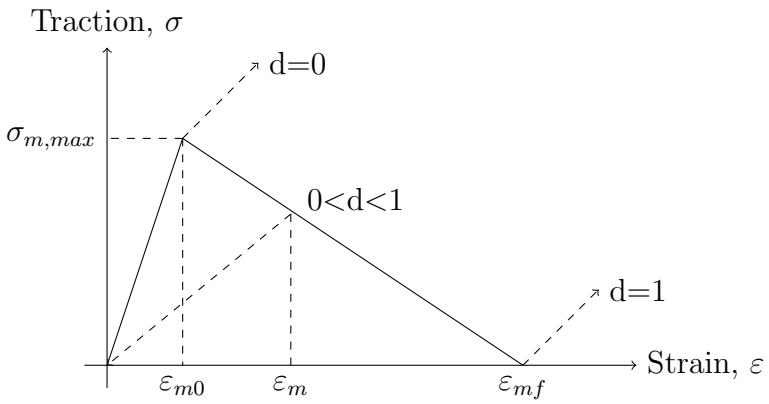

Figure 10: Triangular law used in UMAT, mixed mode, with degradation due to damage.

A.3.1 DCB model

Two models were created to reproduce the tests performed using Abaqus®. For quasi-static and intermediate speed a DCB test was modelled by applying a displacement at a constant speed to one of the extremities, for the impact tests a mass was positioned in the same position and a velocity field was applied in that mass to recreate the impact of the drop-weight machine.

Both models were two dimensional and used solid elements for the substrates and cohesive elements for the adhesive. The substrates has the properties mentioned above, and the adhesive was connected to the UMAT developed.

The mesh was created considering that near the crack tip it should be refined, using the element spacing of 0.2 mm, corresponding to the adhesive thickness, increasing in size until the end of the bondline where the element spacing is 5 mm.

Quasi-static and intermediate speed. The boundary conditions, Figure 11, were set to replicate the performed test, with the bottom substrate being fixed by an encastre in the position of the lower pin, and the upper substrate with an upwards displacement applied in the position of the upper pin.

Figure 11: Boundary conditions for the DCB test simulation for quasi-static and intermetiate speed.

The displacement applied and the duration of the test define the loading rate tested, which can be seen in Table 1.

Table 1: Displacement and duration inputted for each testing condition.

Loading rate / mm·min $^{-1}$	Displacement / mm	Duration of the test / s
0.2	30	$9 \cdot 10^3$
$6 \cdot 10^3$	30	0.3

Impact. For the simulation of impact conditions, a 26 kg mass was attached to the position of the upper pin. In that mass a velocity field of 3 m·s^{-1}, or $180 \cdot 10^{-3}$ mm·min^{-1}. Those boundary conditions can be seen in Figure 12.

Figure 12: Boundary conditions for the DCB test simulation for impact conditions.

A.4 Experimental results and discussion

A.4.1 Tensile tests

The stress, σ, strain, ε, curves obtained for the tensile tests were similar to the one observed in Figure 13, which is for Betamate^{TM}120EU at quasi-static conditions, 1 mm·min $^{-1}$.

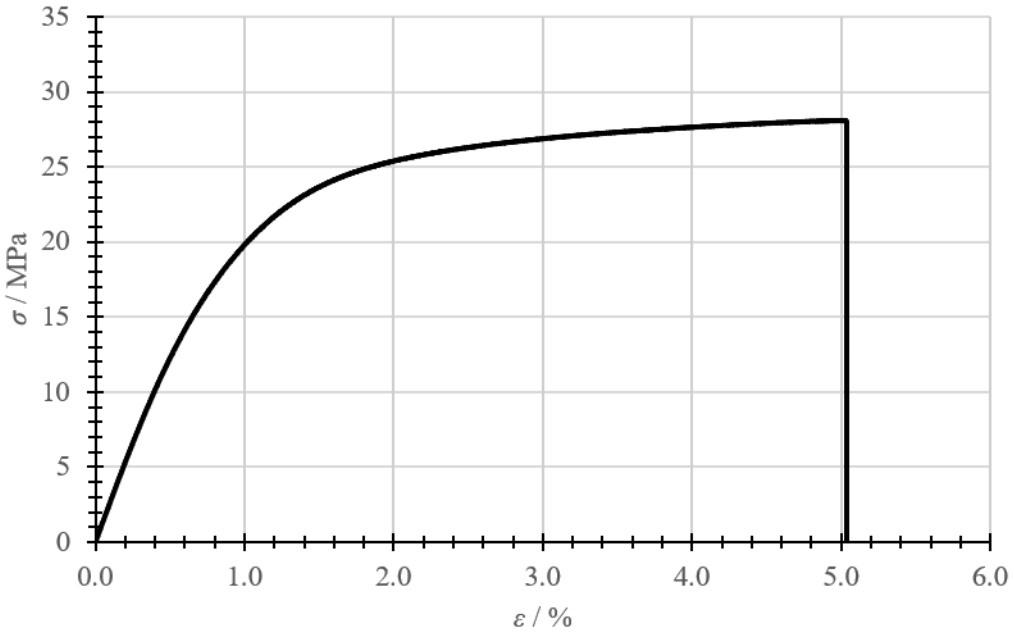

Figure 13: Representative stress strain curves for tensile tests of Betamate^{TM}120EU.

With the increase of loading rate, the adhesive has shown a higher strength and lower maximum strain. This is expected for viscoelastic materials, because, with low loading rates, the time it takes for the adhesive's molecules to find new equilibrium conditions is lower then the time of loading, and the material has a more viscous behaviour. In impact conditions, because the loading time is very short, the time of the loading is lower then the time it takes for the molecules of the adhesive to accommodate, which translates in a more elastic behaviour. The results for maximum stress for the three loading rates tested can be seen in Table 2.

Table 2: Maximum stress, σ_{max}, for the three different loading rates, $\dot{\delta}$, tested.

Adhesive	$\dot{\delta}$ / mm·min^{-1}	σ_{max} /MPa
Betamate^{TM}120EU	0.2	28.1 ± 0.61
	$6 \cdot 10^3$	47.3 ± 1.21
	$180 \cdot 10^3$	92.5 ± 10.1
Betamate^{TM}1480R	0.2	38.1 ± 0.43
	$6 \cdot 10^3$	54.4 ± 1.06
	$180 \cdot 10^3$	96.0 ± 8.3

Ultimate stress, as a function of strain rate, can be seen in Figure 14.

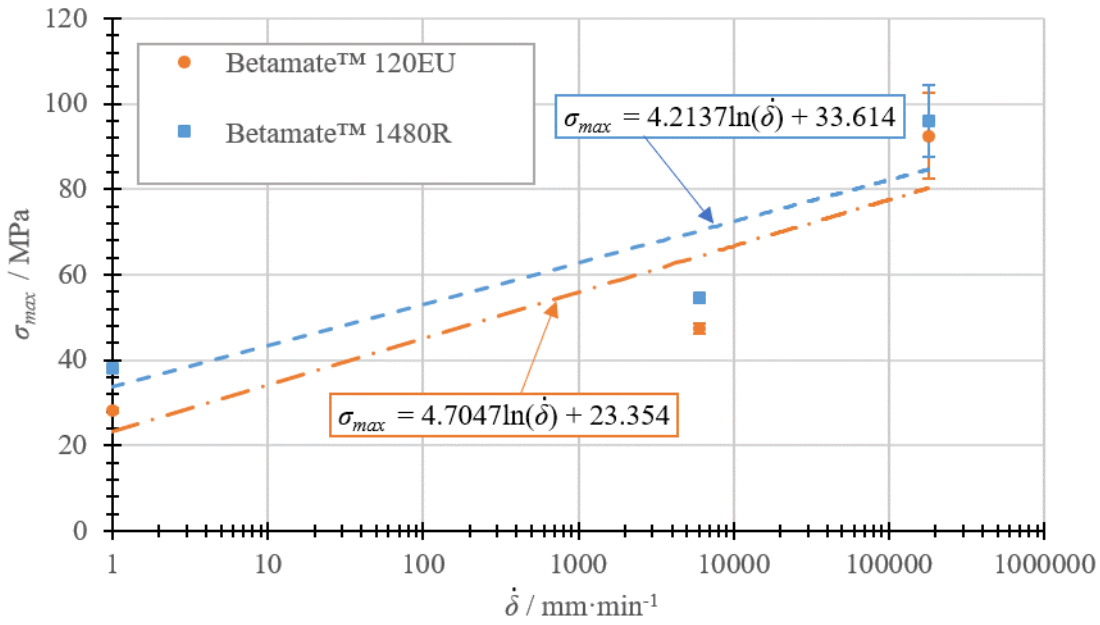

Figure 14: Ultimate stress as a function of loading rate for Betamate^{TM}120EU and Betamate^{TM}1480R.

Young's modulus has been considered approximately constant by different authors [7–9]. Thus, the Young's modulus will be considered equal to its quasi-static value in the numerical model. The values for the Young's modulus for both adhesives can be seen in Table 3.

Table 3: Young's modulus for the two adhesives tested.

Adhesive	E / MPa
Betamate^{TM}120EU	2522 ± 104
Betamate^{TM}1480R	2209 ± 64

A.4.2 DCB tests

The results of the DCB tests exhibited cohesive failure in the adhesive and, with increasing strain rate, the adhesive exhibited an increase in load. The measurement of displacement, for the impact tests, was measured using a high speed camera and the Photron FASTCAM Analysis®, represented in Figure 15.

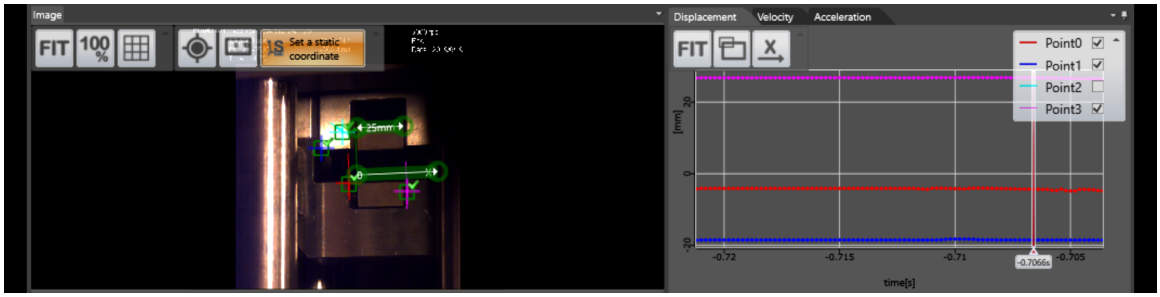

Figure 15: Measurement of displacement in impact tests.

The load displacement curves recorded for the universal testing machines and with the impact machine can be seen in Figure 16 and 17, for Betamate^{TM}120EU and Betamate^{TM}1480R, respectively.

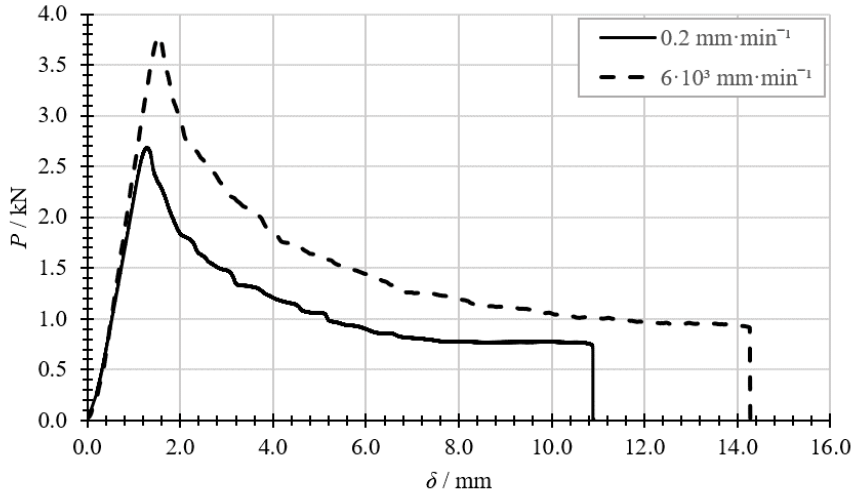

(a) Load displacement curves recorded using universal testing machines.

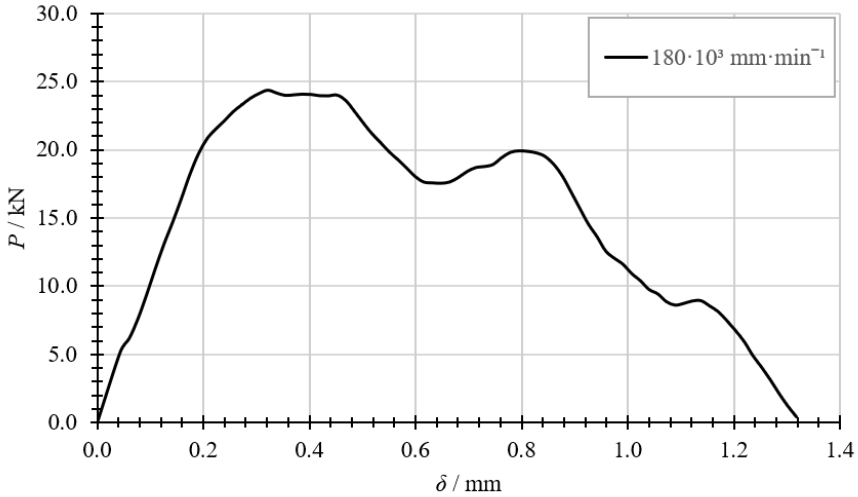

(b) Load displacement curve recorded with the impact machine.

Figure 16: Representative load displacement curves recorded for Betamate^{TM}120EU.

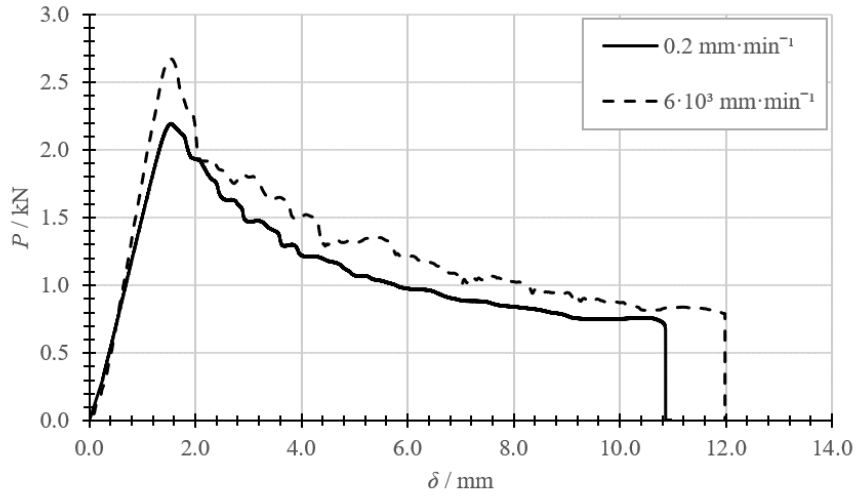

(a) Load displacement curves recorded using universal testing machines.

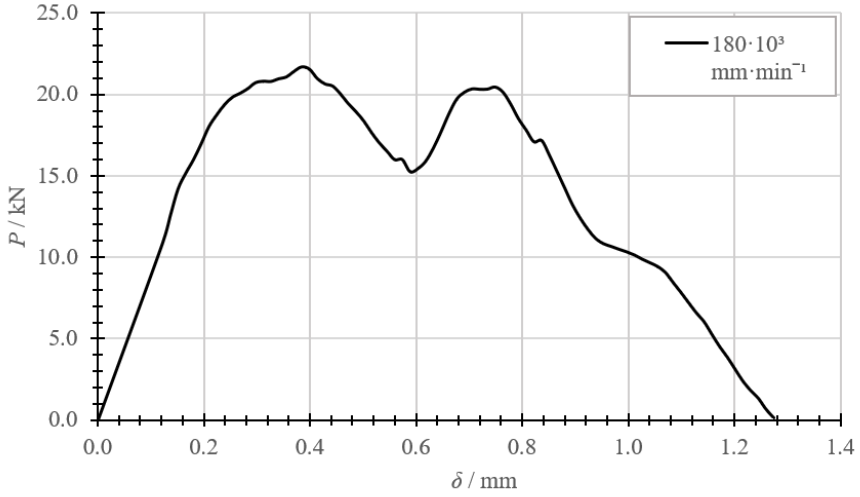

(b) Load displacement curve recorded with the impact machine.

Figure 17: Representative load displacement curves recorded for Betamate^{TM}1480R.

Based on the load displacement curves, and using CBBM, the respective R-curve was determined, and consequently the critical energy release rate in mode I was obtained, Figure 18 and 19, respectively.

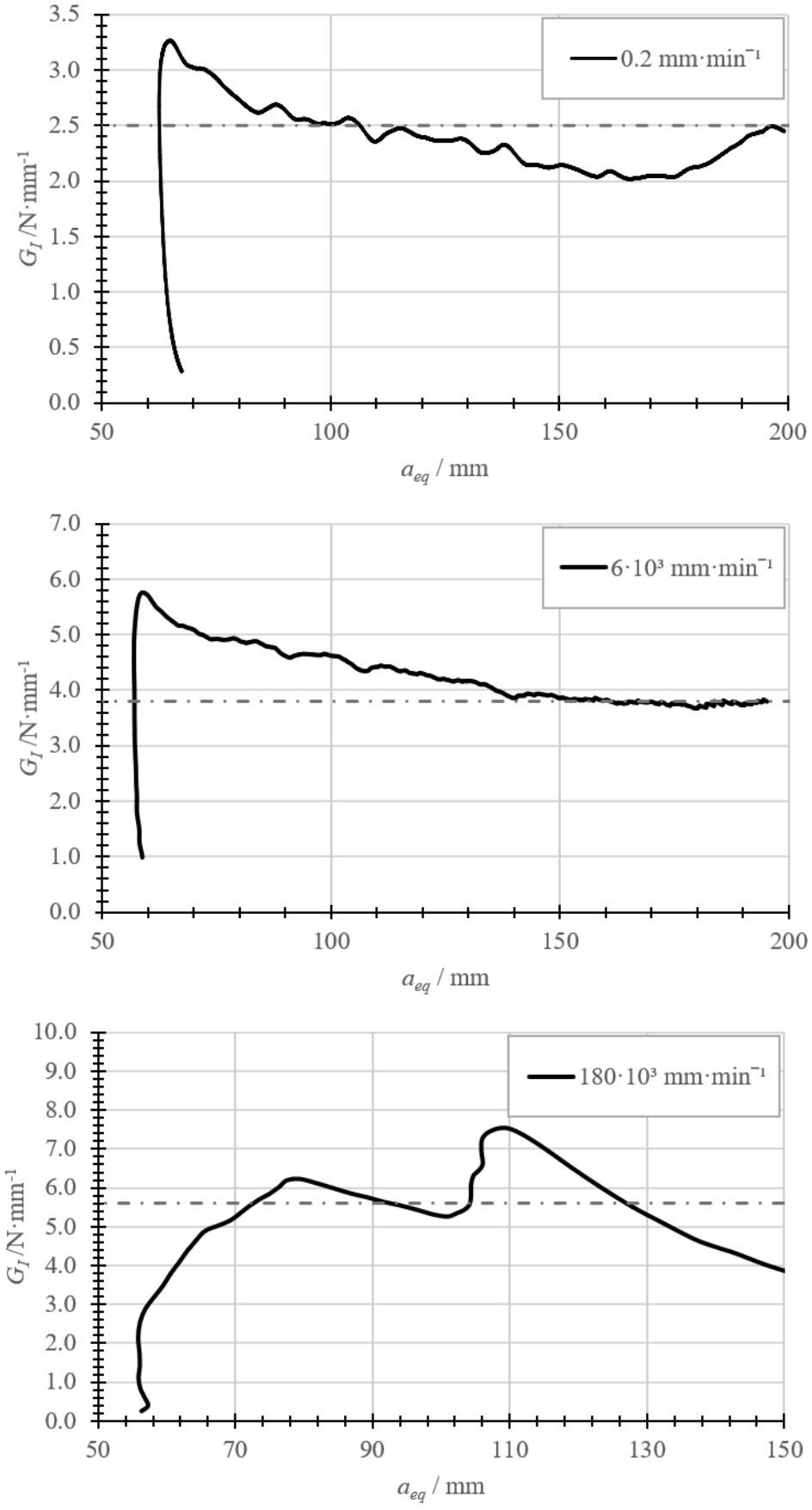

Figure 18: Representative R-curves for Betamate^{TM}120EU.

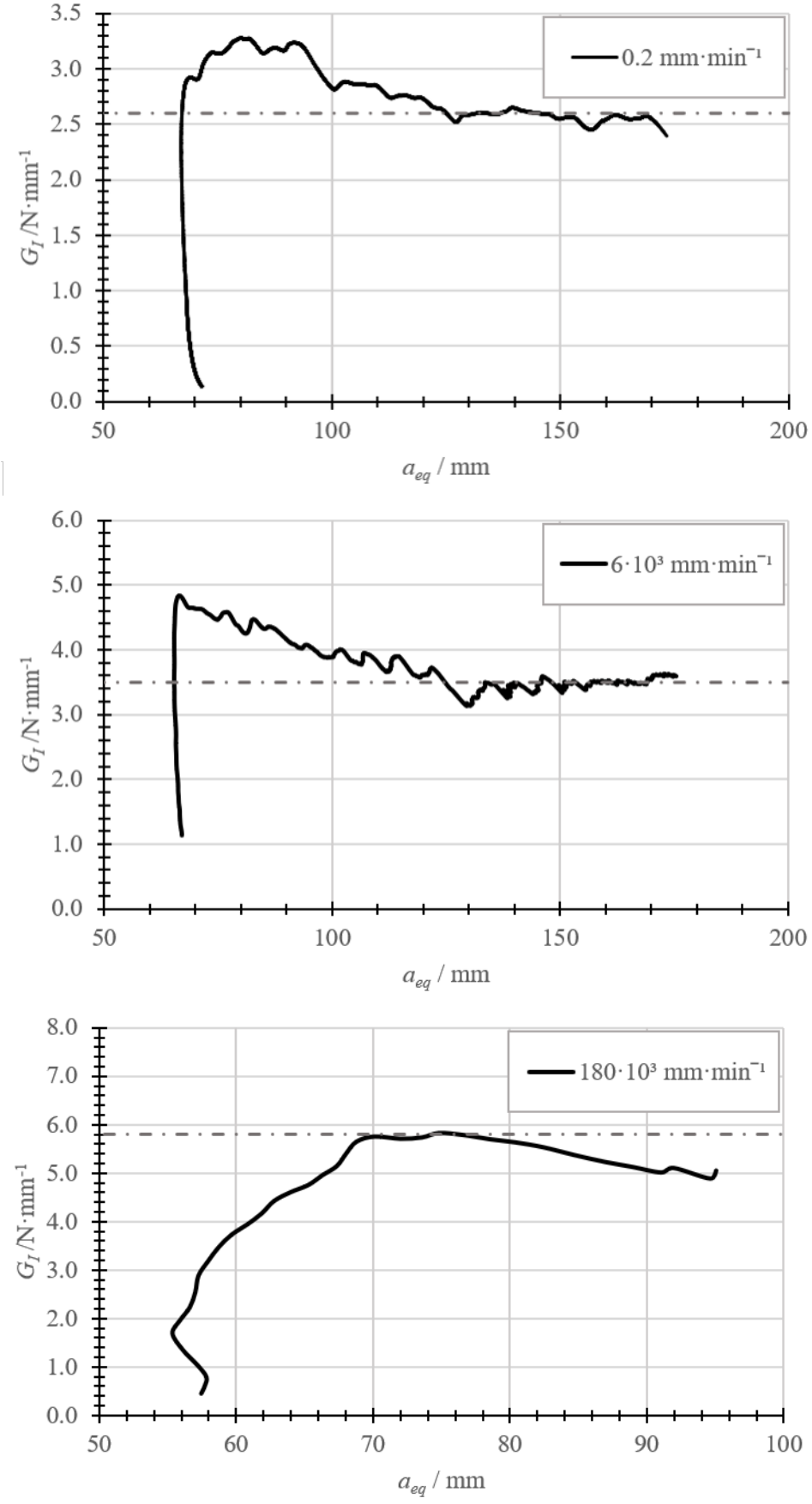

Figure 19: Representative R-curves for Betamate^{TM}1480R.

The results obtained for all tests can be seen in Table 4.

Table 4: Energy release rate, G_{IC}, for the three different loading rates, $\dot{\delta}$, tested.

Adhesive	$\dot{\delta}$ / mm·min $^{-1}$	G_{IC} / N·mm^{-1}
Betamate^{TM}120EU	0.2	2.5 ± 0.2
	$6 \cdot 10^3$	3.7 ± 0.2
	$180 \cdot 10^3$	4.5 ± 0.3
Betamate^{TM}1480R	0.2	2.6 ± 0.1
	$6 \cdot 10^3$	3.4 ± 0.1
	$180 \cdot 10^3$	5.0 ± 0.3

With the critical energy release rates calculated, G_{IC} as a function of loading rate, $\dot{\delta}$ can be plotted. The results were approximated by a logarithmic expression, Figure 20.

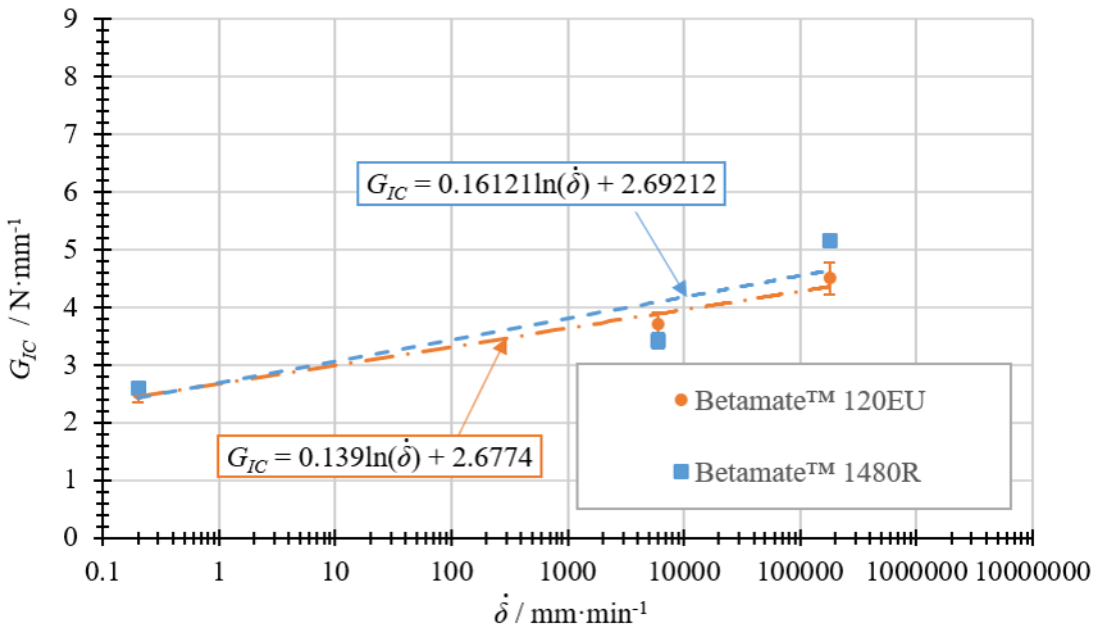

Figure 20: Critical energy release rate as a logarithmic function of loading rate for Betamate^{TM}120EU and Betamate^{TM}1480R.

As observed before by other authors, the energy release rate increases with increasing strain rate, which can be once again related to the viscoelastic behaviour of the adhesive. Aditionally, the curve that proved to have the best fit to replicate the experimental results for both adhesives was a line in a semi-logarithmic scale, this was previously suggested by Carlberger et al. [26] and Avendaño et al. [29], and has been the basis of many extrapolations for impact loads.

A.5 Properties as a function of the strain rate

The application of the numerical model for a wide variety of geometries and loading conditions requires the definition of the properties as a function of strain rate and not as a function of loading rate, which is intimately connected to the specific test performed. For this, the strain rate was determined for each test, and the curves characterizing the adhesive properties as a function of strain rate determined.

A.5.1 Strength properties

Strain rate determination. Strain rate for the tensile tests was determined based on the displacement recorded by the extensometer, for the quasi-static and intermediate speed, and the a high speed camera, for impact loading, and the sample rate of the devices. Strain rate was recorded during the tests and an average value determined. Strenght was, then, plotted as a function of strain rate, Figure 21.

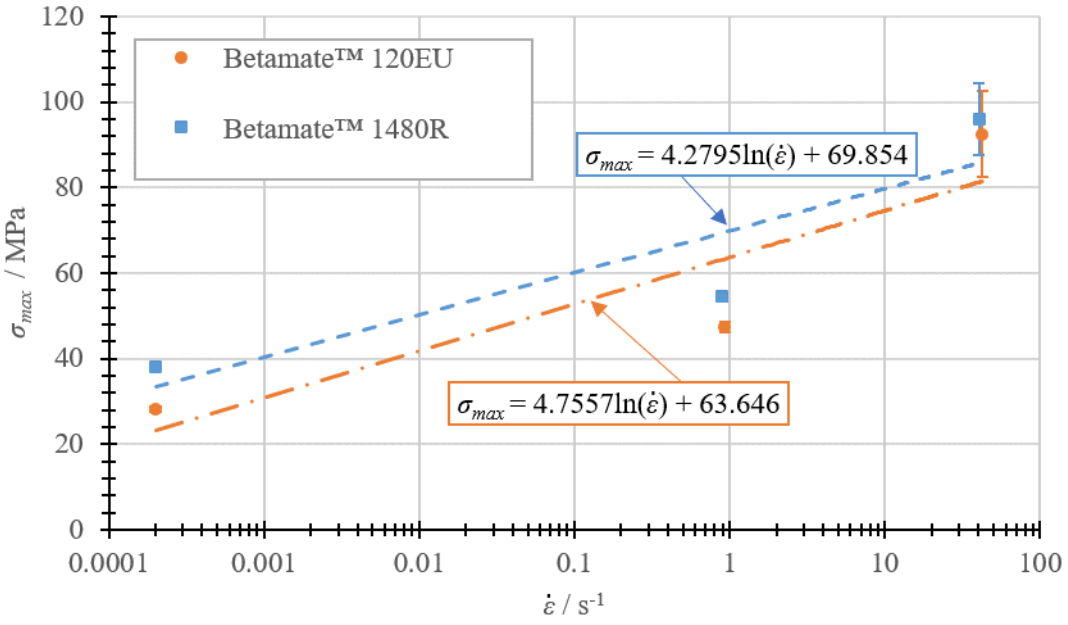

Figure 21: Maximum stress as a function of strain rate for Betamate^{TM}120EU and Betamate^{TM}1480R.

A.5.2 Fracture properties

Strain rate determination. Strain rate during the experimental tests was indirectly determined through the numerical model. The conditions of each test performed were recreated in a numerical simulation in Abaqus®, using UMAT. UMAT has different outputs, two of which are damage and strain rate in mode I. For each element, the strain rate was determined in the moment of failure ($d = 1$), and those strain rates were plotted as a function of the distance to the crack tip. The trendlines obtained for the strain rate

for each test speed are represented in Figure 22 and all loading rates are compared in Figure 23, considering a pre-crack of 45 mm. Both figures refer to Betamate^{TM}120EU.

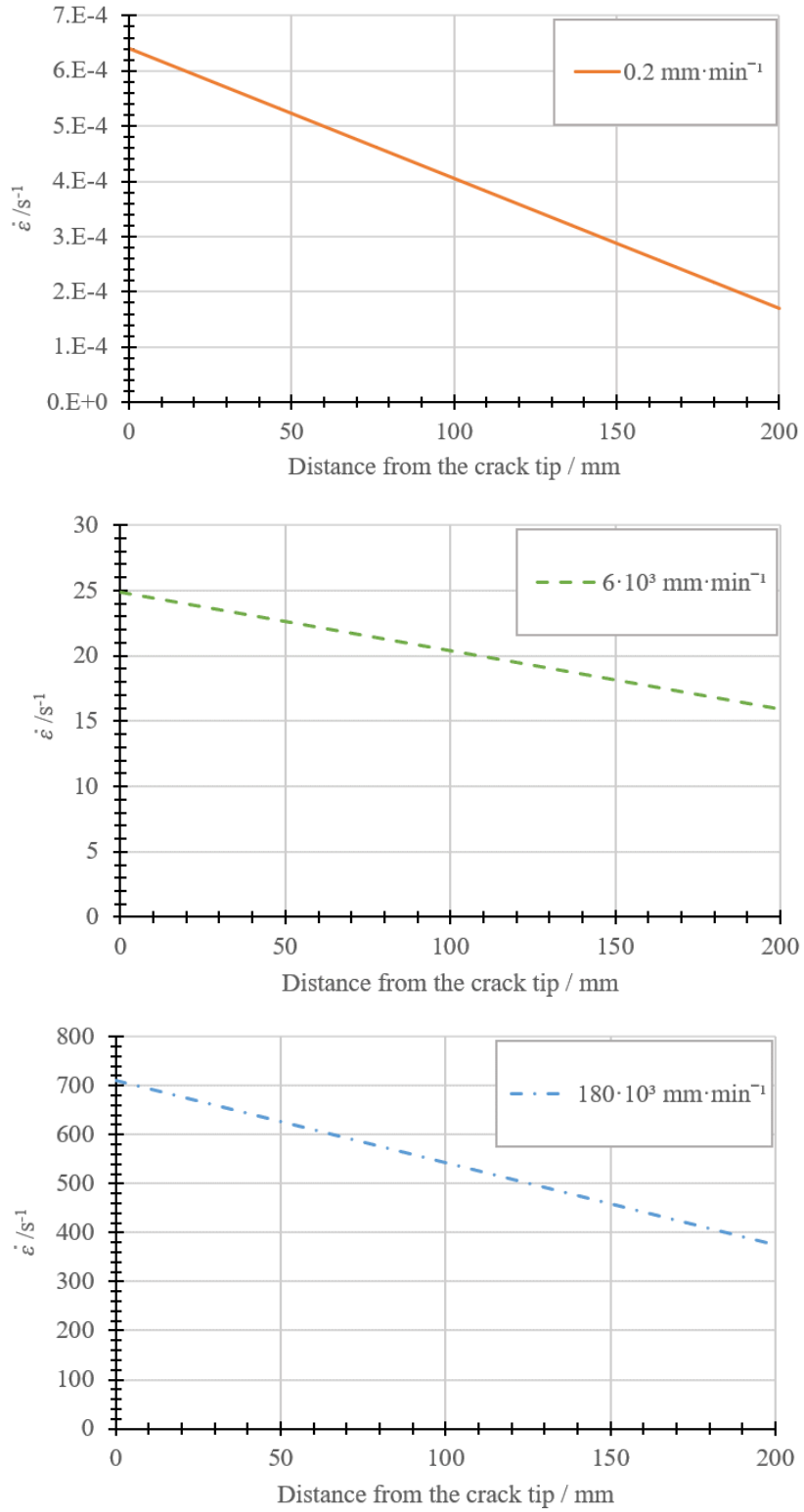

Figure 22: Strain rate for each loading rates tested, with a pre-crack length of 45 mm.

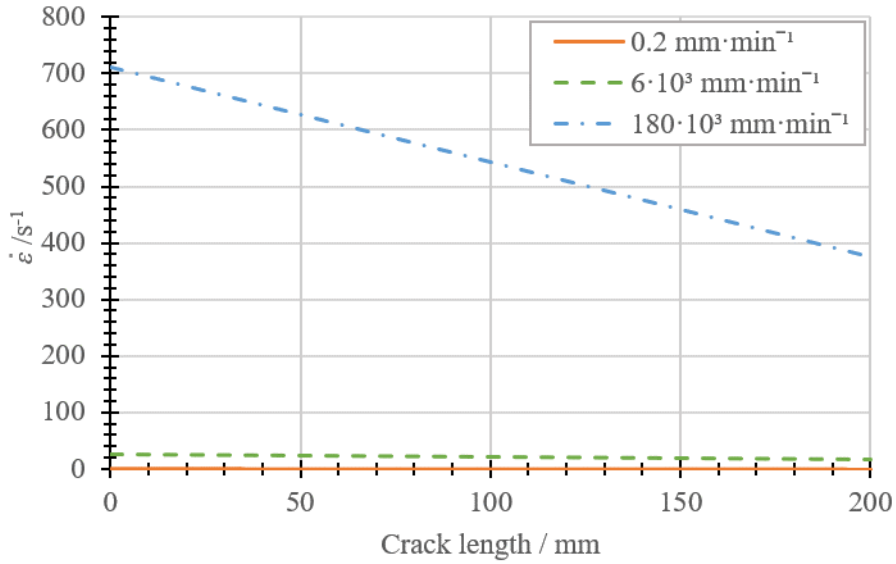

Figure 23: Strain rate for all loading rates tested, with a pre-crack length of 45 mm.

The strain rate at which the adhesive fails, along the specimen, shows a decrease. According to the experimental results, fracture energy changes with strain rate, thus, for each point along the specimen, the energy release rate considered should be different.

Energy release rate as a function of strain rate. As previously mentioned, the strain rate for each test was determined in the moment the adhesive breaks along the bondline, then, for each experimental test, the R-curves were analysed, and the stable zone of the curve zone where the critical energy release rate was determined is recorded, and the correspondent strain rate range established. Figure 24 clarifies this procedure for using a test from the Betamate^{TM}1480R adhesive for a loading rate of $6 \cdot 10^3$ mm·min $^{-1}$.

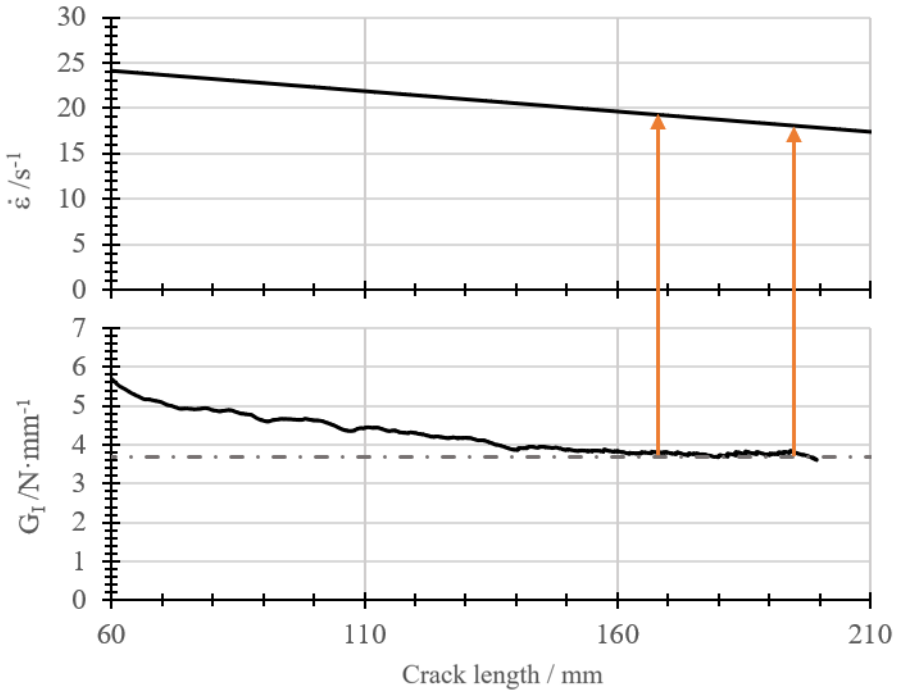

Figure 24: Determination of G_{IC} as a function of strain rate.

Using the strain rate ranges and the correspondent value of energy release rate, critical energy release rate as a function of strain rate was plotted, which can be seen in Figure 25.

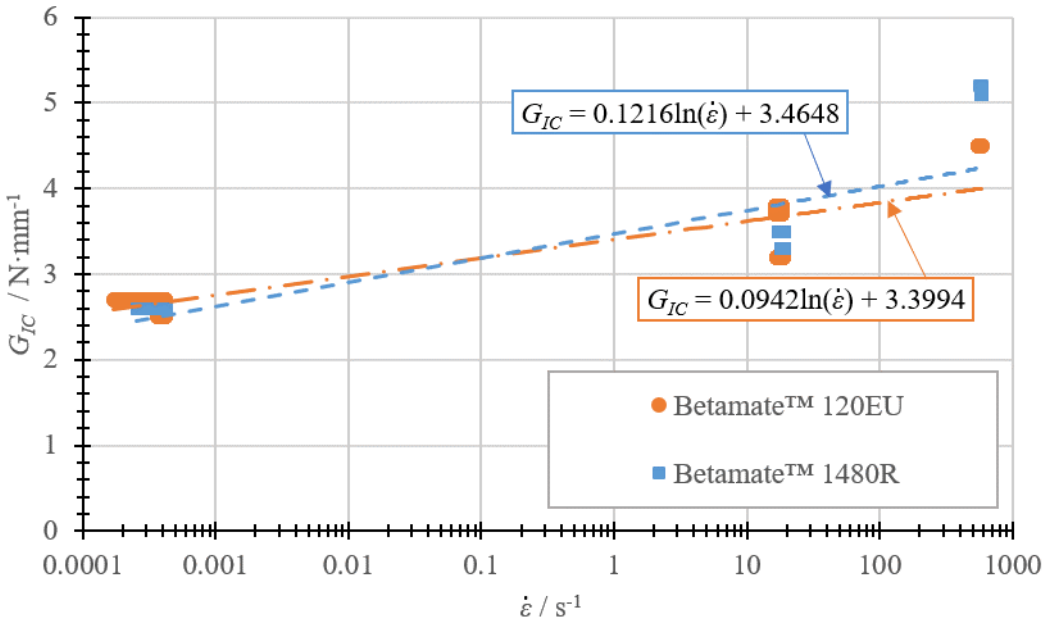

Figure 25: G_{IC} as a function of strain rate.

A.6 Numerical results

The numerical model requires the input of the ultimate tensile stress σ_{max}, and energy release rate in mode I, G_{IC}, as a function of strain rate. As the test progresses, the variation of strain rate can also be seen along the bondline. Therefore, this, the expressions developed in section A.5 were used. The tests performed were then reproduced using the numerical model.

The numerical model developed has, as output variables, damage, strain rate in mode I and energy release rate in mode I, for each element along the bondline and for each time increment. The results for the model will be presented using Betamate^{TM}120EU loaded at $6 \cdot 10^3$ mm·min $^{-1}$. The crack propagation can be seen, along the test, through damage evolution. When damage is equal to one, $d = 1$, it is considered that the element does not resist the loading anymore, and it is equivalent to the element disappearing. Damage evolution can be seen in Figure 26..

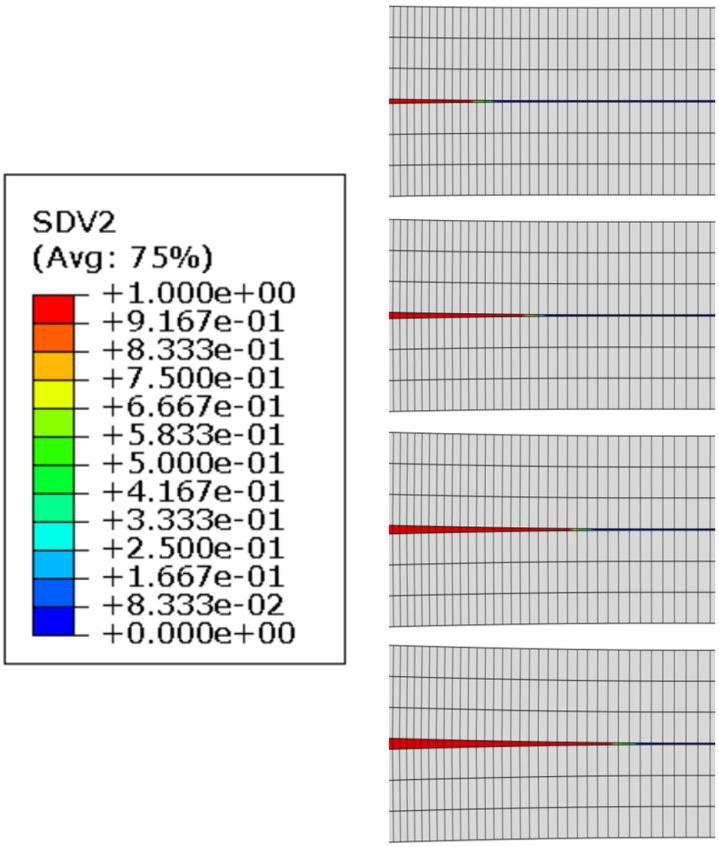

Figure 26: Crack propagation during the numerical simulation, where $SDV2$ is the variable damage, d.

And, because energy release rate is determined as a function of strain rate, it can be seen for each element during the test. Both variations are represented in Figure 27.

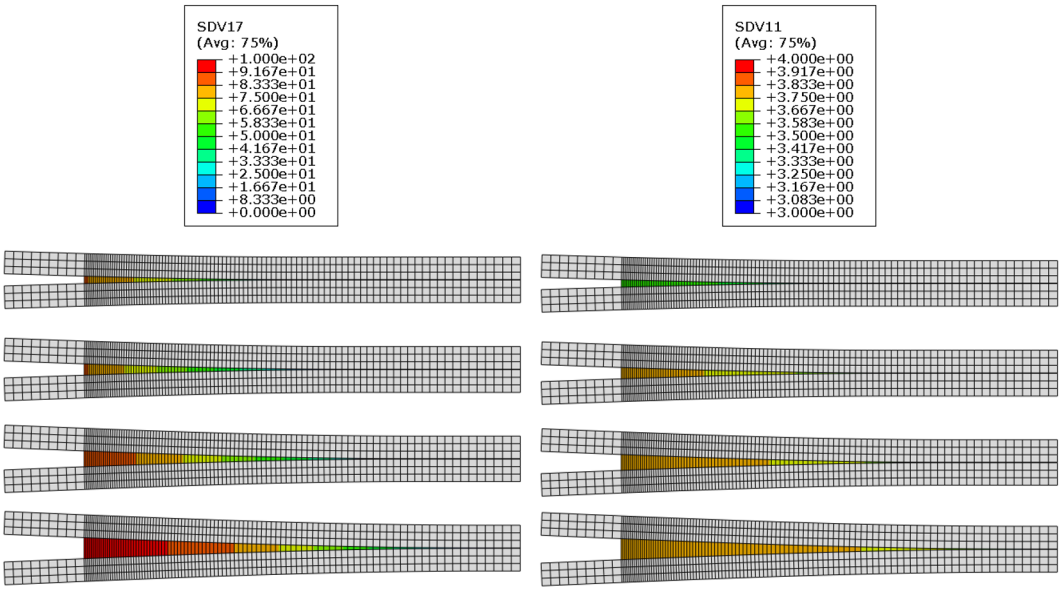

Figure 27: Strain rate, $\dot{\varepsilon}_I$, and energy release rate, G_{IC}, during the numerical simulation, where $SDV17$ is $\dot{\varepsilon}_I$, in s^{-1}, and $SDV11$ is G_{IC}, in N·mm^{-1}.

Afterwards, and to compare with the experimental results, the load and displacement obtained in the model were treated using CBBM, to obtain G_{IC}. The R-curve for Betamate^{TM}120EU at $6 \cdot 10^3$ mm·min $^{-1}$, compared with the experimental result can be seen in Figure 28.

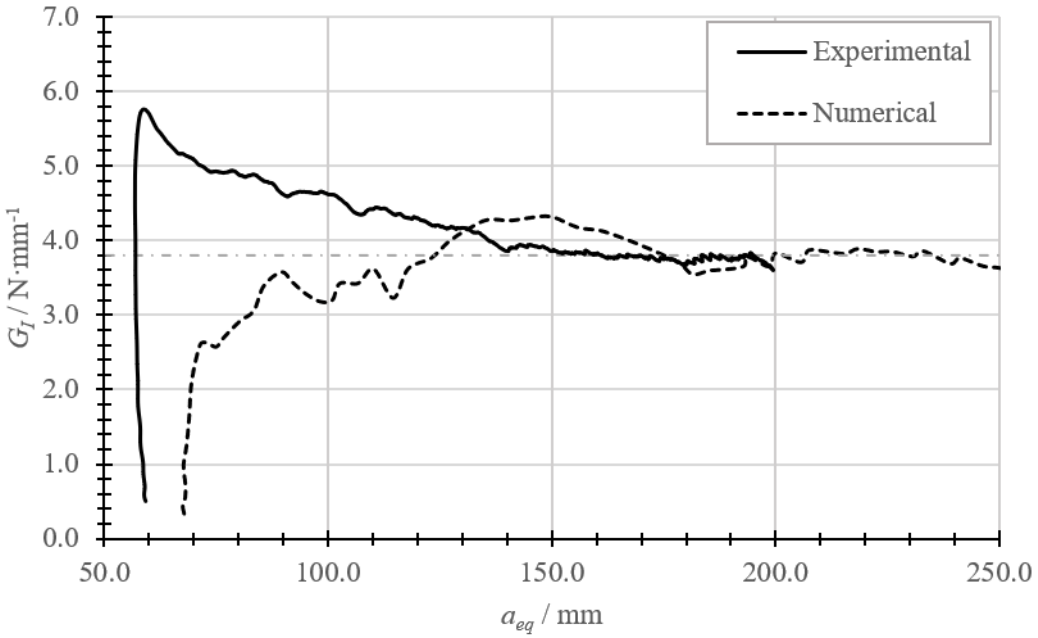

Figure 28: Experimental and numerical R-curve for Betamate^{TM}120EU at $6 \cdot 10^3$ mm·min $^{-1}$.

The numerical values of G_{IC}, compared with the experimental values obtained can be

observed in Figure 29 and Table 5.

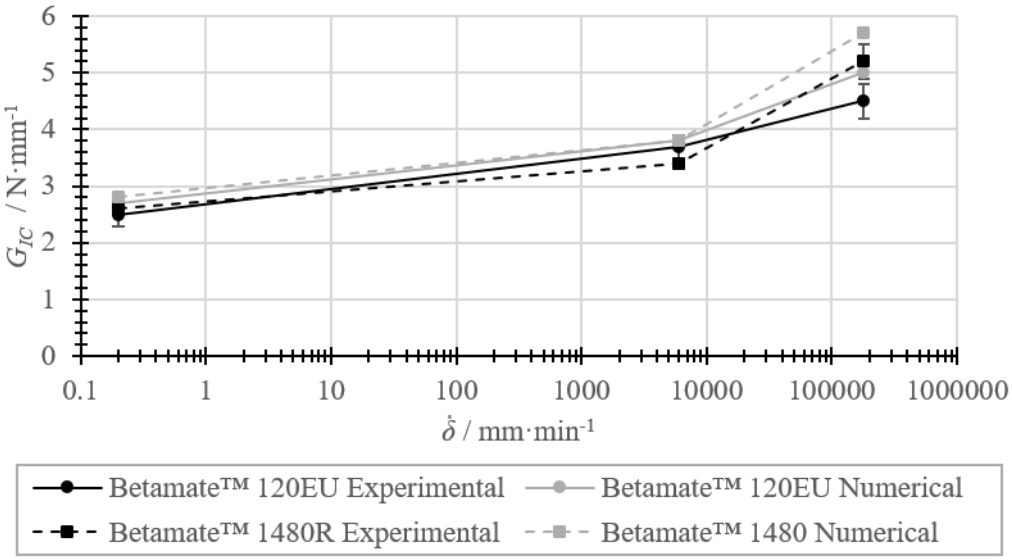

Figure 29: Comparison between experimental and numerical energy release rate, G_{IC}, for the three different loading rates, $\dot{\delta}$, tested.

Table 5: Experimental and numerical energy release rate, G_{IC}, for the three different loading rates, $\dot{\delta}$, tested.

Adhesive	$\dot{\delta}$ / mm·min^{-1}	Experimental G_{IC} / N·mm^{-1}	Numerical G_{IC} / N·mm^{-1}	Error / %
Betamate^{TM}120EU	0.2	2.5 ± 0.2	2.7	8.0
	$6 \cdot 10^3$	3.7 ± 0.2	3.8	2.7
	$180 \cdot 10^3$	4.5 ± 0.3	5.0	11.1
Betamate^{TM}1480R	0.2	2.6 ± 0.1	2.8	7.7
	$6 \cdot 10^3$	3.4 ± 0.1	3.8	11.8
	$180 \cdot 10^3$	5.2 ± 0.3	5.7	9.6

As it can be seen both in Figure 29 and Table 5, the energy release rate in mode I displays, for the Betamate^{TM}120EU, a higher error for impact tests than for quasi-static and intermediate speed. This may be due to the nature of the drop-weight tests, which present a load displacement curve with a lot of noise. Energy release rate for the Betamate^{TM}1480R also presents a high error for the intermediate speed, which may be mainly due to the fact that the higher difference between the trend traced for energy release rate in mode I and the experimental details occurs for this point.

A.7 Conclusions

The aim of this work was the development of a numerical model that takes into account the variation of mechanical properties, in mode I, as a function of strain rate. For that purpose, the mechanical characterization of the adhesive was conducted through strength tensile tests, and fracture tests (DCB). Ultimate tensile stress, determined through bulk tensile tests, and energy release rate in mode I, determined using DCB tests, were established for three different loading rates: quasi-static, intermediate speed and impact.

The main conclusions which can be drawn from this work are the following:

- The tensile behaviour of the adhesives exhibited a large dependency on strain rate, with an increase in maximum tension and decrease in maximum strain, which was consistent with what is expected for viscoelastic materials.

- Critical energy release rate in mode I, G_{IC}, showed an increase when increasing the loading rate, which can be considered as linear in a logarithmic scale.

- Strain rate along each specimen tested was determined based on a numerical simulation developed, where the adhesive was modelled using UMAT, an Abaqus® subroutine. The strain rate at the moment the adhesive fails, determined by this subroutine, changed along the specimen, decreasing with the increase in distance from the crack tip.

- Energy release rate was then determined as a function of the strain rate. G_{IC} also changes linearly in a logarithmic scale as a function of strain rate.

- The numerical model was updated with the expression for G_{IC} as a function of strain rate and the tests performed were reproduced using Abaqus®. The numerical results showed good agreement with the experimental results.

References

[1] Lucas FM Da Silva, Andreas Öchsner, and Robert D Adams. *Handbook of adhesion technology*. Springer Science & Business Media, 2011.

[2] Robert D Adams, Robert D Adams, John Comyn, William Charles Wake, and WC Wake. *Structural adhesive joints in engineering*. Springer Science & Business Media, 1997.

[3] JJM Machado, EAS Marques, and Lucas FM da Silva. Adhesives and adhesive joints under impact loadings: an overview. *The Journal of Adhesion*, 94(6):421–452, 2018.

[4] Lucas FM da Silva, Alessandro Pirondi, and Andreas Öchsner. *Hybrid adhesive joints*, volume 6. Springer Science & Business Media, 2011.

[5] HP Tardif and H Marquis. Some dynamic properties of plastics. *Canadian Aeronautics and Space Journal*, 9:205–213, 1963.

[6] US Lindholm. Some experiments with the split hopkinson pressure bar. *Journal of the Mechanics and Physics of Solids*, 12(5):317–335, 1964.

[7] PD Chalkley and WK Chiu. An improved method for testing the shear stress/strain behaviour of adhesives. *International Journal of Adhesion and Adhesives*, 13(4):237–242, 1993.

[8] Moudar Zgoul. *Characterising the rate dependent response of adhesively bonded structures*. PhD thesis, University of Surrey, 2002.

[9] Toru Sugaya, Tatsuya Obuchi, and Chiaki Sato. Influences of loading rates on stress-strain relations of cured bulks of brittle and ductile adhesives. *Journal of Solid Mechanics and Materials Engineering*, 5(12):921–928, 2011.

[10] Aleksandar Karac, BRK Blackman, V Cooper, AJ Kinloch, S Rodriguez Sanchez, WS Teo, and A Ivankovic. Modelling the fracture behaviour of adhesively-bonded joints as a function of test rate. *Engineering Fracture Mechanics*, 78(6):973–989, 2011.

[11] GD Dean, Bryan Eric Read, and BC Duncan. *An evaluation of yield criteria for adhesives for finite element analysis*. National Physical Laboratory, 1999.

[12] W Chen, F Lu, and M Cheng. Tension and compression tests of two polymers under quasi-static and dynamic loading. *Polymer testing*, 21(2):113–121, 2002.

[13] Amos Gilat, Robert K Goldberg, and Gary D Roberts. Strain rate sensitivity of epoxy resin in tensile and shear loading. *Journal of Aerospace Engineering*, 20(2):75–89, 2007.

[14] Luca Goglio, L Peroni, M Peroni, and M Rossetto. High strain-rate compression and tension behaviour of an epoxy bi-component adhesive. *International journal of adhesion and adhesives*, 28(7):329–339, 2008.

[15] WD Bascom, RY Ting, RJ Moulton, CK Riew, and AR Siebert. The fracture of an epoxy polymer containing elastomeric modifiers. *Journal of Materials Science*, 16(10):2657–2664, 1981.

[16] JL Bitner, JL Rushford, WS Rose, DL Hunston, and CK Riew. Viscoelastic fracture of structural adhesives. *The Journal of Adhesion*, 13(1):3–28, 1981.

[17] DL Hunston and GW Bullman. Viscoelastic fracture behaviour for different rubber-modified epoxy adhesive formulations. *International journal of adhesion and adhesives*, 5(2):69–74, 1985.

[18] JL Lataillade, D Grapotte, and F Cayssials. The impact resistance of ctbn-modified epoxy adhesive joints. *Le Journal de Physique IV*, 4(C8):C8–771, 1994.

[19] BRK Blackman, AJ Kinloch, AC Taylor, and Y Wang. The impact wedge-peel performance of structural adhesives. *Journal of materials science*, 35(8):1867–1884, 2000.

[20] BRK Blackman, AJ Kinloch, FS Rodriguez Sanchez, WS Teo, and JG Williams. The fracture behaviour of structural adhesives under high rates of testing. *Engineering Fracture Mechanics*, 76(18):2868–2889, 2009.

[21] D Raghavan, J He, D Hunston, and D Hoffman. Strain rate dependence of fracture in a rubber-toughened epoxy system. *The Journal of Adhesion*, 78(8):723–739, 2002.

[22] Zhemin Jia, Guoqing Yuan, David Hui, Xiaoping Feng, and Yun Zou. Effect of high loading rate and low temperature on mode i fracture toughness of ductile polyurethane adhesive. *Journal of Adhesion Science and Technology*, 33(1):79–92, 2019.

[23] Michael May, Holger Voß, and Stefan Hiermaier. Predictive modeling of damage and failure in adhesively bonded metallic joints using cohesive interface elements. *International Journal of Adhesion and Adhesives*, 49:7–17, 2014.

[24] AJ Kinloch, GA Kodokian, and MB Jamarani. Impact properties of epoxy polymers. *Journal of materials science*, 22(11):4111–4120, 1987.

[25] Anders Biel. *Constitutive behaviour and fracture toughness of an adhesive layer*. PhD thesis, Chalmers tekniska högskola, 2005.

[26] Thomas Carlberger, Anders Biel, and Ulf Stigh. Influence of temperature and strain rate on cohesive properties of a structural epoxy adhesive. *International Journal of Fracture*, 155(2):155–166, 2009.

[27] S Marzi, O Hesebeck, M Brede, and F Kleiner. A rate-dependent cohesive zone model for adhesively bonded joints loaded in mode i. *Journal of Adhesion Science and Technology*, 23(6):881–898, 2009.

[28] S Marzi. Measuring the critical energy release rate in mode ii of tough, structural adhesive joints using the tapered end-notched flexure (tenf) test. *The European Physical Journal Special Topics*, 206(1):35–40, 2012.

[29] R Avendaño, RJC Carbas, EAS Marques, LFM da Silva, and AA Fernandes. Effect of temperature and strain rate on single lap joints with dissimilar lightweight adherends bonded with an acrylic adhesive. *Composite Structures*, 152:34–44, 2016.

[30] G Viana, J Machado, R Carbas, M Costa, LFM da Silva, M Vaz, and MD Banea. Strain rate dependence of adhesive joints for the automotive industry at low and high temperatures. *Journal of Adhesion Science and Technology*, 32(19):2162–2179, 2018.

[31] JJM Machado, A Hayashi, PDP Nunes, EAS Marques, RJC Carbas, C Sato, and LFM da Silva. Strain rate dependence of a crash resistant adhesive as a function of temperature for the automotive industry. *Proceedings of the Institution of Mechanical Engineers, Part L: Journal of Materials: Design and Applications*, page 1464420719836914, 2019.

[32] NF T 76-142. Méthode de préparation de plaques d'adhésifs structuraux pour la réalisation d'éprouvettes d'éssai de caractérisation, 1988.

[33] BS 2782-0:2011. Methods of testing plastics, part 2011, 2011.

[34] Diogo PC Antunes, António M Lopes, Carlos MS Moreira da Silva, Lucas FM da Silva, Paulo DP Nunes, Eduardo AS Marques, and Ricardo JC Carbas. Development of a drop weight machine for adhesive joint testing. Accepted for publication, 2019.

[35] MFSF De Moura, RDSG Campilho, and JPM Gonçalves. Crack equivalent concept applied to the fracture characterization of bonded joints under pure mode i loading. *Composites Science and Technology*, 68(10-11):2224–2230, 2008.

B Paper B

Influence of mode mixity and loading rate on the fracture behaviour of adhesives.

C.S.P. Borges[1], P.D.P. Nunes[1], A. Akhavan[1], E.A.S. Marques[1], L.F.M. Silva[2]

1 Instituto de Ciência e Inovação em Engenharia Mecânica e Engenharia Industrial (INEGI), Portugal

2 Departamento de Engenharia Mecânica, Faculdade de Engenharia (FEUP), Universidade do Porto, Portugal

Abstract

The automotive industry, among other sectors, is progressively replacing traditional mechanical fasteners by adhesives. In this sector, passengers' safety is a priority. Thus, the behaviour of the automotive structure, including the adhesive joints within it, should be carefully studied. Adhesives are commonly subjected to loads that result from a combination of peel and shear, therefore, when studying their behaviour, both modes should be accounted for. The main aim of this work is the determination of the strength and fracture envelopes of two epoxy based crash-resistant adhesives at quasi-static conditions, an intermediate speed and impact conditions. Mode I and tensile behaviour were already known thus, for the characterization of the strength envelope, thick adherend shear tests (TAST) were performed. For the establishment of the fracture envelope, mode II fracture toughness was studied using energy release rate (ENF) tests, and mixed mode was studied with two in-house developed apparatus, one for quasi-static conditions and a more robust one for intermediate speed and impact. Strength increased for tensile and shear loading with increasing strain rate. An increase was also recorded for the energy release rate at all mode-mixities studied, following a logarithmic trend.

B.1 Introduction

Key players in the transportation sector, such as the automotive, aerospace and aeronautical industries, have increasingly adopted adhesive joints as an alternative to classical joining methods, due to their better strength to weight ratio as well as their ability to create a more uniform stress distribution, which increases load transmission, stiffness and fatigue resistance [1–3]. Adhesives also suppress the need for holes in the structure, which not only diminishes the stress concentration sites, but also promotes the use of composite materials, which are very sensitive to notches. These materials are also able to easily joint dissimilar substrates. All those changes in the structure lead to lower weight and, consequently, lower energy consumption and emissions.

The most important factor when designing a vehicle is the safety of its passengers, specially in case of a collision therefore, the behaviour of the automobile structure under impact, including the adhesive joints within it, should be fully understood.

The dynamic behaviour of adhesives has not been yet extensively studied but, as polymers, they are known to be sensitive to strain rate. Among the first researchers to record this property variation of polymeric materials for different loading rates were Tardif and Marquis [4] and Lindholm [5], in the 1960s.

Although, the number of authors recording a strain rate dependence of adhesive joints has been increasing in recent years, different trends have been recorded for the property variation, both for tensile and shear properties and fracture properties.

Regarding tensile and shear properties, the stiffness of the adhesive has been shown to increase with increasing strain rate by some authors [4–9], while others reported that it was approximately constant over the tested spectrum of strain rates [10–12].

Maximum stress and maximum strain are more unanimous subjects, with most authors recording an increase in maximum stress with strain rate and a decrease in maximum strain, paired with an increasingly more brittle behaviour [4, 5, 9–11, 13].

The fracture behaviour of adhesives at high strain rates, although fracture energy is an extensively studied topic, presents limited research, once again exhibiting contradictory results.

A decrease in fracture energy in mode I has been shown by Bascom et al. [14], Bitner et al. [15], Hunston et al. [16], Lataillade et al. [17], Blackman et al. [18, 19], Raghavan et al. [20], Karac et al. [7] and Jia et al. [21]. This decrease was justified by Raghavan et al. [20] saying that lower loading rates grant a grater crack-tip deformation, resulting in higher toughness. May et al. [22] presented a different explanation, stating that when a critical crack propagation speed is reached, the conditions at the crack-tip change from isothermal to adiabatic and, because of the increase in temperature, the fracture toughness decreases due to thermally induced degradation of the adhesive properties.

However, other authors, such as May et al. [22], Biel et al. [23], Carlberger et al. [24], Marzi et al. [25] and Machado et al. [9], recorded an increase in fracture energy in mode I with increasing strain rate. Carlberger et al. [24], additionally, it was stated that the

fracture energy increased linearly in a semi-logarithmic scale. May et al. [22] reached the same conclusion, adding that above and below two limit strain rates, the fracture energy was constant. The increase in fracture toughness with increasing strain rate follows the trend expected for viscoelastic materials.

The fracture process of adhesives is generally restricted by the adherends, resulting from a combination of mode I and II loadings. Therefore, mode II and mixed mode I+II should also be carefully determined. For that, the fracture envelope, which comprehends energy release rate in mode I, II and all mode mixities between them can be used.

However, mode II and mixed-mode variation of fracture energy with strain rate have been much less studied. Lataillade et al. [17] stated that in mode II the fracture energy deacreses with increasing strain rate, a result also reported by Carlberger et al. [24]. Marzi et al. [26], when studying the fracture behaviour in mode II of adhesives came to the conclusion that it increased with increasing strain rate. An insensitivity to strain rate variation in mode II was also reported by May et al. [22].

The main aim of this work is understanding the fracture behaviour of adhesives with the variation of loading rate. In adhesive joints, crack propagation is generally restricted by the adherends, occuring due to a combination of mode I and II [27] thus, although mode I is the most commonly studied, to understand the full fracture behaviour mode II and mixed mode I+II should also be analysed.

With that in mind, mode I, mode II and mixed mode I+II tests were performed to generate the fracture envelope of the adhesives. This envelope defines, for each mode mixity the corresponding energy release rate in mode I and II. Fracture tests were performed at three different test speeds: quasi-static 0.2 mm·min $^{-1}$, intermediate speed, $6 \cdot 10^3$ mm·min $^{-1}$ or 100 mm·s^{-1}, and impact, $180 \cdot 10^3$ mm·min $^{-1}$ or 3 m·s^{-1}. Thus, three different fracture envelopes were generated, one for each test speed.

Critical energy release rate in mode I, for all test speeds, was previously detemined [28] for the same loading rates using double cantilever beam (DCB) tests. Fracture energy in mode II was determined using end notched flexure (ENF) tests. Mixed mode tests were performed using two in-house developed apparatus, one for quasi-static conditions and other for higher loading rates.

Additionally, the strength envelope of the adhesive was also determined. Tensile properties were previously determined using bulk tensile tests at three different test speeds: quasi-static, 1 mm·min $^{-1}$, intermediate speed, $6 \cdot 10^3$ mm·min $^{-1}$ or 100 mm·s^{-1}, and impact, $180 \cdot 10^3$ mm·min $^{-1}$ or 3 m·s^{-1}. Thick adherend shear tests (TAST) were performed at the same displacement rates to analyse the shear properties of both adhesives.

B.2 Experimental details

In this work, the strength and fracture envelopes of two epoxy adhesives were experimentally determined at three different loading rates.

Strength properties were determined at the loading rates of: $1\ mm \cdot min^{-1}$, quasi-static, $6 \cdot 10^3\ mm \cdot min^{-1}$, intermediate speed, and $180 \cdot 10^3\ mm \cdot min^{-1}$, impact. Tensile properties have been previously determined using bulk tensile tests [28]. Shear properties were determined using TAST.

Fracture properties were determined for quasi-static conditions, $0.2\ mm \cdot min^{-1}$, intermediate speed, $6 \cdot 10^3\ mm \cdot min^{-1}$, and impact speed, $180 \cdot 10^3\ mm \cdot min^{-1}$. Mode I properties have been previously determined for all previously mentioned test speeds using DCB tests [28].

Mode II was analysed using ENF tests. When performing ENF tests under impact, plastic deformation of the substrates was detected. An additional speed of $9 \cdot 10^3\ mm \cdot min^{-1}$ was then tested, where plastic deformation was also found. Therefore, results for test speeds over $6 \cdot 10^3\ mm \cdot min^{-1}$ were not considered.

Mixed mode tests were performed using two in-house developed apparatus. For quasi-static conditions, an existing apparatus was used [29]. However, this apparatus was not designed to sustain high loading rates, thus, for intermediate and impact conditions a new apparatus for mixed mode testing was used.

At quasi-static and intermediate speed the phase angle adopted, φ, was 45°. In impact conditions, and because ENF tests were not possible, two mode mixities were tested: 45° and 72.5°

B.2.1 Crash resistant adhesive

In this study, two one component adhesives from DOW Automotive (Michigan, USA) were used, the Betamate™ 120EU and the Betamate™ 1480R. These adhesives are classified as crash resistant and were developed to increase durability, crash performance and body stiffness. Both adhesives require a curing stage of 30 minutes at $180°C$.

B.2.2 Specimen fabrication

TAST. TAST specimens were manufactured following the standard ISO 11003-2:2019 [30]. Those specimens use steel substrates, creating an adhesive joint with a bondline thickness of 0.7 mm and an overlap of 5 mm, as shown in Figure 1. Prior to the application of the adhesive, the specimens were grit blasted and degreased with acetone. Calibrated tape, with a thickness of 1.5 mm was inserted between the adherends, after the adhesive was applied. The adhesive was then cured under the appropriate pressure and temperature conditions.

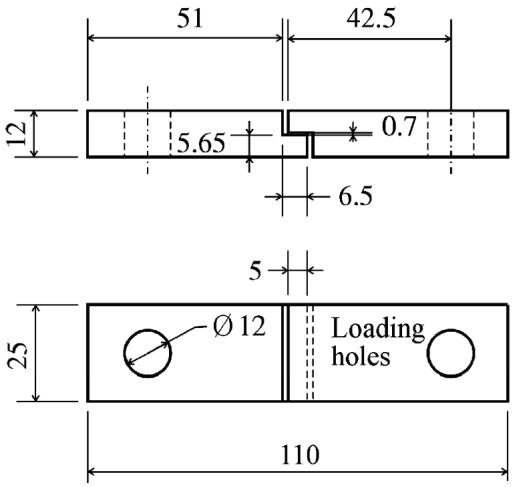

Figure 1: Representation of TAST specimen's geometry, in mm.

ENF and mixed mode tests. The specimens used for ENF and mixed mode tests are similar, Figure 2, and have the same geometry as the specimens traditionally used for DCB tests, manufactured following the relevant standard [31]. Hard steel substrates were used in DCB specimens, in order to avoid plastic deformation during the test. Before applying the adhesives, the substrates should be grit blasted and degreased with acetone.

The initial crack was induced by positioning a sharp razor blade in the mid-thickness of the bondline, the initial crack length was 45 mm. The bondline thickness of 0.2 mm is then achieved using calibrated tape.

The specimens were subjected to appropriate pressure and temperature conditions to perform the cure of the adhesive. The curing includes heating ramp, stage time and the cooling process, at the constant pressure of 25 bar, using a hot plate press.

After curing, a small pre-crack was created, in mode I, by loading the specimen until crack propagation was detected. This procedure promotes stable crack propagation during the test. The new initial crack length, a_0, was recorded.

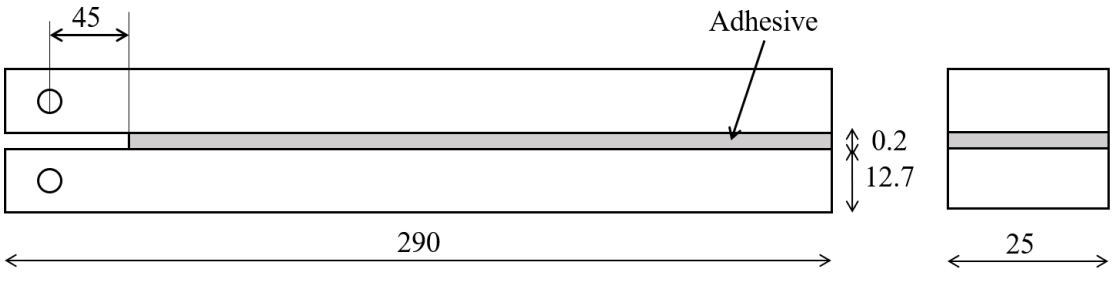

Figure 2: Representation of ENF and mixed mode test specimens' geometry, in mm.

B.2.3 Testing procedures

TAST, ENF and mixed mode tests were performed at quasi-static, intermediate and impact conditions.

The quasi-static tests were conducted in an INSTRON® 3367 with a load cell of 30 kN. The tests at an intermediate rate were conducted on an INSTRON® 8801 with a load cell of 100 kN. Impact tests were conducted in an in-house developed drop-weight machine [32], with a load cell of 30 kN, which is capable of dropping a mass up to 56 kg from a height of 1.27 m, with impact speeds of 5 m·s^{-1}. For each condition, at least three specimens were tested.

TAST. Shear strength properties were obtained using thick adherend shear tests. For the data treatment, the displacement was measured using both the testing machine displacement data and a camera for quasi-static and intermediate conditions and a high-speed camera, with a frame rate of 5000 fps for impact conditions.

ENF tests. The fracture toughness in mode II was determined using ENF tests, Figure 3.

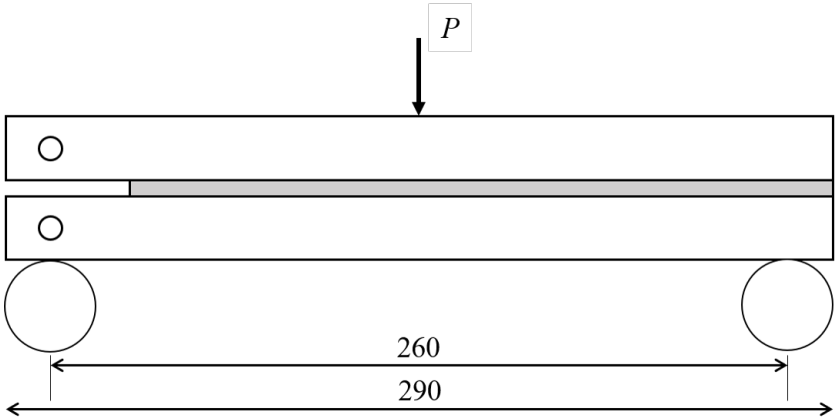

Figure 3: Schematic representation of ENF test, in mm.

Before the test, all blades were removed and a Teflon sheet, lubricated with oil, was placed between the substrates, at the pre-crack location, to avoid friction during the test. Load and displacement were recorded for each test, and the fracture energy was determined using a data reduction scheme, The compliance based beam method (CBBM), which has the advantage of not needing the exact crack length determination, because it relies on the compliance of the substrates. The energy release rate, in mode II, is given by [27]:

$$G_{II} = \frac{9P^2 a_{eq}^2}{16B^2 E h^3} \tag{1}$$

where P is the load, a_{eq} is the length of the equivalent crack, B the specimen width, E_f the corrected flexural modulus of the substrates and h its thickness.

Mixed mode tests. Mixed mode tests were performed using two in-house developed apparatus for mixed mode testing.

The apparatus used for quasi-static tests, represented in Figure 4, the configuration of the phase angles can be done by adjusting the beam lengths (s_1,s_2,s_3 and s_4). This apparatus allows the analysis of a wide range of mode mixities between 0° and 90°.

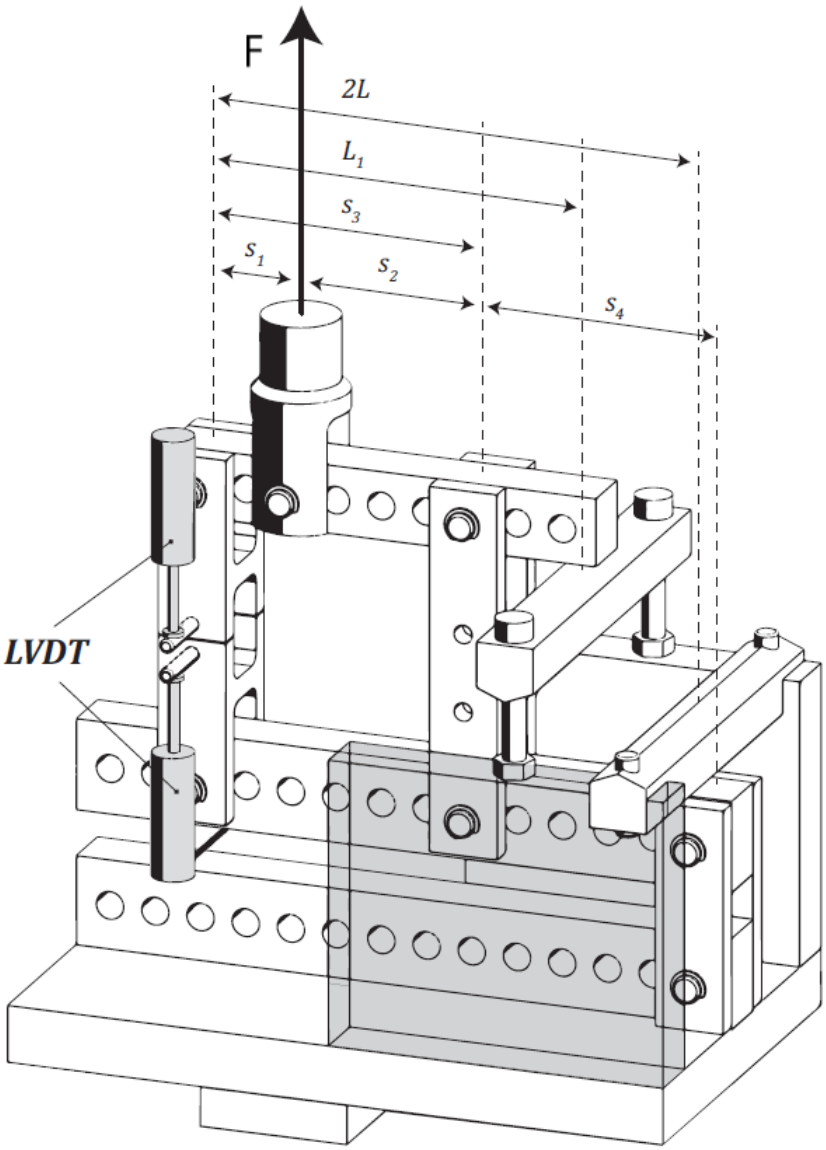

Figure 4: Schematic representation of the apparatus used for mixed mode testing in quasi-static conditions.

The theoretical phase angle, as a function of the upper beam load, F_1 and the lower beam load, F_2 is given by [29]:

$$\varphi = tan^{-1} \frac{\sqrt{3}\left(\frac{F_1}{F_2} + 1\right)}{2\left(\frac{F_1}{F_2} - 1\right)} \tag{2}$$

The load applied is a combination of mode I and II, as shown in Figure 5, and can be decomposed in F_1 and F_2 by:

$$F_1 = F\frac{s_2}{s_3}; \qquad F_2 = F\frac{s_1 s_4}{s_3(s_3 + s_4)} \tag{3}$$

Mode I and II load components, P_I and P_{II} are then determined by:

$$P_I = \frac{F_1 - F_2}{2}; \qquad P_{II} = F_1 + F_2 \tag{4}$$

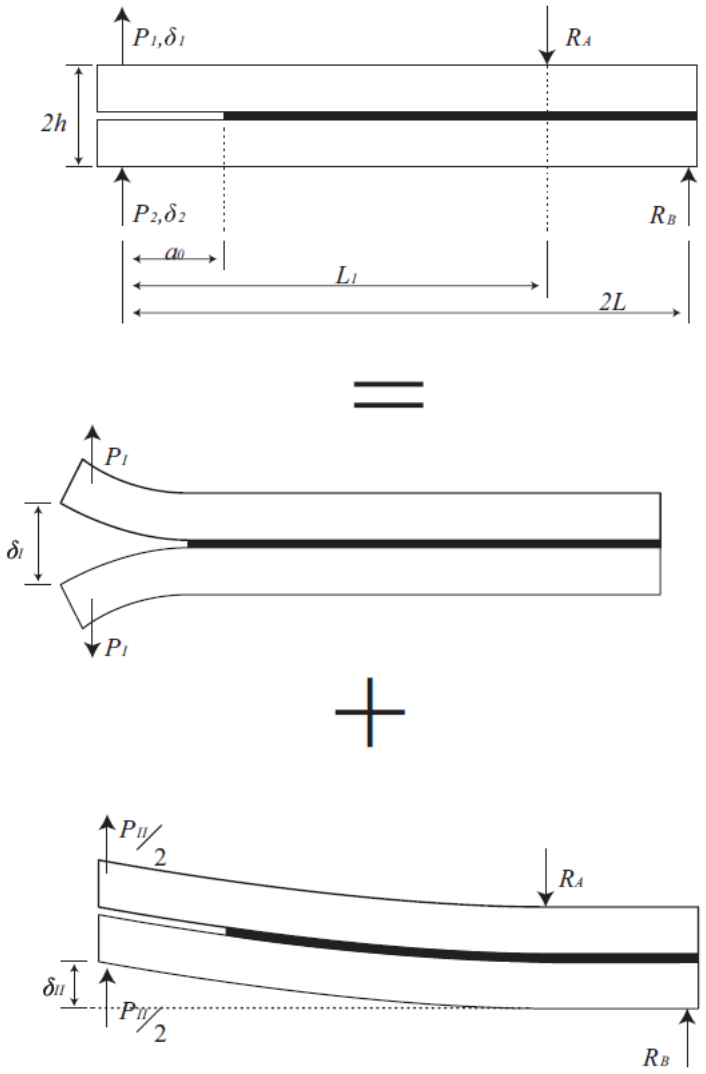

Figure 5: Schematic representation of the mixed mode test [29].

The new apparatus for mixed mode testing has the same working principle as the previous one, as far as load decomposition and phase angle calculation are concerned. However, as this apparatus is intended for operating under impact loads, it was designed with a more robust configuration, with thicker beams paired with less holes, which leads to fewer stress concentration zones, Figure 6.

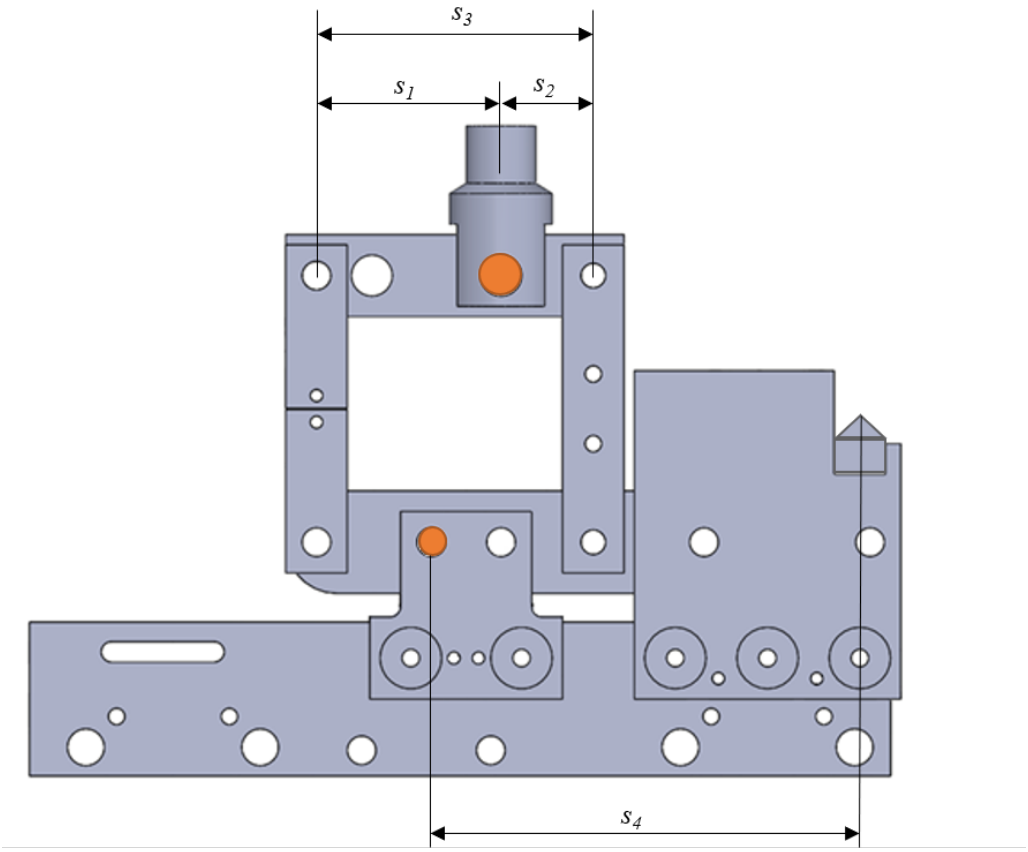

Figure 6: Schematic representation of the apparatus used for mixed mode testing under impact conditions and at intermediate speed.

This lower number of holes, allows for fewer combinations of the lengths s_i ($i = 1, 2, 3, 4$) and consequently, the analysis of less mode mixities - $\varphi = 0°$, $22.5°$, $45°$, $72.5°$ and $90°$. The pins should be placed in the positions shown in Figure 7 to test the specimen under each of those mixed mode conditions.

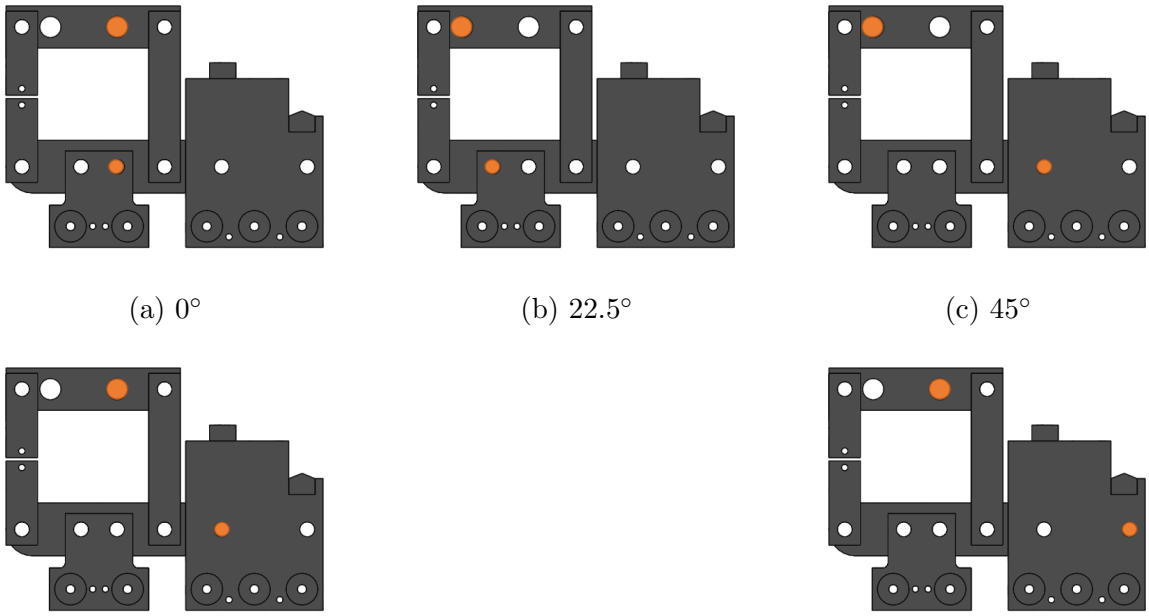

(a) 0° (b) 22.5° (c) 45°

(d) 72.5° (e) 90°

Figure 7: Positions where the pins should be placed to perform tests under each mode mixity.

The apparatus is prepared to perform impact tests using a drop-weight machine, as shown in Figure 8, where the arrow represents the impactor.

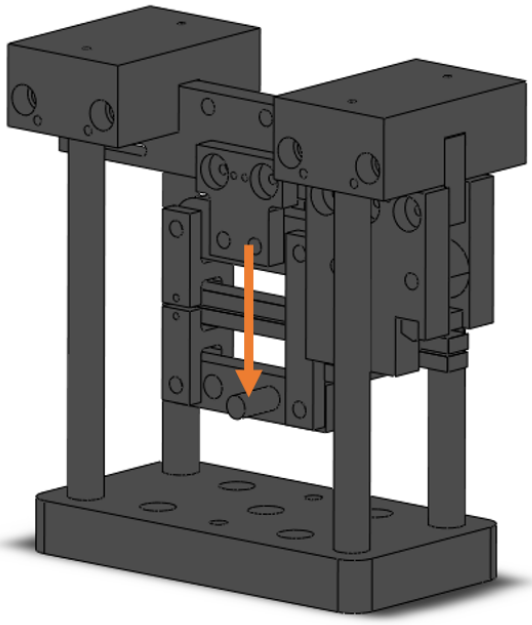

Figure 8: Schematic representation of the new apparatus for mixed mode testing, configured for impact tests.

In mixed mode I+II, after the load and displacement decomposition, the same data reduction scheme, used in ENF tests, is adopted. The corresponding energy release rate, in mode II, is given by equation (1), and in mode I by [33]:

$$G_I = \frac{6P^2}{B^2 h}\left(\frac{2a_{eq}^2}{h^2 E_f} + \frac{1}{5G_{13}}\right) \tag{5}$$

where G_{13} is its shear modulus.

B.3 Experimental results

B.3.1 Shear tests

TAST

TAST were performed to determine ultimate shear stress. The stress, τ, strain, ε, curves obtained are similar to the representative curve shown in Figure 9.

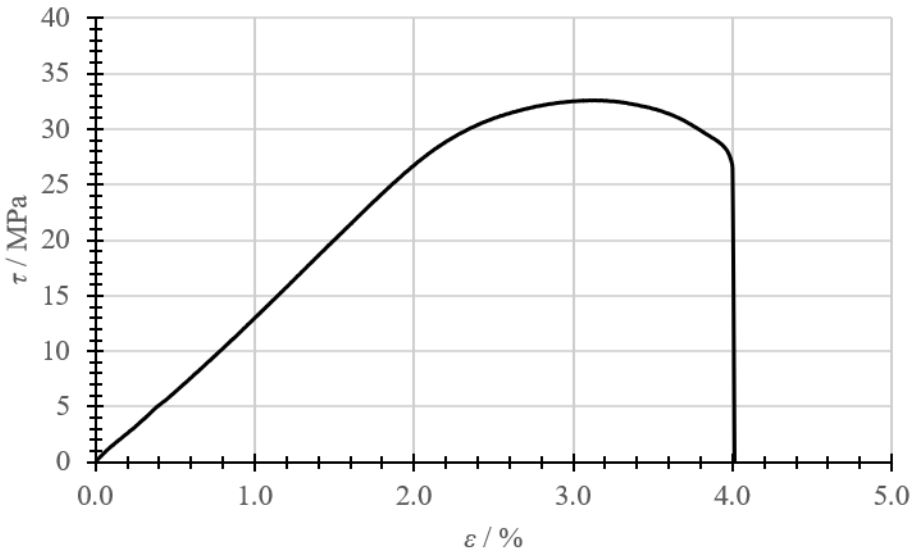

Figure 9: Representative stress strain curve for TAST.

The values of maximum stress obtained for all the testing conditions can be found in Table 1.

Table 1: Maximum shear stress, τ_{max}, for the two adhesives tested.

Adhesive	$\dot{\delta}$ / mm·min^{-1}	τ_{max} / MPa
Betamate^{TM}120EU	1	30.9 ± 0.9
	$6 \cdot 10^3$	41.6 ± 0.9
	$180 \cdot 10^3$	53.6 ± 6.7
Betamate^{TM}1480R	1	35.6 ± 1.3
	$6 \cdot 10^3$	44.6 ± 1.7
	$180 \cdot 10^3$	49.5 ± 6.1

B.3.2 Fracture tests

All fracture specimens tested exhibited cohesive failure in the adhesive. Additionally, with increasing loading rate, the specimens presented a smoother fracture surface. An example of this can be observed in Figure 10, for Betamate^{TM}120EU.

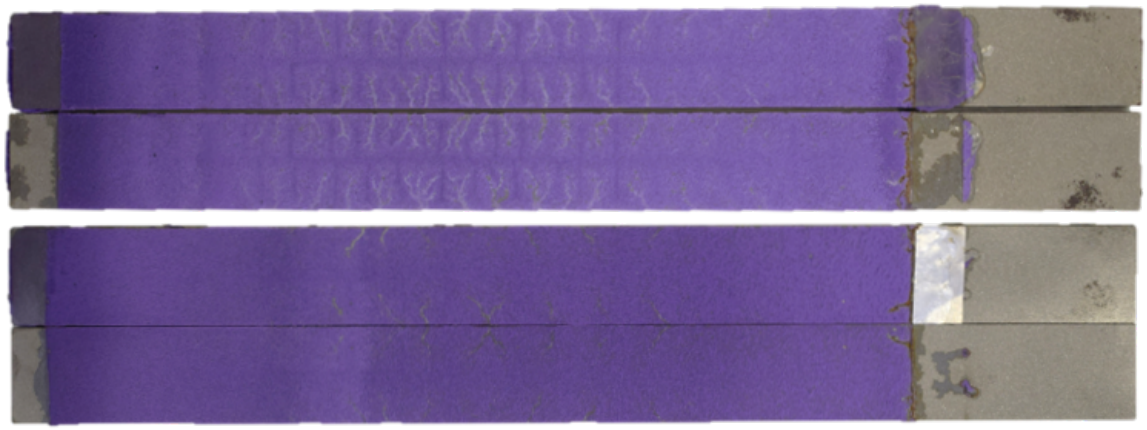

Figure 10: Fracture surface of the Betamate^{TM}120EU after testing at quasi-static conditions (top) and impact (bottom).

ENF tests

Fracture energy in mode II was determined using ENF tests. The typical R-curve for this test can be observed in Figure 11. This Figure represents a quasi-static test performed using Betamate^{TM}120EU under quasi-static conditions.

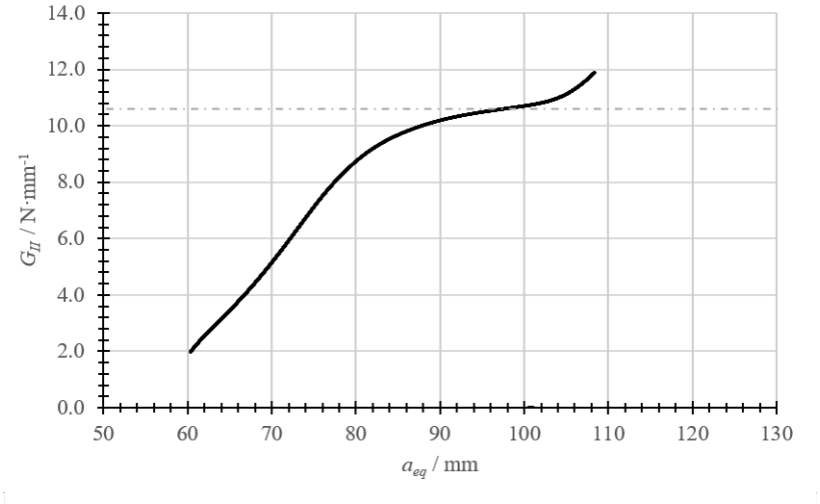

Figure 11: Representative R-curve for ENF tests.

The results for energy release rate in mode II, G_{IIC}, for all test speeds, $\dot{\delta}$, and for both studied adhesives can be seen in Table 2.

Table 2: Critical energy release rate in mode II, G_{IIC}, for the two adhesives tested.

Adhesive	$\dot{\delta}$ / mm·min^{-1}	G_{IIC} / N·mm^{-1}
Betamate$^{\text{TM}}$120EU	0.2	10.7 ± 0.1
	$6 \cdot 10^3$	10.7 ± 0.6
Betamate$^{\text{TM}}$1480R	0.2	10.1 ± 0.2
	$6 \cdot 10^3$	10.3 ± 0.1

Mixed mode tests

In mixed mode, the load and displacement components are decomposed in mode I and II, and both components of the fracture energy, energy release rate in mode I, G_I, and in mode II, G_{II} are determined. The R-curves typically obtained from this tests can be seen in Figure 12. The curve presented is for Betamate$^{\text{TM}}$120EU under quasi-static conditions and for a theoretical phase angle of 45°.

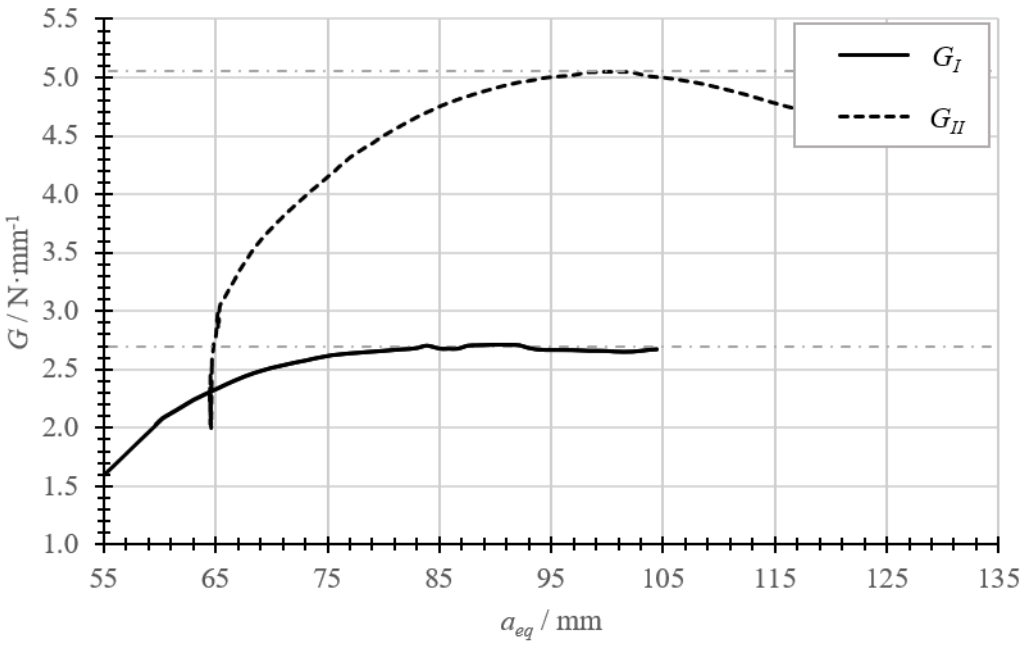

Figure 12: Representative R-curve curve for mixed mode tests.

The values for energy release rate in mode I, G_I, energy release rate in mode II, G_{II}, and experimental phase angles φ, can be seen in Tables 3 and 4, for the theoretical phase angles of 45° and 72.5°. respectively.

Table 3: Energy release rate for mixed mode for a theoretical phase angle of 45°.

Adhesive	$\dot{\delta}$ / mm·min^{-1}	G_I / N·mm^{-1}	G_{II} / N·mm^{-1}	φ / °
Betamate^{TM}120EU	0.2	2.9 ± 0.4	4.9 ± 0.3	52.4 ± 1.3
	$6 \cdot 10^3$	4.4 ± 0.1	5.8 ± 0.4	48.8 ± 0.4
	$180 \cdot 10^3$	5.8 ± 0.3	6.2 ± 0.3	46.0 ± 1.4
Betamate^{TM}1480R	0.2	3.2 ± 0.1	4.3 ± 0.4	49.4 ± 1.1
	$6 \cdot 10^3$	4.4 ± 0.1	5.3 ± 0.3	47.7 ± 1.2
	$180 \cdot 10^3$	6.1 ± 0.4	6.6 ± 0.3	46.5 ± 1.4

Table 4: Energy release rate for mixed mode for a theoretical phase angle of 72.5°.

Adhesive	$\dot{\delta}$ / mm·min^{-1}	G_I / N·mm^{-1}	G_{II} / N·mm^{-1}	φ / °
Betamate^{TM}120EU	$180 \cdot 10^3$	1.1 ± 0.3	12.1 ± 0.8	73.3 ± 1.5
Betamate^{TM}1480R	$180 \cdot 10^3$	1.4 ± 0.4	12.3 ± 0.6	71.7 ± 1.9

B.4 Results analysis and discussion

B.4.1 Strength envelope

The variation of tensile strength with loading rate was previously determined by Borges et al. [28]. Authors reported that the variation of strength with loading rate can be represented by a logarithmic trendline [8,24] and, in the present case, it also provided the best fit for the experimental data obtained by testing the two adhesives under study.

The variation of tensile strength with increasing loading rate can be seen, for both adhesives, in Figure 13.

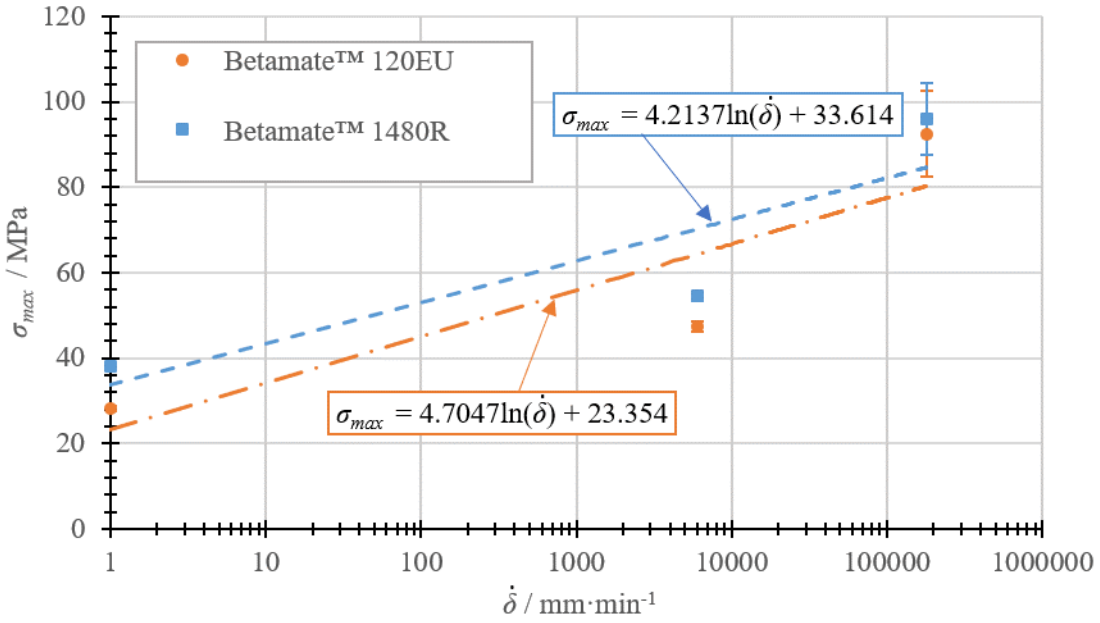

Figure 13: Tensile strength as a function of strain rate for both adhesives under study.

For an increase of six orders of magnitude in the loading rate, the tensile strength of the adhesive increases to 3.2 times of its quasi-static value for Betamate^{TM}120EU and 2.5 times for Betamate^{TM}1480R.

Shear strength as a function of loading rate was also plotted, Figure 14.

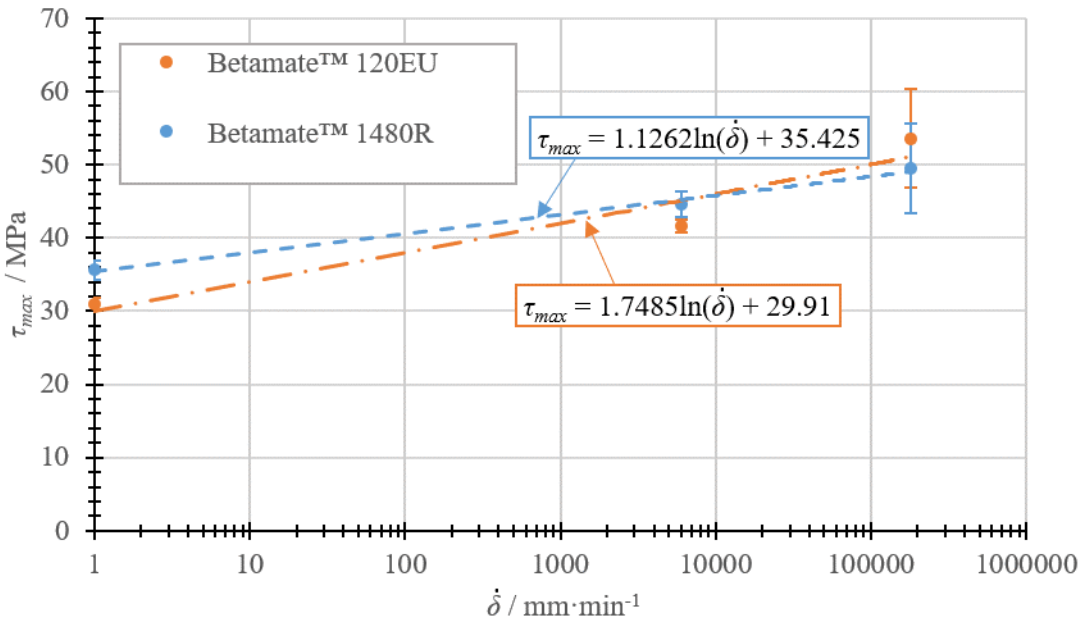

Figure 14: Shear strength as a function of loading rate for both adhesives under study.

Shear strength increases with increasing loading rate, and the trend can also be defined by a logarithmic line.

With the same increase of six orders of magnitude, the shear strength increased by 73% of its quasi-static value for Betamate^{TM}120EU and 39% Betamate^{TM}1480R.

Comparing the increase in tensile strength with the increase in shear strength, based on the experimental results, it is safe to say that tensile strength is more sensitive to loading rate variations. Figures 13 and 14 also show that the slope of the logarithmic variation of tensile strength with loading rate has a slope 3.7 times higher than the slope of the variation of shear strength for Betamate^{TM}120EU and 2.7 times for Betamate^{TM}1480R.

Finally, the envelope for the strength properties of the adhesives was plotted and can be observed in Figures 15 and 16 for the Betamate^{TM}120EU and Betamate^{TM}1480R, respectively.

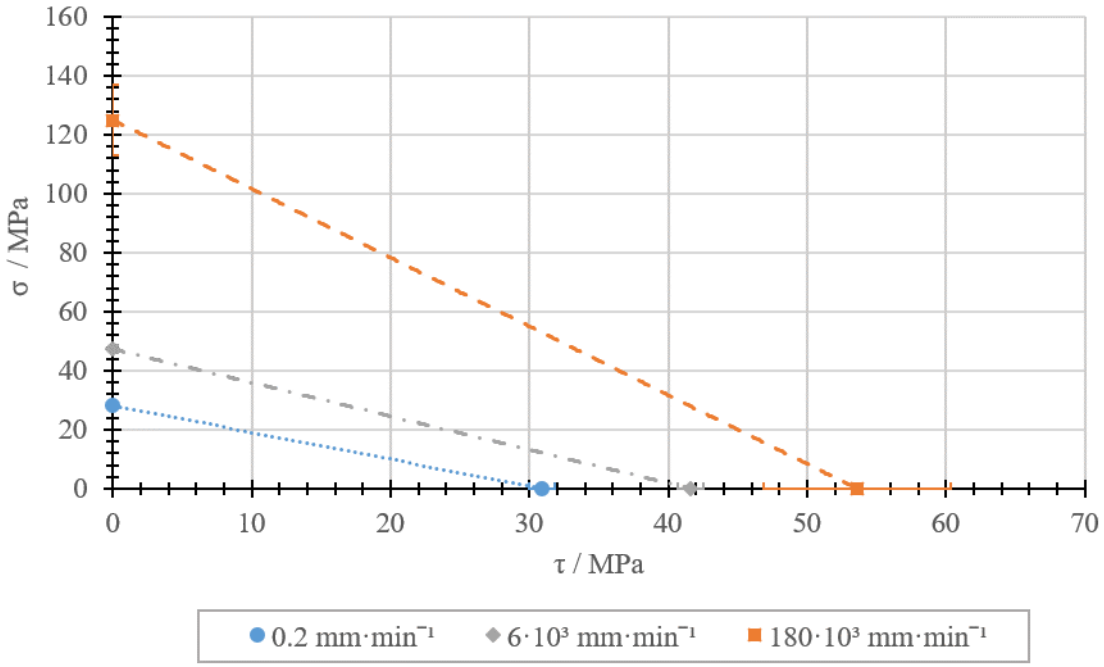

Figure 15: Strength envelopes for three loading rates for Betamate^{TM}120EU.

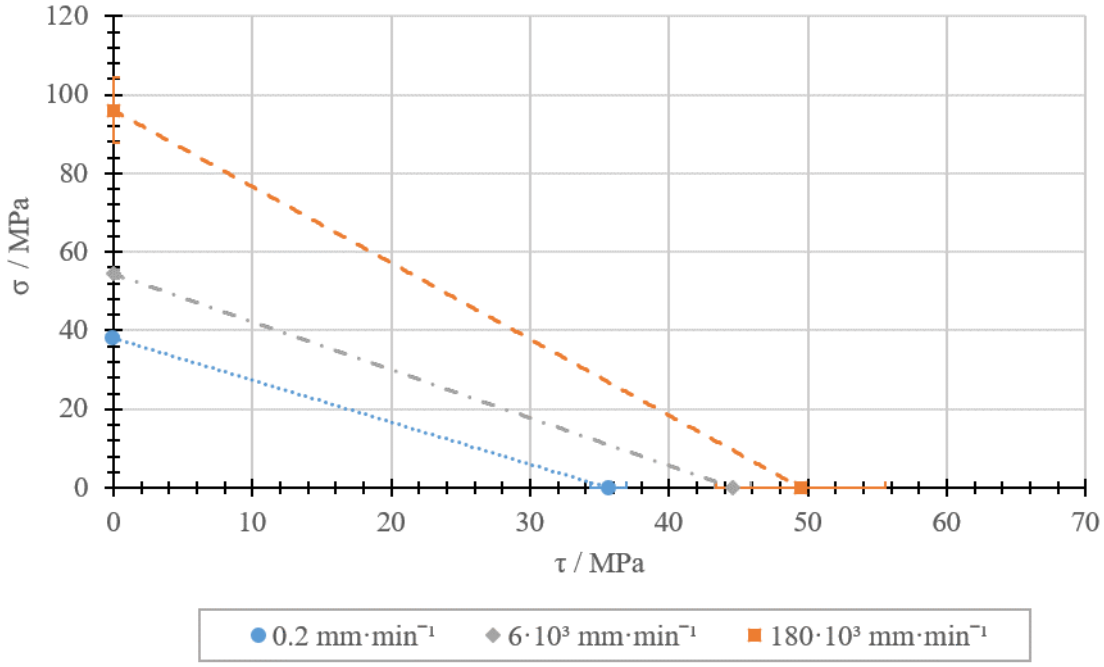

Figure 16: Strength envelopes for three loading rates for Betamate^{TM}1480R.

A linear fracture envelope was assumed due to lack of points combining shear and tensile loading. However, the strength envelope is also commonly defined using quadratic expressions.

B.4.2 Fracture envelope

Energy release rate in mode I was previously determined by Borges et al. [28], Figure 17. As for the strength properties, it was stated previously by other authors [8, 22, 24, 25] that energy release rate in mode I depends on loading rate following a logarithmic function. For the experimental data recorded, this tend also proved to be the best fit.

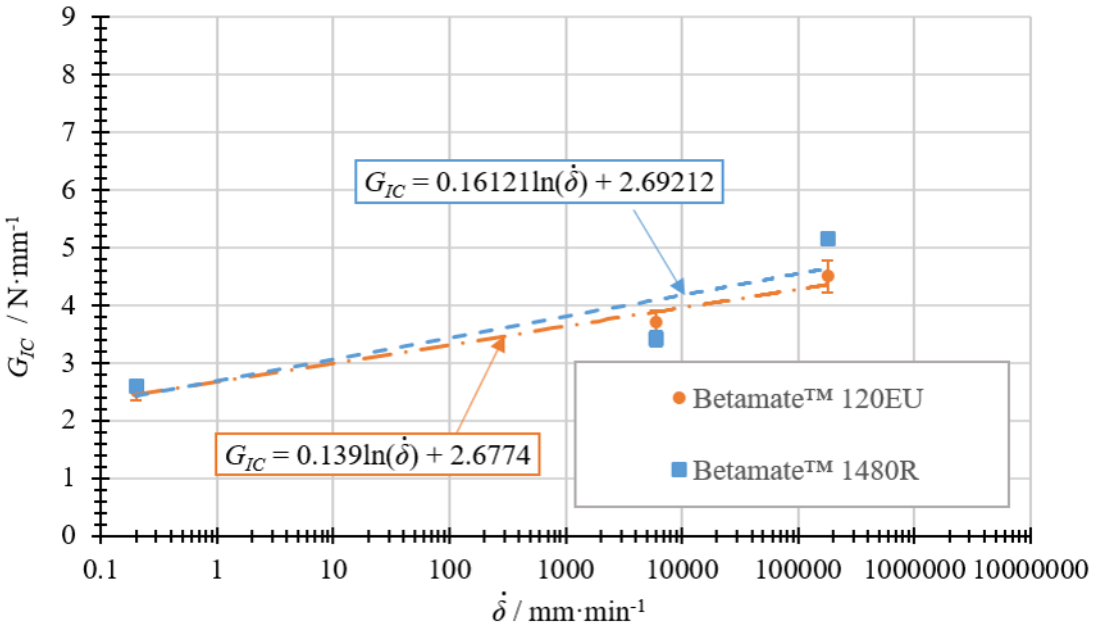

Figure 17: Critical energy release rate in mode I, G_{IC}, as a function of loading rate for both adhesives under study.

It was impossible to determine energy release rate in mode II using ENF tests for impact conditions due to the plastic deformation of the substrates. Thus, although for quasi-static conditions and intermediate speed only one mixed mode was tested, two mixed modes were analysed for impact, the fracture envelope was traced and, then, energy release rate in mode II was established.

The fracture envelopes for the three loading rates tested can be seen in Figures 18 and 19 for the Betamate^{TM}120EU and for the Betamate^{TM}1480R.

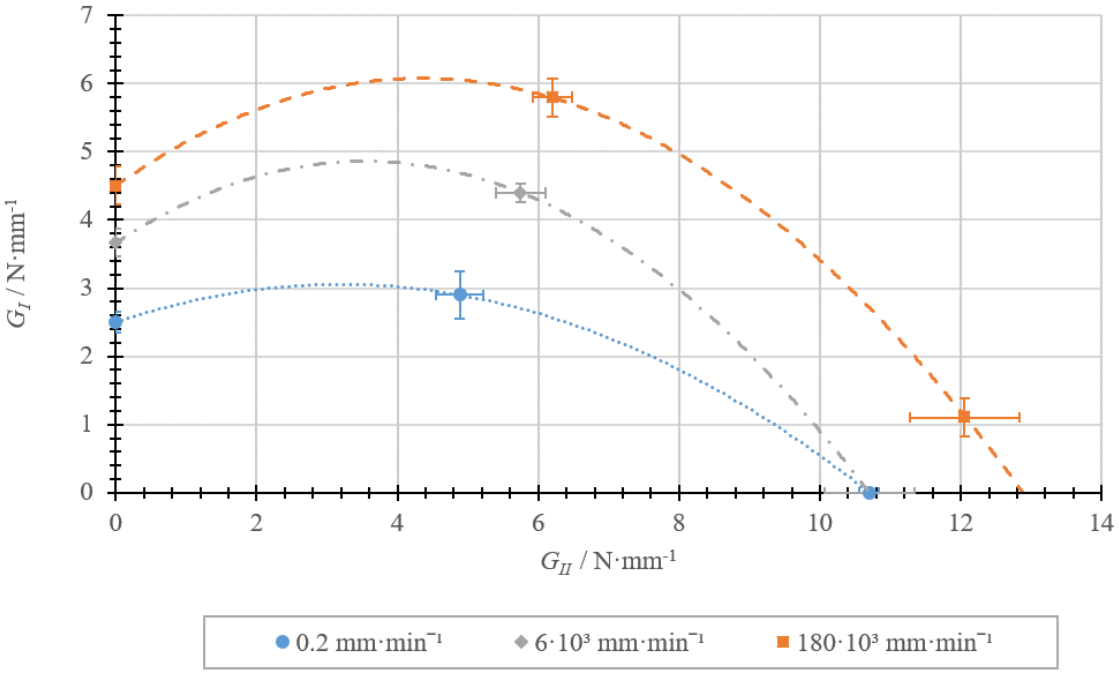

Figure 18: Fracture envelopes for three loading rates for Betamate^{TM}120EU.

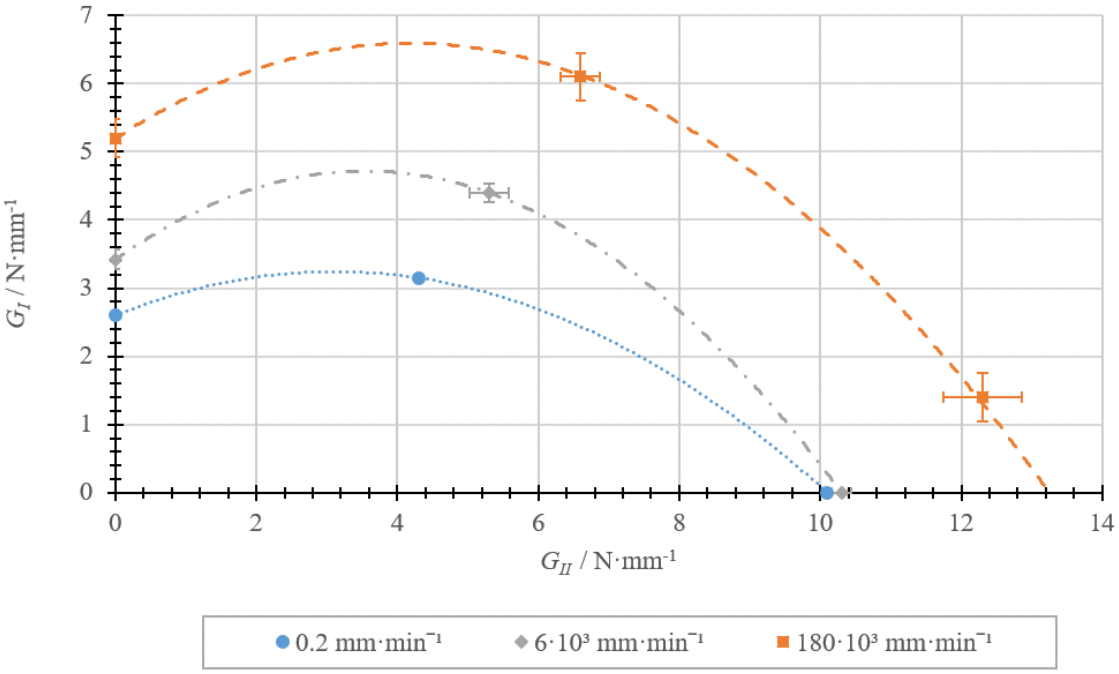

Figure 19: Fracture envelopes for three loading rates for Betamate^{TM}1480R.

The fracture envelopes, for each adhesive, present similar shapes, clearly showing an increase in the energy release rate with increasing loading rate, for all mode mixities studied.

With the impact fracture envelope, taking into account the values of energy release rate in mode I and for two mixed modes (with phase angles of 45° and 72.5°), the critical

energy release rate in mode II, G_{IIC}, can be extrapolated, leading to the values presented in Table 5.

Table 5: Critical energy release rate in mode II, G_{IIC}, determined from the impact fracture envelope.

Adhesive	G_{IIC} / $N \cdot mm^{-1}$
Betamate™120EU	12.9
Betamate™1480R	13.2

The critical energy release rate in mode II, G_{IIC}, was then plotted as a function of loading rate, considering the value established for impact conditions through the fracture envelope and the values determined for quasi-static and intermediate speed, Figure 20.

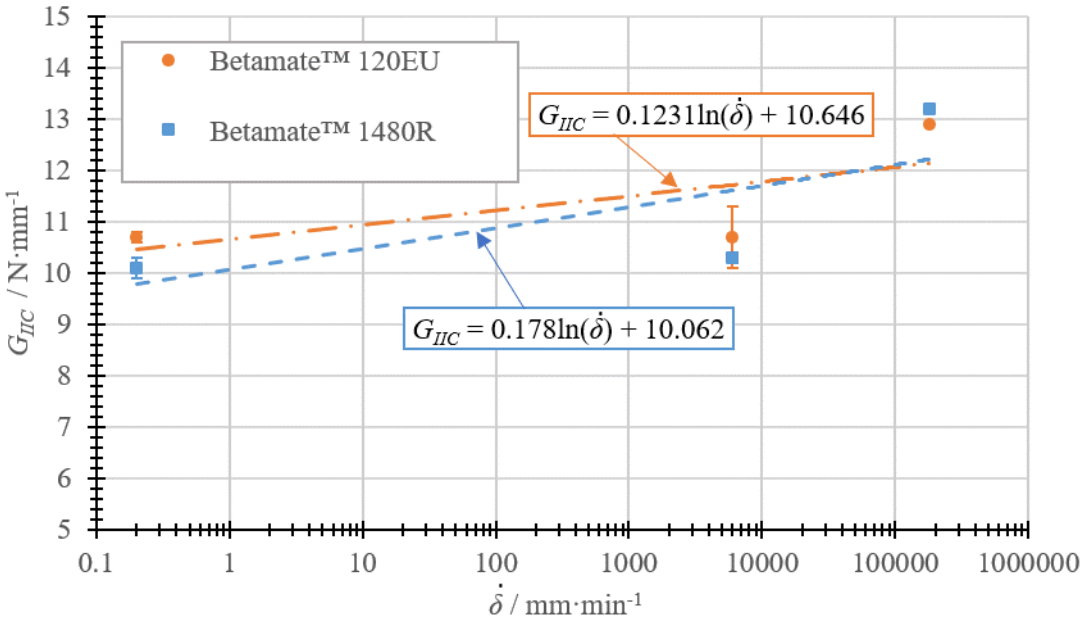

Figure 20: Critical energy release rate in mode II, G_{IIC}, as a function of loading rate for both adhesives under study.

A logarithmic trend was successfully adjusted to the points recorded and determined. However, analysing the experimental results for ENF tests, it is easily concluded that the difference between G_{IIC} at $6 \cdot 10^3$ mm·min^{-1} and $180 \cdot 10^3$ mm·min^{-1} is significantly higher than the difference between 0.2 mm·min^{-1} and $6 \cdot 10^3$ mm·min^{-1}. In literature, for mode I, some authors [22, 25] reported that energy release rate was constant bellow a certain value of strain rate, then increasing following a logarithmic relation and reaching a new constant value after a second critical value of strain rate. Jia et al. [34] suggests that strain rate for ENF tests can be determined by:

$$\dot{\varepsilon} = \frac{3EH^2\dot{\delta}}{L^3G} \tag{6}$$

where E is the Young's modulus of the substrates, H the total height of the specimen, $\dot{\delta}$ the loading rate, L the distance between the lower supports and G the shear modulus of the adhesive. Considering that it would be possible to perform the test at $180 \cdot 10^3$ mm·min^{-1} without deformation of the substrates, the strain rate for Betamate^{TM}120EU would be $1.5 \cdot 10^{-4}$ s^{-1} for a loading rate of 0.2 mm·min^{-1}, 4.4 s^{-1} for a loading rate of $6 \cdot 10^3$ mm·min^{-1} and 132.9 s^{-1} for a loading rate of $180 \cdot 10^3$ mm·min^{-1}. In this case, and in if the trend observed for mode I can be applied for mode II, the critical strain rate at which the energy release rate changes from a constant value to a logarithmic relation may be close to 4.4 s^{-1}, displaying an approximately constant value between $1.5 \cdot 10^{-4}$ and 4.4 s^{-1}. To detect this behaviour, more loading rates should be analysed.

Energy release rate was also determined in mixed mode for a theoretical phase angle of 45°. For that purpose, load and displacement were decomposed in mode I and mode II and energy release rate for each component determined. Energy release rate in mode I, G_I, and in mode II, G_{II}, as well as the experimental phase angle, φ are represented in Figure 21 and 22, for for Betamate^{TM}120EU and Betamate^{TM}1480R, respectively.

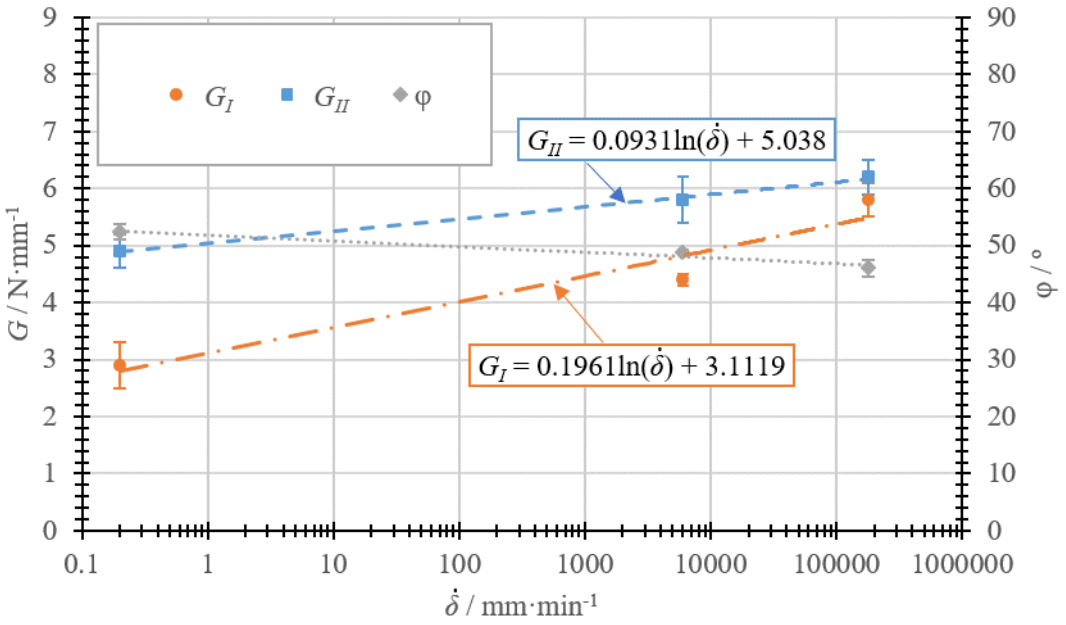

Figure 21: Energy release rate in mode I, G_I, II, and experimental phase angle, φ, for a theoretical angle of 45° as a function of loading rate for Betamate^{TM}120EU.

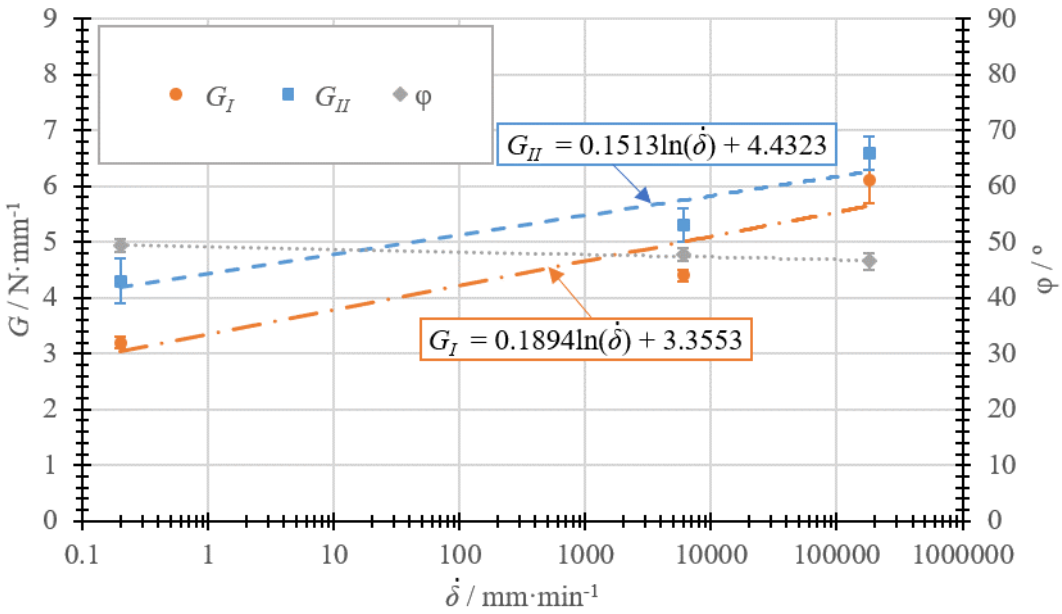

Figure 22: Energy release rate in mode I, G_I, II, and experimental phase angle, φ, for a theoretical angle of 45° as a function of loading rate for Betamate^{TM}1480R.

In mixed mode, the mode II component of energy release rate revealed a smaller influence of loading rate, when compared to mode I for both adhesives. Energy release rate, both in mode I and II, for mixed mode conditions can also be approximated using a logarithmic relation. The phase angle promoted by the apparatus used for mixed mode testing is also approximately constant and close to 45°.

B.4.3 Conclusions

The main aim of this work is the experimental determination of the strength and fracture envelopes for two epoxy adhesives at three different loading rates: quasi-static (1 mm·min $^{-1}$ for strength tests and 0.2 mm·min $^{-1}$ for fracture tests), intermediate speed ($6 \cdot 10^3$ mm·min $^{-1}$), and impact ($180 \cdot 10^3$ mm·min $^{-1}$).

For the determination of the strength envelopes, tensile and shear strength were used. Tensile strength as a function of loading rate had been previously determined [28] using bulk tensile tests. The shear strength was determined using TAST.

For the determination of the fracture envelopes, pure mode I, pure mode II and mixed mode I+II, at 45°, were analysed. Critical energy release rate in mode I as a function of loading rate had been previously determined [28]. Critical energy release rate in mode II was determined using ENF tests. However, for loading rates over $6 \cdot 10^3$ mm·min $^{-1}$ the specimens showed plastic deformation and, therefore, the results were not considered. Thus, to establish the impact fracture energy, an additional mode mixity, 72.5°, was analysed. Mixed mode was studied using two different apparatus, one for quasi-static conditions and a more robust one for intermediate speed and impact.

The main conclusions which can be drawn from this work are the following:

- Tensile and shear strength increase with increasing loading rate and the evolution can be described by a line in a semi-logarithmic scale.

- Fracture envelopes present a quadratic shape, which is similar for all loading rates analysed.

- Energy release rate, for all mode mixities studied, increases as a function of loading rate, which could be also approximated by a logarithmic relation.

References

[1] Lucas FM Da Silva, Andreas Öchsner, and Robert D Adams. *Handbook of adhesion technology*. Springer Science & Business Media, 2011.

[2] Robert D Adams, Robert D Adams, John Comyn, William Charles Wake, and WC Wake. *Structural adhesive joints in engineering*. Springer Science & Business Media, 1997.

[3] Lucas FM da Silva, Alessandro Pirondi, and Andreas Öchsner. *Hybrid adhesive joints*, volume 6. Springer Science & Business Media, 2011.

[4] HP Tardif and H Marquis. Some dynamic properties of plastics. *Canadian Aeronautics and Space Journal*, 9:205–213, 1963.

[5] US Lindholm. Some experiments with the split hopkinson pressure bar. *Journal of the Mechanics and Physics of Solids*, 12(5):317–335, 1964.

[6] Luca Goglio, L Peroni, M Peroni, and M Rossetto. High strain-rate compression and tension behaviour of an epoxy bi-component adhesive. *International journal of adhesion and adhesives*, 28(7):329–339, 2008.

[7] Aleksandar Karac, BRK Blackman, V Cooper, AJ Kinloch, S Rodriguez Sanchez, WS Teo, and A Ivankovic. Modelling the fracture behaviour of adhesively-bonded joints as a function of test rate. *Engineering Fracture Mechanics*, 78(6):973–989, 2011.

[8] R Avendaño, RJC Carbas, EAS Marques, LFM da Silva, and AA Fernandes. Effect of temperature and strain rate on single lap joints with dissimilar lightweight adherends bonded with an acrylic adhesive. *Composite Structures*, 152:34–44, 2016.

[9] JJM Machado, A Hayashi, PDP Nunes, EAS Marques, RJC Carbas, C Sato, and LFM da Silva. Strain rate dependence of a crash resistant adhesive as a function of temperature for the automotive industry. *Proceedings of the Institution of Mechanical Engineers, Part L: Journal of Materials: Design and Applications*, page 1464420719836914, 2019.

[10] PD Chalkley and WK Chiu. An improved method for testing the shear stress/strain behaviour of adhesives. *International Journal of Adhesion and Adhesives*, 13(4):237–242, 1993.

[11] Moudar Zgoul. *Characterising the rate dependent response of adhesively bonded structures*. PhD thesis, University of Surrey, 2002.

[12] Toru Sugaya, Tatsuya Obuchi, and Chiaki Sato. Influences of loading rates on stress-strain relations of cured bulks of brittle and ductile adhesives. *Journal of Solid Mechanics and Materials Engineering*, 5(12):921–928, 2011.

[13] Amos Gilat, Robert K Goldberg, and Gary D Roberts. Strain rate sensitivity of epoxy resin in tensile and shear loading. *Journal of Aerospace Engineering*, 20(2):75–89, 2007.

[14] WD Bascom, RY Ting, RJ Moulton, CK Riew, and AR Siebert. The fracture of an epoxy polymer containing elastomeric modifiers. *Journal of Materials Science*, 16(10):2657–2664, 1981.

[15] JL Bitner, JL Rushford, WS Rose, DL Hunston, and CK Riew. Viscoelastic fracture of structural adhesives. *The Journal of Adhesion*, 13(1):3–28, 1981.

[16] DL Hunston and GW Bullman. Viscoelastic fracture behaviour for different rubber-modified epoxy adhesive formulations. *International journal of adhesion and adhesives*, 5(2):69–74, 1985.

[17] JL Lataillade, D Grapotte, and F Cayssials. The impact resistance of ctbn-modified epoxy adhesive joints. *Le Journal de Physique IV*, 4(C8):C8–771, 1994.

[18] BRK Blackman, AJ Kinloch, AC Taylor, and Y Wang. The impact wedge-peel performance of structural adhesives. *Journal of materials science*, 35(8):1867–1884, 2000.

[19] BRK Blackman, AJ Kinloch, FS Rodriguez Sanchez, WS Teo, and JG Williams. The fracture behaviour of structural adhesives under high rates of testing. *Engineering Fracture Mechanics*, 76(18):2868–2889, 2009.

[20] D Raghavan, J He, D Hunston, and D Hoffman. Strain rate dependence of fracture in a rubber-toughened epoxy system. *The Journal of Adhesion*, 78(8):723–739, 2002.

[21] Zhemin Jia, Guoqing Yuan, David Hui, Xiaoping Feng, and Yun Zou. Effect of high loading rate and low temperature on mode i fracture toughness of ductile polyurethane adhesive. *Journal of Adhesion Science and Technology*, 33(1):79–92, 2019.

[22] Michael May, Holger Voß, and Stefan Hiermaier. Predictive modeling of damage and failure in adhesively bonded metallic joints using cohesive interface elements. *International Journal of Adhesion and Adhesives*, 49:7–17, 2014.

[23] Anders Biel. *Constitutive behaviour and fracture toughness of an adhesive layer*. PhD thesis, Chalmers tekniska högskola, 2005.

[24] Thomas Carlberger, Anders Biel, and Ulf Stigh. Influence of temperature and strain rate on cohesive properties of a structural epoxy adhesive. *International Journal of Fracture*, 155(2):155–166, 2009.

[25] S Marzi, O Hesebeck, M Brede, and F Kleiner. A rate-dependent cohesive zone model for adhesively bonded joints loaded in mode i. *Journal of Adhesion Science and Technology*, 23(6):881–898, 2009.

[26] S Marzi. Measuring the critical energy release rate in mode ii of tough, structural adhesive joints using the tapered end-notched flexure (tenf) test. *The European Physical Journal Special Topics*, 206(1):35–40, 2012.

[27] M Costa, R Carbas, M Benedita, E Marques, G Viana, LFM da Silva, E Yokoi, S Nakada, and T Furusawa. Static assessment of the mixed-mode behaviour of three epoxy adhesives. *Engineering Fracture Mechanics*, 182:552–565, 2017.

[28] CSP Borges, PDP Nunes, A. Akhavan, and Lucas FM da Silva. A strain rate dependent cohesive zone element for mode i modelling of the fracture behaviour of adhesives. -, 2019.

[29] M Costa, R Carbas, E Marques, G Viana, and LFM Da Silva. An apparatus for mixed-mode fracture characterization of adhesive joints. *Theoretical and Applied Fracture Mechanics*, 91:94–102, 2017.

[30] ISO 11003-2:2019. Adhesives - determination of shear behaviour of structural bonds - part 2: Thick-adherend tensile-test method. *International Organization for Standardization*, 2019.

[31] ASTM D3433-99. Standard test method for fracture strength in cleavage of adhesives in bonded metal joints. *Adhesives, American Society for Testing and Materials*, 1999.

[32] Diogo PC Antunes, António M Lopes, Carlos MS Moreira da Silva, Lucas FM da Silva, Paulo DP Nunes, Eduardo AS Marques, and Ricardo JC Carbas. Development of a drop weight machine for adhesive joint testing. Accepted for publication, 2019.

[33] MFSF De Moura, RDSG Campilho, and JPM Gonçalves. Crack equivalent concept applied to the fracture characterization of bonded joints under pure mode i loading. *Composites Science and Technology*, 68(10-11):2224–2230, 2008.

[34] Zhemin Jia, Guoqing Yuan, David Hui, Xiaoping Feng, and Yun Zou. Effect of high strain rate and low temperature on mode ii fracture toughness of ductile adhesive. *International Journal of Adhesion and Adhesives*, 86:105–112, 2018.